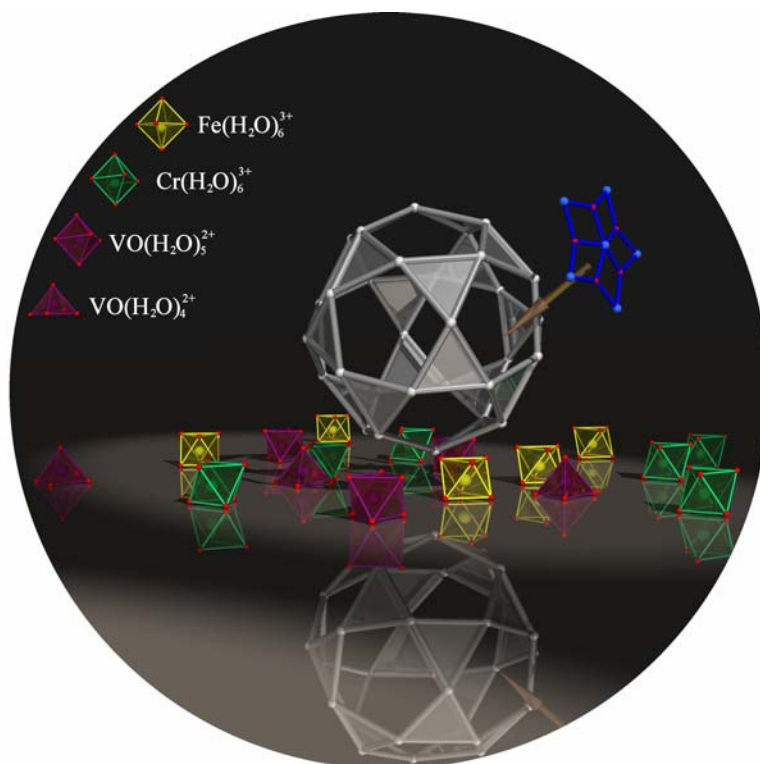


New Routes in Polyoxometalate Chemistry: From Keplerates to Chemistry under Confined Conditions



– Cumulative Dissertation –

Ana Maria Todea

Fakultät für Chemie
Universität Bielefeld

January 2008

This thesis is the result of research carried out during the period of February 2004 to June 2007 under the supervision of Prof. Dr. Dr. h. c. mult. Achim Müller, Fakultät für Chemie, Universität Bielefeld.

Referee: Prof. Dr. Dr. h. c. mult. Achim Müller

Second referee: Prof. Dr. Lothar Weber

Acknowledgement

First of all I'm grateful to my supervisor Prof. Dr. Dr. h.c. mult. Achim Müller for offering me the possibility to join his group, for his guidance, as well as the provision of financial support during the course of this investigation.

I am also grateful to Prof. Dr. Mariana Rusu for introducing me to the wonderful field of polyoxometalates.

Special thanks regard Filipa (F. Sousa Lourosa), my lab colleague from the first day, Raul (Dr. A. R. Tomsa) for all their support on professional and personal level. I am especially grateful to Marc Schmidtmann, Dr. Alice Merca and Dr. Hartmut Bögge for their help with the X-ray diffraction measurements and crystal structure determinations. This thesis would not have been possible without their permanent involvement. I am grateful to Ms. Gabi Heinze-Brückner for the Infrared and Raman measurements, to Ursula Stuphorn for the UV-Vis measurements, to Ms. Brigitte Michel for the C,H,N analyses and to Alois Berkle for his help with the analytical measurements. A number of other people have made my stay in a foreign country possible and enjoyable. My thanks in this regard go to K. Lacey, Prof. Dr. E. Diemann, E. Krickemeyer, B. Ostheider, Dr. A. Bell, T. Mitra (special thanks for the nice idea and for all the work in preparing the cover picture), C. Schäffer, J. Szakacs.

And finally I would like to thank my parents for all their love and support.

Contents

1. Introduction	1
1.1. Synopsis.....	1
1.2. Basic principles and highlights of the field.....	2
1.2.1. Polyoxotungstates.....	3
1.2.2. Polyoxomolybdates.....	5
1.3. Goals of the project: defining the problem.....	10
2. Publications	13
2.1. <i>Triangular Geometrical and Magnetic Motifs Uniquely Linked on a Spherical Capsule Surface</i> A. Müller, A. M. Todea, J. van Slageren, M. Dressel, H. Bögge, M. Schmidtman, M. Luban, L. Engelhardt, M. Rusu <i>Angew. Chem.</i> , 2005 , 117, 3925-3929.....	14
2.2. <i>Formation of a "less stable" polyanion directed and protected by electrophilic internal surface functionalities of a capsule in growth: $[\{Mo_6O_{19}\}^{2-} \subset \{Mo^{VI}_{72}Fe^{III}_{30}O_{252}(ac)_{20}(H_2O)_{92}\}]^+$</i> A. Müller, A. M. Todea, H. Bögge, J. van Slageren, M. Dressel, A. Stammler, M. Rusu <i>Chem. Commun.</i> , 2006 , 3066-3068.....	14

2.3. <i>Extending the $\{(Mo)Mo_5\}_{12}M_{30}$ Capsule Sequence: New Cr_{30} Cluster of $s = 3/2$ Metal Centres with a $\{Na(H_2O)_{12}\}$ Encapsulate</i>	
A. M. Todea, A. Merca, H. Bögge, J. van Slageren, M. Dressel, L. Engelhardt, M. Luban, T. Glaser, M. Henry, A. Müller	
<i>Angew. Chem.</i> , 2007 , <i>119</i> , 6218-6222.....	15
2.4. <i>Unique Properties of $Mo_{72}Fe_{30}$ Cluster in Solution</i>	
A. Müller, A. M. Todea	
Manuscript in preparation.....	15
2.5. <i>Metal-Oxide-Based Nucleation Process under Confined Conditions: Two Mixed-Valence V_6-Type Aggregates Closing the W_{48} Wheel-Type Cluster Cavities</i>	
A. Müller, M. T. Pope, A. M. Todea, H. Bögge, J. van Slageren, M. Dressel, P. Gouzerh, R. Thouvenot, B. Tsukerblat, A. Bell	
<i>Angew. Chem.</i> , 2007 , <i>119</i> , 4561-4564.....	16
2.6. <i>Nucleation process in the cavity of a 48-tungstophosphate wheel resulting in a 16 metal center iron-oxide nanocluster</i>	
Sib Sankar Mal, Michael H. Dickman, Ulrich Kortz, Ana Maria Todea, Alice Merca, Hartmut Bögge, Thorsten Glaser, Achim Müller, Saritha Nellutla, Narpinder Kaur, Johan van Tol, Naresh S. Dalal, Bineta Keita, Louis Nadjjo	
<i>Chem. Eur. J.</i> , 2008 , <i>14</i> , 1186-1195.....	16
2. Summary	17
3. Appendix	20
4. Curriculum Vitae	28

Chapter 1

Introduction

1.1 Synopsis

The emergence of the term “nanotechnology” and its increasing use in the scientific and popular scientific literature reflects the expanding interest in the ability to gain control over the organisation of material, in order to fabricate and exploit entities with dimensions of less than 100 nm. This fascinating field opens up many new exciting possibilities for example in materials science, biomolecular transport systems, and bio-sensor technology.

A fundamental question is: how can the appropriate material be organised in the desired arrangements to provide such nano-sized entities? One strategy for achieving such entities reproducibly is the “top-down” approach. In this approach usually the desired nanostructure is designed starting from a macroscopic structure. A second strategy is a “bottom-up” approach. In this approach the nanostructures are generated from a library of building blocks, which might be a group of atoms, molecules, ions or an iterative structural moiety. It is inevitably a zone where chemists can exhibit extreme creative prowess.

Polyoxometalate chemistry, the chemistry of the inorganic metal-oxygen cluster anions, mostly based on Mo, W or V, uses the advantages of self assembly but based on covalent linking, to synthesise a variety of nano-sized entities which are based on the linking of transferable building blocks, under "one-pot" conditions. This type of chemistry has already yielded a multitude of compounds containing polyanions which display a fascinating degree of structural and functional variety comparable to that of proteins [1]. Optimal conditions for linking of fragments leading to a large variety of structures are:

1. the potential of the system to generate a versatile library of linkable units,
2. the ability to generate groups (intermediates) with high free enthalpy to drive polymerization or growth processes, e.g. based on formation of H₂O,
3. the possibility for easy structural changes in the building units and blocks, the ability to include hetero elements in the fragments,
4. the possibility to form larger groups which can be linked in different ways,
5. the ability to control the structure-forming processes by templates,
6. the ability to generate structural defects in reaction intermediates (e.g. leading to lacunary structures) e.g. by removing building blocks from (large) intermediates due to the presence of appropriate reactants,
7. the ability to localize and delocalize electrons in different ways in order to gain versatility,
8. the ability to control and vary the charge of building parts (e.g. by protonation, electron transfer reactions, or substitution) and to limit growth by the abundance of appropriate terminal ligands,
9. the possibility of generating fragments with energetically low-lying unoccupied molecular orbitals [2].

These conditions can be optimally fulfilled in polyoxometalate systems which possess the relevant variety of structural and electronic versatility. It is not only possible to perform a new type of chemistry with the clusters in aqueous solution but also to dissolve them in organic solvents, e.g. after encapsulating them with suitable surfactant molecules, with the option of forming monolayers, thin films, liquid crystals and hybrid materials [3]. Furthermore, it is possible to study their aggregation behavior in solution leading to the formation of novel vesicles [4].

1.2 Basic principles and highlights of the field

The basic structural principle for polyoxotungstates and molybdates is the same, since the structures are governed by the principle that each metal atom occupies an $\{MO_x\}$ coordination

polyhedron, in which the metal atom is displaced, as a result of M-O π bonding, toward those polyhedral vertices that form the surface of the structure. However, a more detailed view of this fascinating area of chemistry shows striking differences for these compound types also with respect to the very large cluster systems [5].

1.2.1 Polyoxotungstates

The structural features of large polyoxotungstate clusters can be visualized in terms of subunits based on lacunary fragments of the Keggin anion (with the classical archetypal $\{W_3O_{13}\}$ units) including its isomers [6].

Keggin-isomers and trilacunary structures

The structure of the classical Keggin anion has overall T_d symmetry and is based on a central XO_4 tetrahedron surrounded by twelve $\{WO_6\}$ octahedra arranged in four groups of three edge-shared octahedra, $\{W_3O_{13}\}$. These $\{W_3O_{13}\}$ groups are linked by sharing corners to each other and to the central XO_4 tetrahedron (Figure 1.1). The Keggin ion can adopt up to five isomers (α - ϵ) and these isomers are related to each other by a rotation of one or more edge-shared $\{W_3O_{13}\}$ groups by $\pi/3$ [7, 8].

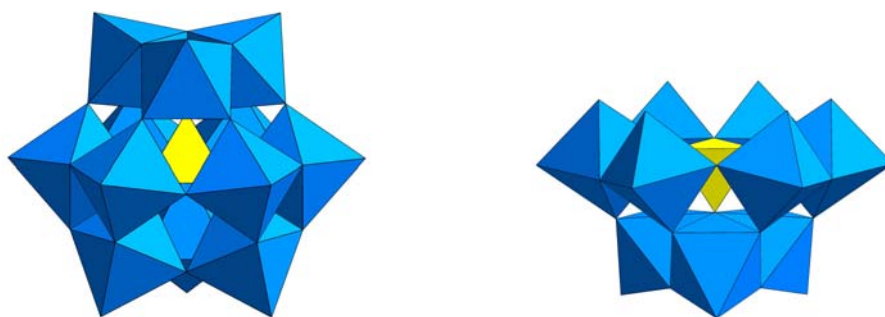


Figure 1.1: Polyhedral representation of the α -Keggin (left) ion and of the trilacunary derivative $\{\alpha\text{-A-XW}_9\}$ (right). The metal ions form the centers of the blue polyhedra and the oxygen atoms form the apexes of the polyhedra. The central heteroatom is shown as yellow polyhedra.

Lacunary derivatives of the Keggin type anions geometrically result from the removal of one or more WO groups. The two tri-vacant species correspond to the loss of a corner-shared group of $\{WO_6\}$ octahedral (A-type) or an edge-shared group (B-type) (Figure 1.1) [5, 6].

Wells-Dawson-isomers and hexalacunary structures

The Wells-Dawson anion $[P_2W_{18}O_{62}]^{6-}$ results from the direct association of two $[A-PW_9O_{34}]^{9-}$ units. The structure has two types of tungsten atoms, six "polar" and twelve "equatorial" (Figure 1.2). Six isomers of this anion are theoretically possible depending upon whether the half-units are derived from α or β -Keggin species and also whether the fragments combined in a staggered (S) or eclipsed (E) fashion [8]. Four of these isomers have been observed for $[As_2W_{18}O_{62}]^{6-}$ and three for $[P_2W_{18}O_{62}]^{6-}$ [9].

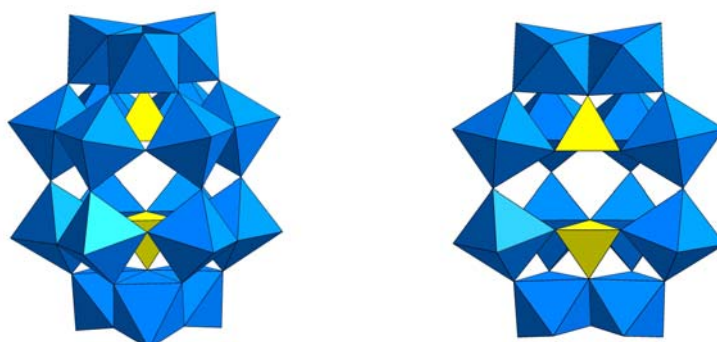


Figure 1.2: Polyhedral representation of the α -Dawson (left) ion and of the hexavacant derivative $\{\alpha\text{-}A\text{-}P_2W_{12}\}$ (right). The metal ions form the centers of the blue polyhedra and the oxygen atoms form the apexes of the polyhedra. The central heteroatom is shown as yellow polyhedra.

As in the case of the Keggin ion, lacunary derivatives of the Well-Dawson structure are also known. The most important of these are based on the most common isomer known as the α -Dawson anion. Lacunary derivatives of the α -Dawson anion include a metastable hexavacant species $\{P_2W_{12}\}$ (Figure 1.2) [10]. A well known polyoxoanion which can be described as a derivative of the $\{P_2W_{12}\}$ unit is the tetramer $[K_8\subset P_8W_{48}O_{184}]^{32-}$ or $\{P_8W_{48}\}$ with the cyclic

structure shown in Figure 1.3. The crystal structure of the related salt reveals that the central cavity of the anion encapsulates potassium cations [11].

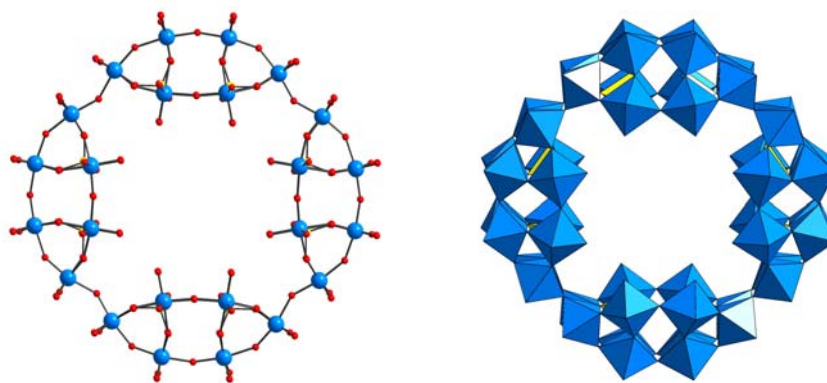


Figure 1.3: Structure of the anion $[P_8W_{48}O_{184}]^{40-}$, $\{P_8W_{48}\}$ as a cyclic assembly of four lacunary $\{P_2W_{12}\}$ groups. A ball and stick representation is shown on the left and a polyhedral representation on the right side.

1.2.2 Polyoxomolybdates

From a unique library containing molybdenum-oxide based building blocks/fragments in aqueous solution under reducing conditions a huge variety of nanoobjects, allowing specific reactions at well-defined positions, can be generated. Examples include: the molecular big-sphere of the type $\{Mo_{132}\}$, the molecular big-wheel of the type $\{Mo_{154}\}/\{Mo_{176}\}$ and in addition the by far largest structurally well characterized cluster $\{Mo_{368}\}$ with the shape of a lemon.

Specifically speaking the reasons for such a versatile behavior of polyoxomolybdates are:

1. The easy change of coordination numbers as well as easy exchange of H_2O ligands at Mo sites.
2. The moderate strength of Mo-O-Mo type bonds allowing "split and link" type processes.
3. The easy change and especially increase of electron densities without the strong tendency to form metal-metal bonds.
4. The presence of terminal Mo = O groups preventing in principle unlimited growth to extended structure [12].

The giant spherical polyoxomolybdates

If we intend to construct a giant species similar in shape to the spherical viruses with icosahedral symmetry (containing C_5 , C_3 and C_2 axes), we have to find a reaction system in which pentagonal units can first be generated, then get linked and be placed at the 12 corners of an icosahedron. Reaction mixture of molybdates under appropriate pH values and reducing conditions house a potential library ideal for such constructions (Figure 1.4). In the giant spherical clusters, the pentagonal $\{(Mo)Mo_5\}$ building blocks, each of which consists of a central pentagonal bipyramidal $\{MoO_7\}$ unit sharing edges with five $\{MoO_6\}$ octahedra, are placed at the 12 vertices of an icosahedron and linked by a set of 30 mono- or dinuclear spacers/linkers, such as $\{Fe^{III}(H_2O)\}^{3+}$ [13], $\{Mo^V O(H_2O)\}^{3+}$ [14], $\{V^{IV} O(H_2O)\}^{2+}$ [15] or $\{Mo^V_2O_4(ligand)\}^{n+}$ (e.g. ligand = $HCOO^-$, CH_3COO^- , SO_4^{2-} , $H_2PO_2^-$, PO_4^{3-}), respectively [16, 17]. In this context it is worthwhile to mention that the linkers span (distorted) Archimedean solids with approximately icosahedral symmetry: in the case of dinuclear metal linkers a (distorted) truncated icosahedron, $\{M_2\}_{30}$ and in the case of mononuclear linkers the unique icosidodecahedron $\{M_{30}\}$ (Figure 1.5).

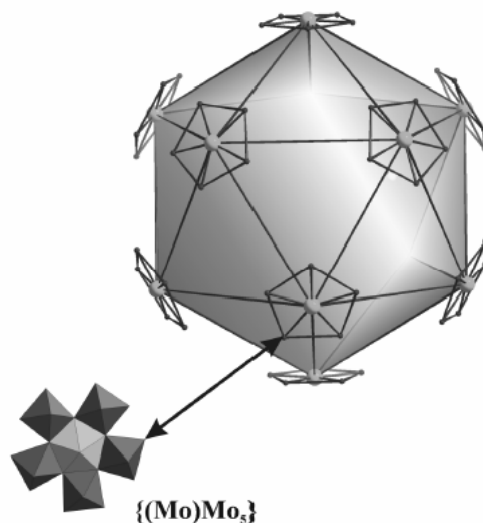


Figure 1.4: Construction principle for a cluster with icosahedral symmetry. The $[(Mo)Mo_5]$ units (polyhedral model with central pentagonal bipyramid in light grey) are the basis for the formation of the $[(pent_{12}(link)_{30})]$ type clusters, where the $[(Mo)Mo_5]$ units define the icosahedron vertices.

All such spherical clusters, which can be described by the general formula $[\{(Mo)Mo_5\}_{12}\{L\}_{30}]$ or $[(pentagon)_{12}(linker)_{30}]$, belong to the family of “Keplerate” type molecules because of their similarity to Kepler's early model of the Universe, as described in his speculative opus *Mysterium Cosmographicum* [18]. A Keplerate has, accordingly to our definition, one central point - whether or not occupied by an atom - and its atoms are organized in one or more spherical shells around this central point while each set of equivalent atoms forms a Platonic or a (generalized) Archimedean solid [19].

These ideas are the base of the present work.

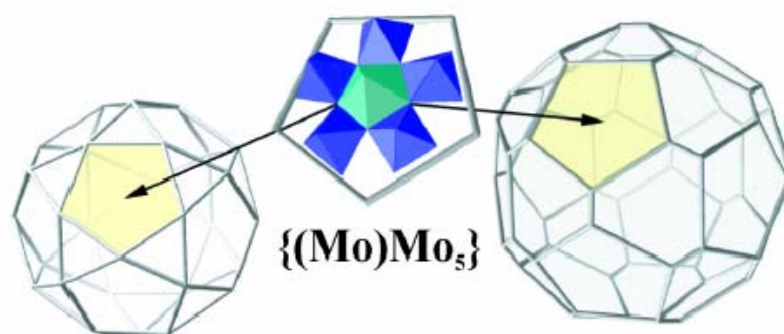


Figure 1.5: "Sizing" the nanospheres is possible. Structure only formed by the linkers: Left: the icosidodecahedron with 12 pentagons and 20 triangles formed by mononuclear linkers. Right: the (distorted) truncated icosahedron with twelve pentagons and twenty hexagons formed by 30 dinuclear $[Mo_2]$ linkers. Colour code: central pentagonal bipyramidal $[MoO_7]$ of $[(Mo)Mo_5]$ in cyan and other octahedra in blue.

The molecular big-wheels

The mentioned spherical Keplerates are results of the spherical disposition of pentagonal $\{(Mo)Mo_5\}$ building blocks with a C_5 symmetry whereas a circular disposition of the deformed $\{(Mo)Mo_5\}$ unit can lead to the formation of $\{Mo_{154}\}$ and $\{Mo_{176}\}$ type clusters, commonly known as the big-wheel and giant wheel type species, respectively [20]. Their structures can formally be represented as $[\{Mo_8\}\{Mo'_2\}\{Mo_1\}]_n$, where $n = 14$ and 16 for $\{Mo_{154}\}$ and $\{Mo_{176}\}$,

respectively. (Figure 1.6) The $\{Mo_8\}$ building block is built up by a central pentagonal $\{(Mo)Mo_5\}$ unit (containing a central $\{MoO_7\}$ or $\{MoO_6(NO)\}$ bipyramid sharing edges with five $\{MoO_6\}$ octahedral) and two more weakly bonded (sharing only corners) $\{MoO_6\}$ octahedra which can be more easily “removed”.

In addition to the $\{Mo_8\}$ unit, the wheel type polyoxomolybdates contain as mentioned above $\{Mo_2\} = \{Mo_2O_5(H_2O)_2\}^{2+}$, formed by two corner-sharing $\{MoO_6\}$ octahedra, together with $\{Mo_1\}$ type units. The cluster anions are 2x14- and 2x16-fold reduced, respectively, with the related Mo (4d) electrons trapped in 14 and 16 $\{Mo_5O_6\}$ -type “compartments”, over which they are delocalized [20]. The $\{Mo_{154}\}$ cluster has an external diameter of 3.4 nm while that of $\{Mo_{176}\}$ is 4.1 nm [21].

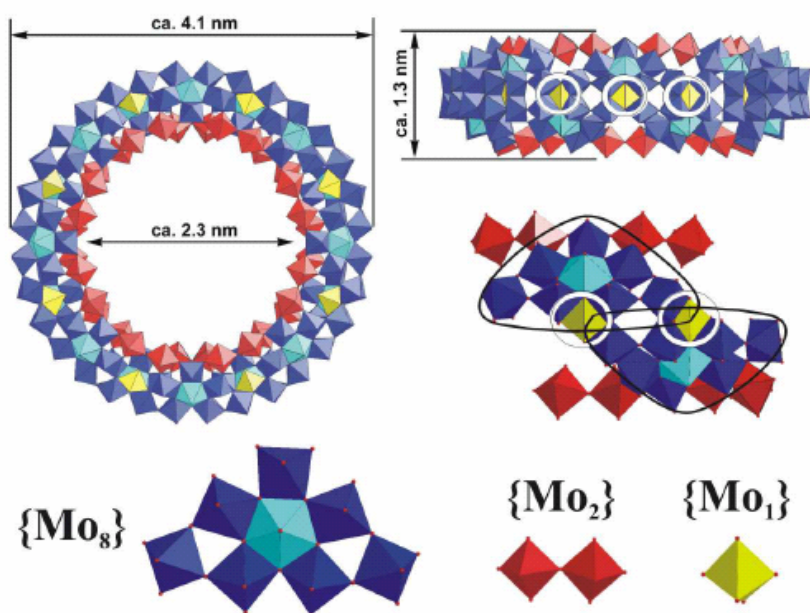


Figure 1.6: Top (left) and side (right) polyhedral views of the hexameric $\{Mo_{176}\}$ cluster. The $\{Mo_8\}$, $\{Mo_2\}$ and $\{Mo_1\}$ building blocks are shown below and the positions of $\{Mo_1\}$ units are ringed on the side view on the right side.

The "Blue Lemon"

The special building units abundant in a "dynamic library" can form, via a type of "split and/or link process" (for instance the mentioned $\{(Mo)Mo_5\}$ units from larger ones which subsequently become linked) a class of molecular architectures upon slight variation of the boundary conditions. The $\{Mo_{368}\}$ cluster [12, 22] is such a molecular type (Figure 1.7); comparable to the size of hemoglobin (external diameter ca. 6 nm), it contains 368 metal (1880 non-hydrogen) atoms formed by the linking of 64 $\{Mo_1\}$, 32 $\{Mo_2\}$, and 40 $\{(Mo)Mo_5\}$ type units (32 with sulfate ligands and 8 without) via a remarkable symmetry breaking process which is nicely recognizable at the cluster surface.

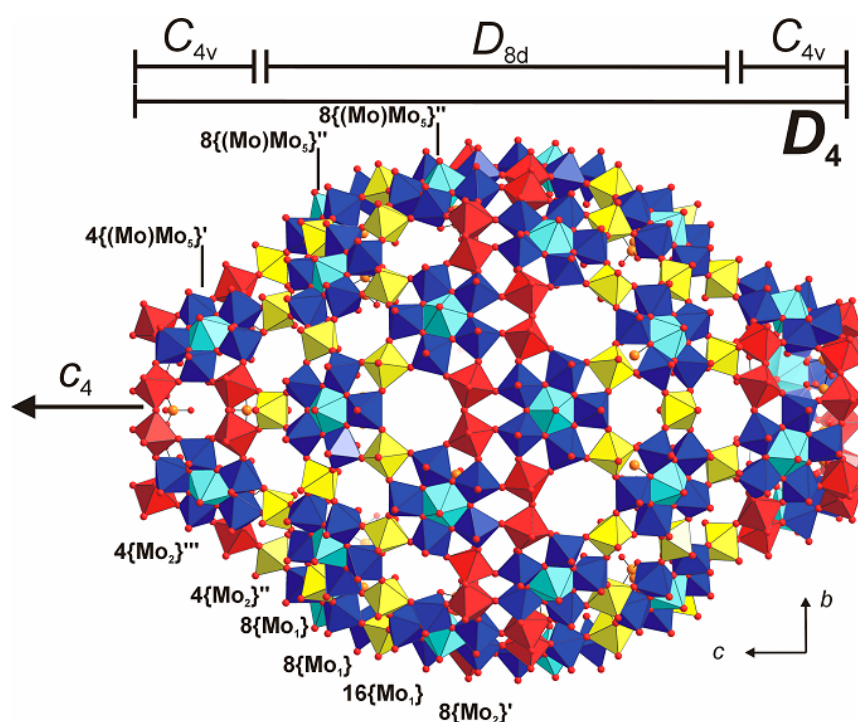


Figure 1.7: $[H_x Mo_{368} O_{1032} (H_2O)_{240} (SO_4)_{48}]^{48-}$ cluster anion in polyhedral representation showing the different building blocks and large areas of different local symmetry; building units $\{Mo_1\}$ (yellow), $\{Mo_2\}$ (red), $\{(Mo)Mo_5\}$ (blue with blue-turquoise pentagonal MoO_7 bipyramids).

In terms of building blocks the $\{Mo_{368}\}$ can be described as $[H_x\{Mo(Mo)_5\}'_8\{Mo(Mo)_5\}''_{32}\{Mo_2\}'_{16}\{Mo_2\}''_8\{Mo_2\}'''_8\{Mo_1\}_{64}]^{48-}$ (x=16) and has an approximate D_4 symmetry with a central ball-shaped fragment with D_{8d} symmetry $\{Mo_{288}\} \equiv \{Mo_{288}O_{784}(H_2O)_{192}(SO_4)_{32}\}$ and two capping fragments $\{Mo_{40}\} \equiv \{Mo_{40}O_{124}(H_2O)_{24}(SO_4)_8\}$ with C_{4v} symmetry. The structure of the cluster anion can be considered as a hybrid between the $\{Mo_{176}\}/\{Mo_{154}\}$ type giant molecular wheels and the $\{Mo_{102}\}$ type clusters.

1.3 Goals of the project: defining the problem

After describing the basic principles and highlights of polyoxometalate chemistry the aims of the research developed in the course of this thesis are as bellow:

- To explore the utility of pentagonal $\{(Mo)Mo_5\}$ -type units, available in a dynamic polyoxomolybdate library as (virtual) building blocks, in the synthesis of giant spherical clusters based on the linking of the units by paramagnetic centers.
- To study metal-oxide based nucleation processes under confined conditions within the cavity of the $\{P_8W_{48}\}$ -type cluster.

The results obtained will be described in the next sections.

Bibliography

1. A. Müller, S. Roy, *Coord. Chem. Rev.*, **2003**, *245*, 153.
2. A. Müller, P. Kögerler, H. Bögge, *Struct. Bond.*, **2000**, *96*, 203.
3. (a) D.G. Kurth, P. Lehmann, D. Volkmer, H. Cölfen, M.J. Koop, A. Müller, A. Du Chesne, *Chem. Eur. J.*, **2000**, *6*, 385; (b) D.G. Kurth, D. Volkmer, M. Ruttorf, B. Richter, A. Müller, *Chem. Mater.*, **2000**, *12*, 2829; (c) D.G. Kurth, P. Lehmann, D. Volkmer, A. Müller, D. Schwahn, *J. Chem. Soc., Dalton Trans.*, **2000**, 3989; (d) F. Caruso, D.G. Kurth, D. Volkmer, M.J. Koop, A. Müller, *Langmuir*, **1998**, *14*, 3462; (e) D. Volkmer, A. Du Chesne, D.G. Kurth, H. Schnablegger, P. Lehmann, M.J. Koop, A. Müller, *J. Am. Chem. Soc.*, **2000**, *122*, 1995; (f) S. Polarz, B. Smarsly, C. Göltner, M. Antonietti, *Adv. Mater.*, **2000**, *12*, 1503; (g) S. Polarz, B. Smarsly, M. Antonietti, *ChemPhysChem.*, **2001**, *2*, 457; (h) L. An, J.M. Owens, L.E. McNeil, J. Liu, *J. Am. Chem. Soc.*, **2002**, *124*, 13688.
4. (a) A. Müller, E. Diemann, C. Kuhlmann, W. Eimer, C. Serain, T. Tak, A. Knöchel, P.K. Pranzas, *Chem. Commun.*, **2001**, 1928; (b) T. Liu, *J. Am. Chem. Soc.*, **2002**, *124*, 10942; *ibid* **2003**, *125*, 312; (c) See also: T. Liu, E. Diemann, H. Li, A. Dress, A. Müller, *Nature*, **2003**, *426*, 59.
5. A. Müller, F. Peters, M. T. Pope and D. Gatteschi, *Chem. Rev.*, **1998**, *98*, 239.
6. M. T. Pope and A. Müller, *Angew. Chem., Int. Ed.*, **1991**, *30*, 34.
7. M. T. Pope, *Heteropoly and Isopoly Oxometalates*, Springer, Berlin, **1983**.
8. L. C. W. Baker, J. S. Figgis, *J. Am. Chem. Soc.*, **1970**, *92*, 3794.
9. R. Contant, R. Thouvenot, *Inorg. Chim. Acta*, **1993**, *212*, 41.
10. R. Contant, J. P. Ciabrini, *J. Chem. Res (M)*, **1977**, *222*, 2601.
11. R. Contant, A. Tézé, *Inorg. Chem.*, **1985**, *24*, 4610.
12. A. Müller, E. Beckmann, H. Bögge, M. Schmidtmann, A. Dress, *Angew. Chem. Int. Ed.*, **2002**, *41*, 1162.

13. A. Müller, S. Sarkar, S. Q. N. Shah, H. Bögge, M. Schmidtman, P. Kögerler, B. Hauptfleisch, A. X. Trautwein, V. Schünemann, *Angew. Chem. Int. Ed. Engl.*, **1999**, *38*, 3238.
14. A. Müller, S. Q. N. Shah, H. Bögge, M. Schmidtman, P. Kögerler, B. Hauptfleisch, S. Leiding, K. Wittler, *Angew. Chem. Int. Ed. Engl.*, **2000**, *39*, 1614.
15. A. Müller, B. Botar, H. Bögge, P. Kögerler, A. Berkle, *Chem. Commun.*, **2002**, 2944.
16. A. Müller, P. Kögerler, C. Kuhlmann, *Chem. Commun.*, **1999**, 1347.
17. A. Müller, E. Krickemeyer, H. Bögge, M. Schmidtman, F. Peters, *Angew. Chem., Int. Ed. Engl.*, **1998**, *37*, 3360.
18. (a) J. Kepler, *Mysterium Cosmographicum* **1956**; see also (b) M. Kemp, *Nature* **1998**, *393*, 123.
19. A. Müller, *Nature*, **2007**, *447*, 1035.
20. A. Müller, C. Serain, *Acc. Chem. Res.*, **2000**, *33*, 2.
21. A. Müller, M. Koop, H. Bögge, M. Schmidtman, C. Beugholt, *Chem. Commun.* **1998**, 1501.
22. A. Müller, B. Botar, S. K. Das, H. Bögge, M. Schmidtman, A. Merca, *Polyhedron*, **2004**, *23*, 2381.

Chapter 2

Publications

2.1. Triangular Geometrical and Magnetic Motifs Uniquely Linked on a Spherical Capsule Surface

A. Müller, A. M. Todea, J. van Slageren, M. Dressel, H. Bögge, M. Schmidtman, M. Luban, L. Engelhardt, M. Rusu
Angew. Chem., **2005**, *117*, 3925-3929

Contribution of A. M. Todea to the publication:

- Synthesis and characterization (electronic absorption as well as vibrational spectra, redox titrations, elemental analysis) of the new compound.

2.2. Formation of a "less stable" polyanion directed and protected by electrophilic internal surface functionalities of a capsule in growth: [$\{Mo_6O_{19}\}^{2-} \subset \{Mo^{VI}_{72}Fe^{III}_{30}O_{252}(ac)_{20}(H_2O)_{92}\}^{4-}$]

A. Müller, A. M. Todea, H. Bögge, J. van Slageren, M. Dressel, A. Stammer, M. Rusu
Chem. Commun., **2006**, 3066-3068

Contribution of A. M. Todea to the publication:

- Synthesis and characterization (electronic absorption as well as vibrational spectra, elemental analysis) of the new compound.

2.3. Extending the $\{(Mo)Mo_5\}_{12}M_{30}$ Capsule Sequence: New Cr_{30} Cluster of $s = 3/2$ Metal Centres with a $\{Na(H_2O)_{12}\}$ Encapsulate
A. M. Todea, A. Merca, H. Bögge, J. van Slageren, M. Dressel, L. Engelhardt, M. Luban, T. Glaser, M. Henry, A. Müller
Angew. Chem., **2007**, *119*, 6218-6222

Contribution of A. M. Todea to the publication:

- Synthesis and characterization (electronic absorption as well as vibrational spectra, elemental analysis) of the new compound.

2.4. Unique Properties of $Mo_{72}Fe_{30}$ Cluster in Solution
A. Müller, A. M. Todea
Manuscript in preparation

Contribution of A. M. Todea to the publication:

- Synthesis and characterization (vibrational spectra) of the deuterated compound.

2.5. Metal-Oxide-Based Nucleation Process under Confined Conditions: Two Mixed-Valence V_6 -Type Aggregates Closing the W_{48} Wheel-Type Cluster Cavities

A. Müller, M. T. Pope, A. M. Todea, H. Bögge, J. van Slageren, M. Dressel, P. Gouzerh, R. Thouvenot, B. Tsukerblat, A. Bell
Angew. Chem, **2007**, *119*, 4561-4564

Contribution of A. M. Todea to the publication:

- Synthesis and characterization (electronic absorption as well as vibrational spectra, redox titrations, elemental analysis) of the new compound.

2.6. Nucleation process in the cavity of a 48-tungstophosphate wheel resulting in a 16 metal center iron-oxide nanocluster

Sib Sankar Mal, Michael H. Dickman, Ulrich Kortz, Ana Maria Todea, Alice Merca, Hartmut Bögge, Thorsten Glaser, Achim Müller, Saritha Nellutla, Narpinder Kaur, Johan van Tol, Naresh S. Dalal, Bineta Keita, Louis Nadjo
Chem. Eur. J., **2008**, *14*, 1186-1195

Contribution of A. M. Todea to the publication:

- Synthesis and characterization (electronic absorption as well as vibrational spectra, elemental analysis) of the new compound.

Triangular Geometrical and Magnetic Motifs Uniquely Linked on a Spherical Capsule Surface**

Achim Müller,* Ana Maria Todea, Joris van Slageren, Martin Dressel, Hartmut Bögge, Marc Schmidtman, Marshall Luban, Larry Engelhardt, and Mariana Rusu

Dedicated to Professor Francis Sécheresse on the occasion of his 60th birthday

Polygons can be placed on spherical surfaces such that periodical structures of a cyclic nature result, while these can be considered as discrete models for two-dimensional (extended) structures. If we wish to construct a chemical structure on a spherical capsule surface in the same way, we have to remember that 1) pentagons are the basic units for sphere constructions, as is well known, for example, from virus structures, 2) they exist, for example, in the form of $\{(Mo^{VI})Mo^{VI}_5\}$ type units, and that 3) they occur in Keplerates of the type $\{(Mo^{VI})Mo^{VI}_5\}_{12}[Linker]_{30}^{[1-5]}$ (linker can be of the mononuclear M (M = metal center) or dinuclear type M_2 ; for the definition of Keplerates, see ref. [5b]). However, until now it was not possible to synthesize a spherical capsule surface directly by the addition of linkers to the pentagonal units that are available in a dynamic library.^[1-5] It is significant that in the Keplerates the linkers describe generic Archimedean solids: in the case of dinuclear linkers M_2 a distorted truncated icosahedron, $\{M_2\}_{30}$, and in the case of mononuclear linkers the unique icosidodecahedron (Figure 1)^[6] $\{M_{30}\}$, which has—geometrically speaking—linked M_3 triangles. Surprisingly the related consequences for chemistry have not been discussed until now. In the $\{M_{30}\}$ situation, there is a

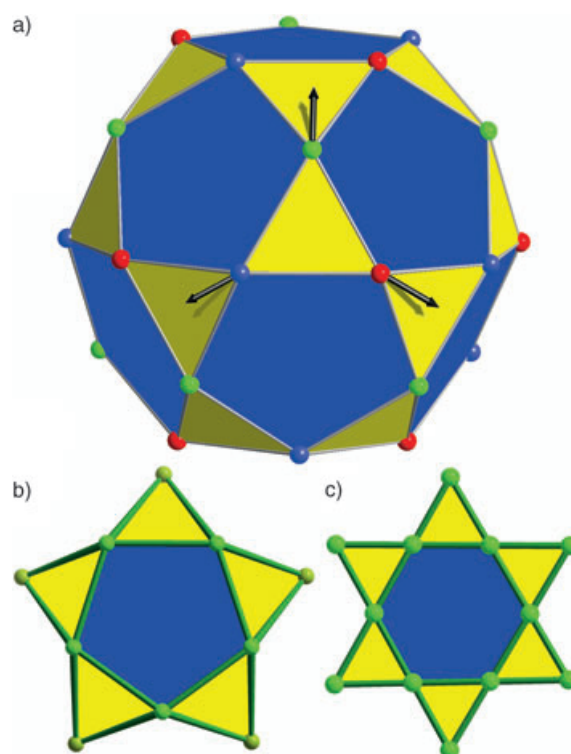


Figure 1. a) The M centers (small colored spheres) of the $\{(Mo^{VI})Mo^{VI}_5\}_{12}M_{30}$ type Keplerates (e.g., $M = V^{IV}$, Fe^{III}) describe the icosidodecahedron shown, which is unique among the icosahedral Archimedean solids as all edges are equivalent and all dihedral angles equal. Referring to the special situation of $M = Fe^{III}$, there are three groups (“sublattices”) of 10 spins (colors: red, blue, green), with all spins of a sublattice pointing in the same direction, while nearest-neighbor spin vectors (three are highlighted) differ in angular orientation by 120° . Also shown: b) A fragment highlighting five linked triangles around a pentagon. c) A fragment of a planar Kagomé lattice with six linked triangles around a hexagon.

network of corner-shared triangles on the sphere surface, this can result unique magnetic properties as in the case of the “classical” Keplerate $\{(Mo^{VI})Mo^{VI}_5\}_{12}Fe^{III}_{30}$.^[7,8] This is the first laboratory example of a “zero-dimensional” system that at low temperatures embodies characteristics of geometrical frustration/magnetic ordering^[8b] which otherwise have only been observed in selected one-, two-, and three-dimensional lattice spin systems.^[9] Herein we report on the spherical cluster **1a** where the twelve $\{(Mo^{VI})Mo^{VI}_5\}$ type units fix 30 $d^1 V^{IV}$ linkers/centers with spin $S = 1/2$ in the form of an icosidodecahedron, and thus 1) demonstrating for the first time that the spherical capsule/Keplerate can be directly constructed from the mononuclear linkers and the appropriate molybdate library,^[5c] 2) providing the chance to obtain new information regarding the unique molecular magnetism of the $\{M_{30}\}$ type network of linkers/triangles, and 3) clarifying the quantum effects of the spin $S = 1/2$ vanadyl linkers especially in connection with the two-dimensional $S = 1/2$ Kagomé lattice which contains linked triangles and exhibits unique magnetic properties.^[9a]

After adding vanadyl sulfate to an acidified molybdate solution, in the presence of K^+ ions, compound **1** precipitates after some time in high yield. (A simpler expression for the

[*] Prof. Dr. A. Müller, A. M. Todea, Dr. H. Bögge, M. Schmidtman
 Lehrstuhl für Anorganische Chemie I
 Fakultät für Chemie der Universität
 Postfach 100131, 33501 Bielefeld (Germany)
 Fax: (+49) 521-106-6003
 E-mail: a.mueller@uni-bielefeld.de

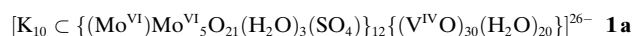
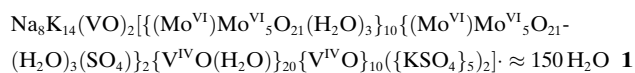
Dr. J. van Slageren, Prof. Dr. M. Dressel
 1. Physikalisches Institut
 Universität Stuttgart
 Pfaffenwaldring 57, 70550 Stuttgart (Germany)

Prof. Dr. M. Luban, L. Engelhardt
 Ames Laboratory and Department of Physics and Astronomy
 Iowa State University, Ames, Iowa 50011 (USA)

Prof. Dr. M. Rusu
 Faculty of Chemistry, Babes-Bolyai University
 3400 Cluj-Napoca (Romania)

[**] A.M., M.D., and J.v.S. gratefully acknowledge the financial support of the Deutsche Forschungsgemeinschaft, A.M. additionally the Fonds der Chemischen Industrie, the German-Israeli Foundation for Scientific Research & Development, the Volkswagenstiftung, and the European Union. M.L. thanks Dr. P. Kögerler and Prof. Dr. C. Schröder for valuable discussions. Ames Laboratory is operated for the U.S. Department of Energy by Iowa State University under Contract No. W-7405-Eng-82.

cluster anion **1a** without referring to structural differences is given as well.)



Compound **1**, which crystallizes in the monoclinic space group $C2/c$, was characterized by elemental analysis, thermogravimetry (to determine the crystal water content), redox titrations (to determine the number of V^{IV} centers), spectroscopic methods (IR, Raman, UV/Vis), single-crystal X-ray structure analysis (including bond valence sum (BVS) calculations),^[10] and susceptibility measurements (including related quantum Monte Carlo calculations).

The cluster anion **1a** of **1** is of the expected $(\text{Pentagon})_{12}(\text{Linker})_{30}$ type and is a slightly compressed sphere, while the heptacoordinate Mo^{VI} centers of the 12 pentagonal units correspondingly describe a slightly distorted icosahedron and the 30 V^{IV} centers—acting as linkers for the pentagonal $\{(\text{Mo}^{\text{VI}})\text{Mo}^{\text{VI}}_5\}$ type units—describe a (slightly distorted) icosidodecahedron (Figure 2; the $\text{V}^{\text{IV}}\text{--V}^{\text{IV}}$ distances in the distorted Archimedean solid vary from 6.3 to 6.6 Å). The distortion is in agreement with the fact that 20 V^{IV} centers in the equatorial region have octahedral coordination and the two sets of five V^{IV} centers in the polar area have square-pyramidal coordination; the distances from the 10 equatorial V^{IV} units to the center of the cluster are a little shorter (10.3 Å) than the related distances of the other 20 V^{IV} units

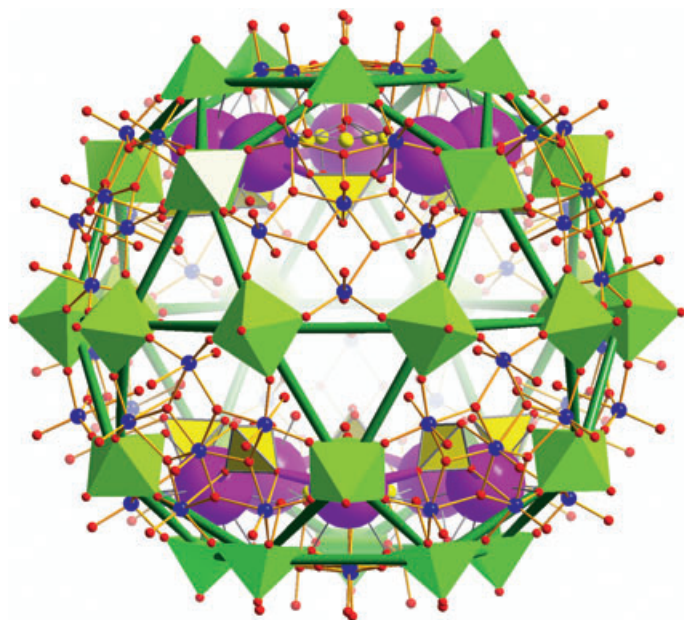


Figure 2. Combined polyhedral and ball-and-stick representation of the structure of **1a** showing the triangles and pentagons of the icosidodecahedron (green sticks), and additionally the basic $\{\text{VO}_3\}$ and $\{\text{VO}_4\}$ units as green polyhedra; as the interaction between the “lattice K^+ ” ions and the 20 pores is not homogeneous, this interaction was not considered here (blue Mo, red O, purple K, yellow tetrahedra: $\{\text{SO}_4\}$ groups; yellow spheres: disordered S atoms).

(10.6 Å). Ten of the twelve $[\text{SO}_4]^{2-}$ ligands are coordinated by three oxygen atoms to three adjacent Mo^{VI} centers of the $\{(\text{Mo}^{\text{VI}})\text{Mo}^{\text{VI}}_5\}$ groups such that two $\{\text{KSO}_4\}_5$ rings parallel to the equator result, with the K^+ ions (formally) bridging the $[\text{SO}_4]^{2-}$ ions (Figure 3). The other two sulfate groups are

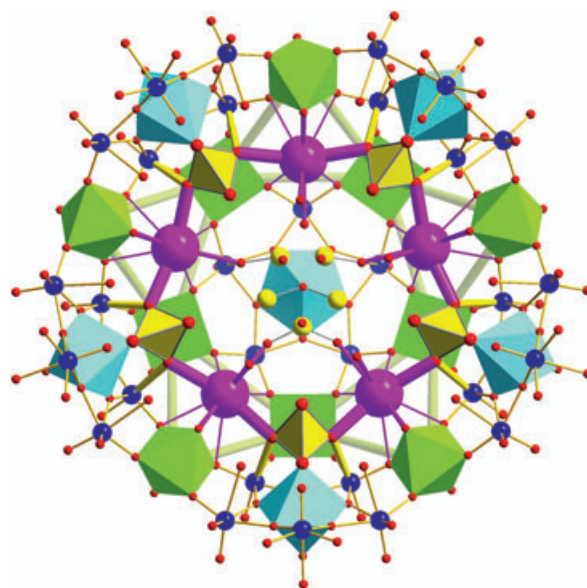
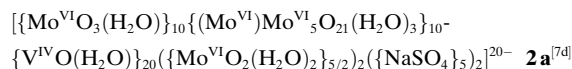


Figure 3. Combined polyhedral and ball-and-stick representation of a fragment of **1a** (view in direction of the C_2 axis) showing one of the two $\{\text{KSO}_4\}_5$ rings and the coordination of $\{\text{SO}_4\}$ groups to Mo centers as well as the disorder of one of the two sulfate groups (color code as in Figure 2, additional light blue pentagonal bipyramids: $\{\text{MoO}_7\}$).

disordered and act as ligands to the two polar $\{(\text{Mo}^{\text{VI}})\text{Mo}^{\text{VI}}_5\}$ groups. The structure of **1a** comprising the twenty triangular and twelve pentagonal faces of the icosidodecahedron built up by 30 V^{IV} centers shows an interesting relation to the much less symmetrical cluster anion **2a** which has a non-complete spherical $\{\text{V}_3\}$ type net. In **2a**, a strongly distorted icosidodecahedron is described by 10 Mo^{VI} and 20 V^{IV} centers, while the equatorial $\{\text{V}_{20}\}$ belt—formed by 10 linked $\{\text{V}_3\}$ triangles—is identical to the related equatorial segment of **1a**.



The presence of K^+ and $[\text{SO}_4]^{2-}$ ions in the reaction medium seems to be of fundamental importance for the structure formation, as the potassium cations of the two $\{\text{KSO}_4\}_5$ rings of **1a** attract the two negatively charged polar $\{(\text{Mo}^{\text{VI}})\text{Mo}^{\text{VI}}_5\}$ units thus causing the slight compression of the sphere. This distortion leads to an inclination of the adjacent $\{\text{VO}_3\}$ polyhedra and thus prevents an octahedral coordination of the 10 polar V^{IV} centers. The sixth (H_2O) ligand required for octahedral coordination would be too close to the $[\text{SO}_4]^{2-}$ ligands of the $\{\text{KSO}_4\}_5$ rings.

The investigations nicely show that $\{(\text{Mo}^{\text{VI}})\text{Mo}^{\text{VI}}_5\}$ type units are potentially available in a dynamic polymolybdate library; remarkably, they can be “used” in the present case as

virtual units in the presence of potential linkers. In aqueous solution at low pH values, the pentagonal structural unit occurs in the $[\text{Mo}^{\text{VI}}_{36}\text{O}_{112}(\text{H}_2\text{O})_{16}]^{8-}$ ion,^[11] which is the only(!) abundant species under those conditions. Correspondingly, **1a** is formed from that solution in the presence of VO^{2+} linkers by a “split-and-link” process with the $\{(\text{Mo}^{\text{VI}})\text{Mo}^{\text{VI}}_5\}$ unit being formed from the $\{\text{Mo}_{36}\}$ species after the addition of the linkers. The option to extend this to mixed-metal species such as $\{\text{Mo}^{\text{V}}_8\text{V}^{\text{IV}}_{22}\}$,^[12] $\{\text{Mo}^{\text{V}}_4\text{V}^{\text{IV}}_{26}\}$, or $\{\text{Fe}^{\text{III}}_{22}\text{V}^{\text{IV}}_8\}$ ^[13] will be reported elsewhere.

Turning to the magnetic properties, two circumstances are of pivotal importance for the possible occurrence of geometrical frustration in the type of system considered herein: First, the 30 mononuclear magnetic Keplerate linkers occupy the vertices of an icosidodecahedron, which may be pictured as 20 linked (corner sharing) triangles arranged around 12 pentagons and corresponds to an equidistant distribution of the spins on the surface of a spherical cluster; second, each magnetic center (“spin vector”) interacts with its four nearest-neighbors by isotropic antiferromagnetic exchange as a consequence of the special geometry of the unique $\{\text{M}_{30}\}$ type quasi-regular solid (Figure 1). Analogous to what occurs for the Kagomé spin system (planar lattice of triangles framed around hexagons; Figure 1c),^[9] the geometric frustration of the individual Keplerate can be achieved by the cooperative interactions among the full set of spin vectors. In the special case of the above mentioned $\{(\text{Mo}^{\text{VI}})\text{Mo}^{\text{VI}}_{512}\text{Fe}^{\text{III}}_{30}\}$, we may refer to it as a “classical” Keplerate (because of the relatively high spin, $S=5/2$, of individual Fe^{III} centers) and the spin frustration/magnetic ordering may therefore be visualized in geometrical terms^[8c] (Figure 1). The 30 spin vectors are composed of three groups (“sublattices”) of 10 spins each; all spins of a given sublattice point in the same direction, and any pair of nearest-neighbor spin vectors differ in angular orientation by 120° (Figure 1).^[8c] In **1a** we have replaced the Fe^{III} centers by VO^{2+} ions which have the much smaller spin of $S=1/2$, that is, “quantum spins”. In addition, in **1a** the 3d electrons are not “localized” at the vertices of the icosidodecahedron as is approximately the case in the $\{\text{Fe}^{\text{III}}_{30}\}$ Keplerate.^[14] However, the spin frustration of these quantum spins can not be visualized in geometric terms. More generally the magnetism of the “quantum” Keplerate **1a** is expected to be significantly different from that of its classical counterpart $\{\text{Fe}_{30}\}$, and more properties are expected to emerge.

Our experimental susceptibility data versus T , recorded for an applied field of $H=0.1$ T, and corrected for the d^1 centers of two VO^{2+} ions which are magnetically/structurally independent from the cluster skeleton **1a**, are shown in Figure 4.^[15] These results show the strong antiferromagnetic coupling in **1a**, in contrast to the $\{(\text{Mo}^{\text{VI}})\text{Mo}^{\text{VI}}_{512}\text{Fe}^{\text{III}}_{30}\}$ case.^[16] The behavior of $T\chi$ at low T is qualitatively what could be expected for a spin system having a ground state with $S=0$ and with very strong exchange coupling. This situation can be explained by a strong delocalization of the 3d electrons which arises because the 3d V levels are comparable in energy with the LUMOs of the molybdate fragment system.^[16] This is a completely different situation than the classical $\{\text{Fe}_{30}\}$ type Keplerate where the exchange interaction is very weak, and

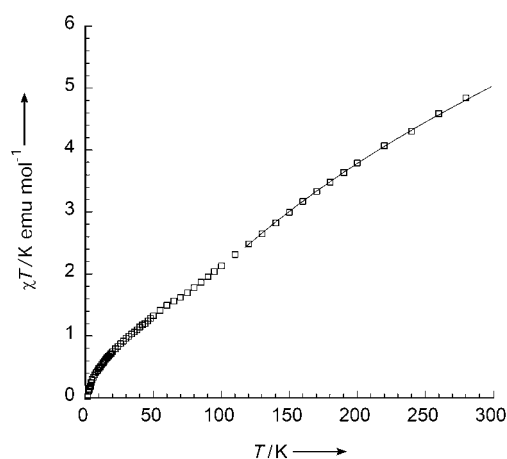


Figure 4. Magnetic susceptibility of $\{\text{V}_{30}\}$ versus temperature: Experimental data corrected for the two d^1/VO^{2+} centers (\square);^[15] quantum Monte Carlo results (solid curve).

therefore the room temperature value of $T\chi$ corresponds to 30 uncoupled $S=5/2$ ions. The quantum Monte Carlo (QMC) method provides accurate values of susceptibility for the Heisenberg model of the $\{\text{V}_{30}\}$ system for $T > 0.5J/k_B$, and as seen in Figure 4, a very good fit to $T\chi$ is achieved for $T > 120$ K for the choices $J/k_B=245$ K and $g=1.95$. Unfortunately, reliable results cannot be obtained for lower temperatures using the QMC method owing to the “sign problem” that occurs for spin systems with antiferromagnetic exchange based on lattice geometries where the classical counterpart exhibits spin frustration.

To summarize: We have demonstrated that it is possible to “use” pentagonal units as “building units” which play, geometrically speaking, the same role as the pentagonal units in other sphere-based constructions, such as spherical viruses, fullerenes, and geodesic domes; in our context they are used as a glue for trapping magnetic centers, such that triangles are linked to form an icosidodecahedron, that is, a part of a Keplerate. As the “quantum” Keplerate **1a** obtained is a new example of a frustrated magnetic system which shares a topological feature with the classical Keplerate $\{(\text{Mo}^{\text{VI}})\text{Mo}^{\text{VI}}_{512}\text{Fe}^{\text{III}}_{30}\}$ and the Kagomé-lattice antiferromagnet, its exploration is expected to provide a deeper understanding of basic aspects of magnetic frustration and the role played by the size of the intrinsic spin of the interacting magnetic ions. This study should also shed light on the parallel problem, and the focus of an intense effort, to characterize and understand the $S=1/2$ Kagomé lattice, which is considered to have unique magnetic/electronic properties originating in the small value of S .^[9] The behavior of the magnetization of the quantum Keplerate **1a** in high magnetic fields will be of key importance in studies aimed at elucidating the characteristics of its magnetic frustration.^[17]

Experimental Section

A solution of $\text{VOSO}_4 \cdot 5\text{H}_2\text{O}$ (2.53 g, 10 mmol) in H_2O (35 mL) was added to a stirred solution of $\text{Na}_2\text{MoO}_4 \cdot 2\text{H}_2\text{O}$ (2.42 g, 10 mmol) in H_2SO_4 (0.5 M; 8 mL) in a conical flask. The resulting dark purple

mixture was stirred at room temperature for 30 min (flask closed with a rubber stopper) and then treated with KCl (0.65 g, 8.72 mmol). After additional stirring for 30 min the solution was stored in the flask which was closed with a rubber stopper. After 5 days, the purple-black rhombic crystals of **1** were collected by filtration, washed with cold water, and finally dried in air. Yield: 1 g; elemental analysis: calcd (%) for $\text{Na}_8\text{K}_{24}\text{Mo}_{72}\text{V}_{32}\text{S}_{12}\text{O}_{538}\text{H}_{412}$: Na 0.96, K 4.92, V 8.55, S 2.02; found: Na 1.0, K 5.1, V 8.5, S 2.1. IR (KBr pellet): $\tilde{\nu} = 1622$ (m), ($\delta(\text{H}_2\text{O})$) 1198 (w), 1130 (w), 1055 (w) ($\nu_{\text{as}}(\text{SO}_4)$ triplet), 964 (s) ($\nu(\text{V}=\text{O})/\nu(\text{Mo}=\text{O})$), 791 (vs), 631 (w), 575 (s), 449 (w) cm^{-1} ; FT-Raman (solid; $\lambda_c = 1064$ nm): $\tilde{\nu} = 941$ (w, $\nu(\text{V}=\text{O})/\nu(\text{Mo}=\text{O})$), 872 (s, $\text{A}_{1g}\text{O}_{\text{br}}$ breathing) cm^{-1} ; UV/Vis (in H_2O): $\lambda = 510$ (vs), 689 (w), 845 (w) nm.

Received: February 24, 2005

Published online: May 25, 2005

Keywords: magnetochemistry · mixed-valence compounds · molybdenum · polyoxometalates · vanadium

- [1] A. Müller, E. Beckmann, H. Bögge, M. Schmidtman, A. Dress, *Angew. Chem.* **2002**, *114*, 1210–1215; *Angew. Chem. Int. Ed.* **2002**, *41*, 1162–1167.
- [2] a) In this context we should refer first to the fact that molybdenum oxide building units—abundant as virtual ingredients in a dynamic library in aqueous solution—display a unique type of flexibility and that the units can adjust their size and shape by a type of “split-and-link process” depending on the relevant boundary conditions.^[1] (Pentagonal $\{(\text{Mo}^{\text{VI}})\text{Mo}^{\text{VI}}\}$ building blocks, for instance, occur in spherical capsules/Keplerates of the $\{\text{Pentagon}\}_{12}\{\text{Linker}\}_{30}$ type.^[1–3]) The flexibility is nicely shown by the reaction of $[\text{PMo}_{12}\text{O}_{40}]^{3-}$ with Fe^{III} leading to a fragmentation of the Keggin ion while the fragments and the Fe^{III} ions form the (present type of) spherical system $\{(\text{Mo}^{\text{VI}})\text{Mo}^{\text{VI}}\}_{12}\text{Fe}^{\text{III}}_{30}$ which has the pentagonal units and encapsulated non-decomposed Keggin ions; see b) A. Müller, S. K. Das, H. Bögge, M. Schmidtman, A. Botar, A. Patrut, *Chem. Commun.* **2001**, 657–658.
- [3] A. Müller, S. Roy, *Coord. Chem. Rev.* **2003**, *245*, 153–166.
- [4] A. Müller, S. Roy in *The Chemistry of Nanomaterials: Synthesis, Properties and Applications* (Eds.: C. N. R. Rao, A. Müller, A. K. Cheetham), Wiley-VCH, Weinheim, **2004**, pp. 452–475.
- [5] a) A. Müller, P. Kögerler, C. Kuhlmann, *Chem. Commun.* **1999**, 1347–1358; b) A. Müller, P. Kögerler, A. W. M. Dress, *Coord. Chem. Rev.* **2001**, *222*, 193–218; c) The related direct synthetic conditions, simply based on addition of the finally appearing linker to the relative medium, are reported herein for the first time. Earlier Keplerate syntheses were more complex.
- [6] The (quasi-regular) icosidodecahedron is a hybrid of the icosahedron and the dodecahedron and thus contains 20 trigonal and 12 pentagonal faces which intersect at each corner. Unlike the other related Archimedean solids, such as the $\{\text{M}_{60}\}$ -type truncated icosahedron, it comprises not only equivalent vertices but also equivalent edges and equal dihedral angles (Figure 1); see a) M. O’Keeffe, B. G. Hyde, *Crystal Structures, I. Patterns and Symmetry*, Mineralogical Society of America, Washington, DC, **1996**; b) H. S. M. Coxeter, *Introduction to Geometry*, Wiley, New York, **1989**; c) H. S. M. Coxeter, *Regular Polytopes*, 3rd ed., Dover, New York, **1973**, in which we read (p. 18): “A quasi-regular polyhedron (like the icosidodecahedron) is defined as having regular faces, while its vertex figures, though not regular, are cyclic and equiangular (i.e., inscriptible in circles and alternate-sided). It follows from this definition that the edges are all equal, say of length $2L$, that the dihedral angles are all equal, and that the faces are of two kinds, each face of one kind being entirely surrounded by faces of the other kind.”; d) A. Holden, *Shapes, Space and Symmetry*, Dover, New York, **1991**.
- [7] a) A. Müller, S. Sarkar, S. Q. N. Shah, H. Bögge, M. Schmidtman, Sh. Sarkar, P. Kögerler, B. Hauptfleisch, A. X. Trautwein, V. Schünemann, *Angew. Chem.* **1999**, *111*, 3435–3439; *Angew. Chem. Int. Ed.* **1999**, *38*, 3238–3241; b) D. Gatteschi, R. Sessoli, A. Müller, P. Kögerler in *Polyoxometalate Chemistry: From Topology via Self-Assembly to Applications* (Eds.: M. T. Pope, A. Müller), Kluwer, Dordrecht, **2001**, pp. 319–328; c) D. Gatteschi, *Europhys. News* **2003**, *34*(6), 214–216 (Magnetism Special Issue); D. Gatteschi in *Organic conductors, superconductors and magnets: from synthesis to molecular electronics* (Eds.: L. Ouahab, E. Yagubskii), Kluwer, Dordrecht, **2004**, pp. 179–196; d) see also A. Müller, M. Koop, H. Bögge, M. Schmidtman, F. Peters, P. Kögerler, *Chem. Commun.* **1999**, 1885–1886. In the related compound discrete hydrated VO^{2+} groups are also present (evidenced by ESR); these can, as usual, be easily integrated into the crystal-water lattice, which leads to a corresponding lower alkali cation concentration.
- [8] a) M. Axenovich, M. Luban, *Phys. Rev. B* **2001**, *63*, 100407; b) C. Schröder, H. Nojiri, J. Schnack, P. Hage, M. Luban, P. Kögerler, *Phys. Rev. Lett.* **2005**, *94*, 017205; c) A. Müller, M. Luban, C. Schröder, R. Modler, P. Kögerler, M. Axenovich, J. Schnack, P. Canfield, S. Bud’ko, N. Harrison, *ChemPhysChem* **2001**, *2*, 517–521.
- [9] When frustration originates purely from the geometry or topology of the lattice it is termed geometric frustration. The corresponding compounds are called geometrically frustrated antiferromagnetic materials (GFAF) and can have exotic magnetic ground states; see: a) J. Greedan, *J. Mater. Chem.* **2001**, *11*, 37–53; b) *Magnetic Systems with Competing Interactions* (Ed.: H. Diep), World Scientific, Singapore, **1994**; c) *Quantum Magnetism* (Eds.: U. Schollwöck, J. Richter, D. J. J. Farnell, R. F. Bishop), Springer, Berlin, **2004**; d) Y. Narumi, K. Katsumata, Z. Honda, J.-C. Domenge, P. Sindzingre, C. Lhuillier, Y. Shimaoka, T. C. Kobayashi, K. Kindo, *Europhys. Lett.* **2004**, *65*, 705–711.
- [10] Crystal data for **1**: $\text{H}_{412}\text{K}_{24}\text{Mo}_{72}\text{Na}_8\text{O}_{538}\text{S}_{12}\text{V}_{32}$, $M_r = 19068.10$ g mol^{-1} , monoclinic, space group $C2/c$, $a = 47.155(2)$, $b = 42.5364(18)$, $c = 26.5344(12)$ Å, $\beta = 90.2510(10)^\circ$, $V = 53222(4)$ Å³, $Z = 4$, $\rho = 2.380$ g cm^{-3} , $\mu = 2.530$ mm^{-1} , $F(000) = 36848$, crystal size = $0.30 \times 0.20 \times 0.02$ mm³. Crystals of **1** were removed from the mother liquor and immediately cooled to 183(2) K on a Bruker AXS SMART diffractometer (three circle goniometer with 1 K CCD detector, MoK_α radiation, graphite monochromator; hemisphere data collection in ω at 0.3° scan width in three runs with 606, 435, and 230 frames ($\phi = 0, 88, \text{ and } 180^\circ$) at a detector distance of 5 cm). A total of 158364 reflections ($1.50 < \theta < 26.99^\circ$) were collected of which 57718 reflections were unique ($R(\text{int}) = 0.0612$). An empirical absorption correction using equivalent reflections was performed with the program SADABS. The structure was solved with the program SHELXS-97 and refined using SHELXL-97 to $R = 0.0567$ for 40563 reflections with $I > 2\sigma(I)$, $R = 0.0916$ for all reflections; max/min residual electron density 3.456 and -2.026 e Å^{-3} . (SHELXS/L, SADABS from G. M. Sheldrick, University of Göttingen **1997**; structure graphics with DIAMOND2.1 from K. Brandenburg, *Crystal Impact GbR*, **2001**.) As usual the cations not bound to the capsule as well as the crystal water molecules could not be found completely due to disorder. As this is also the case for the $[\text{VO}(\text{H}_2\text{O})_5]^{2+}$ centers, the H_2O ligand sphere was not considered in the formula. Further details on the crystal structure investigations may be obtained from the Fachinformationszentrum Karlsruhe, 76344 Eggenstein-Leopoldshafen, Germany (fax: (+49) 7247-808-666; e-mail: crysdata@fiz-karlsruhe.de), on quoting the depository number CSD-415055.
- [11] See for example, a) P. Kögerler, A. Müller in *Polyoxometalate Molecular Science* (Eds.: J. J. Borrás-Almenar, E. Coronado, A.

- Müller, M. T. Pope), Kluwer, Dordrecht, **2003**, pp. 297–323; b) A. Müller, F. Peters, M. T. Pope, D. Gatteschi, *Chem. Rev.* **1998**, *98*, 239–271.
- [12] A. Müller, B. Botar, H. Bögge, P. Kögerler, A. Berkle, *Chem. Commun.* **2002**, 2944–2945.
- [13] A. Müller, S. K. Das, H. Bögge, M. Schmidtman, M. Dressel, J. van Slageren, unpublished results.
- [14] In spite of these expected differences, there are some important features common to the two Keplerates, such as similar characteristics of the ground state and the low-lying excitation states, which arise because of their otherwise common geometrical structure and the existence of antiferromagnetic exchange between nearest-neighbor spins. As one example, the total spin quantum number of the ground state eigenvector for the “quantum” Keplerate **1** is expected to be $S = 0$, as it is for the “classical” Keplerate $\{\text{Fe}_{30}\}$, and its direct manifestation would be in the vanishing of T_χ (proportional to $\langle S^2 \rangle$), in the low-temperature regime; χ is the zero-field susceptibility.
- [15] The raw M/H ($\equiv \chi$) data display a rapid rise on decreasing the temperature below 50 K that is very accurately simulated by a term proportional to $1/T$ (Curie behavior). This observation suggests the presence of additional non-interacting paramagnetic centers in the sample. In fact, fitting the low temperature data leads to a value of approximately $2 S = 1/2$ centers. These centers are considered to be the non-interacting VO^{2+} (d^1) ions. In large cluster systems like **1**, they can take the same place as the other diamagnetic cations, which are usually disordered in the large voids between the clusters and can therefore not be discovered by single-crystal structure analysis (see ref. [10]). On subtracting the contribution of these discrete paramagnetic centers, we obtain a corrected magnetization M' as well as the corrected susceptibility data, $T_\chi \equiv T'/H$, shown in Figure 4. The Curie behavior of the paramagnetic centers shows that they do not interact with each other and with the $\{\text{V}_{30}\}$ cluster. The possibility that the finite T_χ value at low temperatures is due to a non-zero spin ground state can be precluded. Regarding the presented T_χ curve: As always there is uncertainty as to the appropriate choices for diamagnetic and temperature-independent paramagnetism (TIP) corrections. Additionally, because of the large voids between the clusters the VO^{2+} groups need not be present stoichiometrically in the compound; correspondingly, there is a very small error limit in the given/used number of two VO^{2+} groups which influences the correction of the raw magnetic data ($(\text{VO})_{1.8}$ could, for example, correspond to $\text{K}_{14.4}$).
- [16] The exchange coupling difference between the classical and quantum Keplerates discussed herein is analogous to that of the cluster pair with 6 V^{IV} and 6 Fe^{III} centers embedded in the $\{\text{Mo}_{57}\}$ type skeleton; see D. Gatteschi, R. Sessoli, W. Plass, A. Müller, E. Krickemeyer, J. Meyer, D. Sölter, P. Adler, *Inorg. Chem.* **1996**, *35*, 1926–1934.
- [17] Note added in proof, April 27, 2005: Very recent measurements by H. Nojiri (Tohoku University) of M versus H at 0.5 K up to 27 Tesla, as well as ESR measurements at 190 GHz for several temperatures, show features which are fully consistent with our physical interpretation of a strong intracluster exchange constant and approximately two VO^{2+} ions per formula unit that are magnetically independent of the $\{\text{V}_{30}\}$ cluster. Full details will be published elsewhere.

Formation of a “less stable” polyanion directed and protected by electrophilic internal surface functionalities of a capsule in growth: $[\{\text{Mo}_6\text{O}_{19}\}^{2-} \subset \{\text{Mo}^{\text{VI}}_{72}\text{Fe}^{\text{III}}_{30}\text{O}_{252}(\text{ac})_{20}(\text{H}_2\text{O})_{92}\}]^{4-}$

Achim Müller,^{*a} Ana Maria Todea,^a Hartmut Bögge,^a Joris van Slageren,^b Martin Dressel,^b Anja Stammer^a and Mariana Rusu^c

Received (in Cambridge, UK) 6th April 2006, Accepted 23rd May 2006

First published as an Advance Article on the web 13th June 2006

DOI: 10.1039/b604977j

The spherical capsule skeleton of the host–guest system $[\{\text{Mo}_6\text{O}_{19}\}^{2-} \subset \{\text{Mo}^{\text{VI}}_{72}\text{Fe}^{\text{III}}_{30}\text{O}_{252}(\text{CH}_3\text{COO})_{20}(\text{H}_2\text{O})_{92}\}]^{4-}$ **1a**—built up by 12 $\{\text{Mo}^{\text{VI}}\text{Mo}^{\text{VI}}_5\}$ type pentagonal units linked by 30 Fe^{III} centers which span the unique icosahedral Archimedean solid, the icosidodecahedron—can now be constructed deliberately and with a simpler composition than before from an acidified aqueous molybdate solution containing the mentioned (virtual) pentagonal units; the encapsulated hexamolybdate—normally not formed in water—is built up in an unprecedented way concomitant with capsule growth, while being directed by the corresponding internal electrophilic surface functionalities.

It is well known that aesthetically beautiful spherical objects can, geometrically speaking, be constructed from pentagons according to the related building block principle known for instance from virology, architecture (geodesic domes) as well as from daily life. But the use of this principle in synthetic chemistry has not been deliberately exploited. Though it became known that pentagonal units of the type $\{\text{Mo}^{\text{VI}}\text{Mo}^{\text{VI}}_5\}$ occur in spherical capsules/Keplerates of the general formula $\{(\text{Mo})\text{Mo}_5\}_{12}\{\text{Linker}\}_{30}$ (the linker can be of a mononuclear (M) or dinuclear metal type $(\text{M}_2)^{1-4}$) it could only be proven in the particular case of $\text{M} \equiv \text{VO}^{2+}$ that the spherical capsules can be directly synthesized by the addition of linkers to the dynamic library containing (virtual) pentagonal units[†] (see also ref. 5 regarding general remarks). The related cluster type with the skeleton $\{(\text{Mo})\text{Mo}_5\}_{12}\{\text{Fe}^{\text{III}}\}_{30}$ could until now not be synthesized in a straightforward reaction and contains inside the capsule—due to the specific preparation process—complex units of the type $\{\text{Mo}_2\text{O}_{8/9}\}^{n-}$ as ligands,⁶ which complicates the structure and, in principle, the interpretation of its (magnetic) properties.

Herein we report on the synthesis of the $\{(\text{Mo})\text{Mo}_5\}_{12}\{\text{Fe}^{\text{III}}\}_{30}$ type cluster **1a** exhibiting several new features: (1) the spherical capsule/Keplerate can be directly constructed based on an appropriate molybdate library containing the above mentioned virtual pentagonal units, (2) the mentioned $\{\text{Mo}_2\text{O}_{8/9}\}^{n-}$ units⁶ are not present, and most important (3) the hexamolybdate

$[\text{Mo}_6\text{O}_{19}]^{2-}$ anion is encapsulated noncovalently bonded, a discovery which will have implications for future theoretical and synthetic work. Furthermore, it should be noted that the inorganic skeleton of **1a** is of tremendous interest because of its unique magnetic properties.^{8,9a-c}

$\text{Na}_4[\{\text{Mo}_6\text{O}_{19}\}^{2-} \subset \{\text{Mo}^{\text{VI}}_{72}\text{Fe}^{\text{III}}_{30}\text{O}_{252}(\text{CH}_3\text{COO})_{20}(\text{H}_2\text{O})_{92}\}] \cdot ca. 120 \text{ H}_2\text{O} \equiv \text{Na}_4 \cdot \mathbf{1a} \cdot ca. 120 \text{ H}_2\text{O}$ **1**

If an acidified aqueous solution of sodium molybdate which contains a rather high concentration of acetic acid is treated with iron(III) chloride, yellow crystals of **1** precipitate after some days.‡ Compound **1**, which crystallizes in the space group $R\bar{3}$, was characterized by elemental analysis (including ESCA), thermogravimetry (to determine the actual(!) crystal water content), spectroscopy (IR, Raman, UV-Vis), and single-crystal X-ray structure analysis (including bond valence sum (BVS) calculations)§ and magnetic susceptibility measurements.

The cluster anion **1a** (the anions occupy in **1** two crystallographically independent positions $\bar{1}$ and $\bar{3}$) is of the expected spherical $\{(\text{Mo})\text{Mo}_5\}_{12}\{\text{Linker}\}_{30}$ type mentioned above. Correspondingly, the heptacoordinated Mo centers of the 12 pentagonal $\{\text{Mo}^{\text{VI}}\text{Mo}^{\text{VI}}_5\}$ type units span an icosahedron, and the 30 Fe^{III} linkers, the quasi-regular icosidodecahedron (Fig. 1) which is a hybrid of the icosahedron and the dodecahedron and contains correspondingly 20 trigonal and 12 pentagonal faces⁷ (Fig. 1). The 20 acetate ligands in **1a**, some of which are disordered, are located inside the sphere and are coordinated in a bidentate fashion to the metal centers, preferentially bridging Fe and Mo sites. **1a** does not contain the $\{\text{Mo}_2\text{O}_{8/9}\}^{n-}$ type units in contrast to the former reported $\{\text{Fe}\}_{30}$ type compound.⁶

The most interesting aspect of the present work is the encapsulation of the hexamolybdate $[\text{Mo}_6\text{O}_{19}]^{2-}$ in the cavity of the capsule (Fig. 2). This polyanion cannot be obtained as other polymolybdates simply in water and is preferably formed in organic solvents, thereby crystallizing together with organic cations.¹⁰ In the present system it is stabilized/protected by the comparably large number of acetates inside the cavity of **1a**, which form a hydrophobic environment. It is important to note that negatively charged polyoxometalates cannot be encapsulated in (highly) negatively charged Keplerates/capsules like the $\{\text{Mo}_{132}\}$ cluster.³ In the present case **1a** is “approximately neutral” and the pure inorganic part/skeleton, *i.e.* without the acetate ligands, is even positively charged. (Note: a few deprotonated H_2O ligands coordinated to the Fe centers cause a small negative charge.) This allows attraction/collection of small anionic fragments with the consequence that the stepwise formation of $[\text{Mo}_6\text{O}_{19}]^{2-}$ can occur

^aFakultät für Chemie, Universität Bielefeld, Postfach 100131, D-33501 Bielefeld, Germany. E-mail: a.mueller@uni-bielefeld.de; Fax: +49 (0)521 106 6003

^b1. Physikalisches Institut, Universität Stuttgart, Pfaffenwaldring 57, D-70550 Stuttgart, Germany

^cFaculty of Chemistry, Babes-Bolyai University, 3400 Cluj-Napoca, Romania

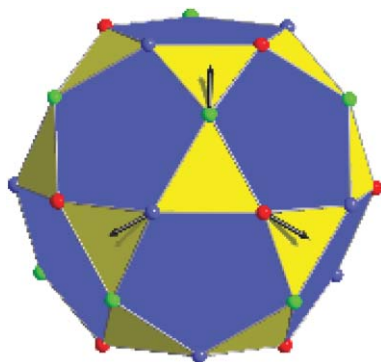


Fig. 1 The unique Archimedean solid: the Fe^{III} centers (small colored spheres) of the $\{(\text{Mo}^{\text{VI}})\text{Mo}^{\text{VI}}_5\}_{12}\{\text{Fe}^{\text{III}}\}_{30}$ type Keplerate **1a** (but also of the corresponding $\{\text{OV}^{\text{IV}}\}_{30}$ system⁴) span the shown icosidodecahedron which is unique among the Archimedean solids.[†] (Note: in the Kagomé lattice, every vertex has the same surroundings in the sense that the polygons meeting at each vertex are in sequence: pentagon (hexagon in the Kagomé case), triangle, pentagon (hexagon), triangle; see ref. 7a, p. 13.) There are three groups (“sublattices”) of 10 spins (red, blue, green, respectively), with all spins of a sublattice having parallel spin vectors, while nearest-neighbor spin vectors (three highlighted) differ in angular orientation by 120° (see text and ref. 9a).

concomitantly with the growth of the capsule skeleton, *i.e.* on its internal electrophilic surface.

With respect to the synthesis the following aspect is important: in aqueous solution, the pentagonal $\{(\text{Mo}^{\text{VI}})\text{Mo}^{\text{VI}}_5\}$ unit “occurs” relatively weakly bound in the $[\text{Mo}_{36}\text{O}_{112}(\text{H}_2\text{O})_{16}]^{8-}$ anion¹¹ (see Fig. 14a of ref. 11b), which is practically the only abundant species at low pH values and furthermore the largest isopolymolybdate to be obtained under non-reducing conditions.¹¹ Correspondingly $\{(\text{Mo})\text{Mo}_5\}_{12}\{\text{Linker}\}_{30}$ type Keplerates, which have—because of their spherical shape (minimum surface–volume ratio)—a high formation tendency, are formed from that solution in the presence of (potential) linkers like Fe^{III} ions. The reaction is based on a “split-and-link” mechanism with the $\{(\text{Mo}^{\text{VI}})\text{Mo}^{\text{VI}}_5\}$ unit being

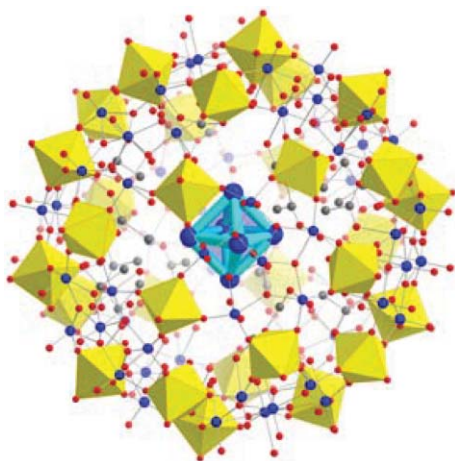


Fig. 2 Structure of **1a** emphasizing the Mo^{VI} positions of the encapsulated hexamolybdate ion within the metal oxide skeleton of the capsule **1a** (Mo blue, O red spheres) and the linkers in the form of FeO_6 octahedra (yellow).

abstracted from the $\{\text{Mo}_{36}\}$ type species.[¶] (Related results regarding mixed metal species like $\{\text{Mo}^{\text{V}}_4\text{V}^{\text{IV}}_{26}\}$, or $\{\text{Fe}^{\text{III}}_{22}\text{V}^{\text{IV}}_8\}$ ¹² will be reported later.) As pentagonal $\{(\text{Mo}^{\text{VI}})\text{Mo}^{\text{VI}}_5\}$ building blocks of the $\{\text{Pentagon}\}_{12}\{\text{Linker}\}_{30}$ type occur in spherical capsules/Keplerates also with the binuclear linkers $\{\text{Mo}^{\text{V}}_2\text{O}_4\}^{2+}$ ^{1–4} it is possible to apply also to them the synthetic principle outlined here for the mononuclear linkers.¹³

To characterize the magnetic properties of **1**, the magnetic susceptibility *versus* temperature as well as the magnetization as a function of field were measured (this had to be done in order to prove whether an influence of the $[\text{Mo}_2\text{O}_{8/9}]^{7-}$ units exists; see above). The room temperature value $\chi T = 120.1 \text{ cm}^3 \text{ K mol}^{-1}$ is slightly smaller than that expected for 30 noninteracting iron(III) ions ($\chi T = 131.3 \text{ cm}^3 \text{ K mol}^{-1}$, assuming $g = 2.00$). On lowering the temperature, the χT product decreases, reaching a value of $\chi T = 10.3 \text{ cm}^3 \text{ K mol}^{-1}$ at $T = 1.8 \text{ K}$, which is indicative of predominant antiferromagnetic exchange interactions. A Curie–Weiss plot of χ^{-1} *versus* T yields a Curie constant of $C = 128.4 \pm 0.2 \text{ cm}^3 \text{ K mol}^{-1}$ and a Weiss temperature of $\theta = -22.3 \pm 0.3 \text{ K}$. This Weiss temperature is virtually identical to that found for the earlier $\{\text{Mo}_7_2\text{Fe}_{30}\}$ cluster,^{9a} which shows that the magnetic properties of the cluster have not been affected by the changed synthetic procedure. This is confirmed by the magnetization curve which is virtually linear as a function of field. The numerical derivative shows the typical minimum at about 5.5 T, which was shown to be due to competing spin configurations.^{9b} Also the low-temperature field-dependence of the magnetization (0–24 Tesla, 0.42 K) of **1** is identical to that of the previously described $\{\text{Mo}_7_2\text{Fe}_{30}\}$ ^{9a,b} (see Acknowledgements).

It has been demonstrated that it is possible to “use” pentagonal “building units” which play, geometrically speaking, in spherical molecules the same role as in spherical constructions in general. In the present context they can be used as a glue for trapping 30 magnetic centers M (*e.g.* $M = \text{V}^{\text{IV}}\text{O}^{2+}$, Fe^{III}) to form the icosidodecahedron $\{M\}_{30}$. As the resulting frustrated magnetic systems share topological features with the highly celebrated Kagomé lattice¹⁴ (see Fig. 1) these types of studies are expected to provide a deeper understanding of basic aspects of geometrical/magnetic frustration and the related role of the spin sizes of the metal centers.^{4a,14} Correspondingly, the method will be extended by us to other magnetic centers in the future, too. The most important aspect of the work refers to the possibility to encapsulate quantum dots like polyoxometalates existing with different electron distributions in host systems. In this context it is important to note that there seems to be a general tendency for practically neutral spherical molybdenum oxide based capsules—but positively charged without the organic ligands—to have a high affinity for the (integration of) polyoxomolybdates.¹⁵ Interestingly, metal oxide cluster encapsulation is also possible in virus cavities (see: Viral Cage Directed Synthesis of Nanoclusters, chapter 10.9, p. 482 in ref. 16).

We thank Prof. H. Nojiri, Prof. M. Luban and Dr P. Kögerler for the high-field magnetization measurement and its interpretation. A.M., M.D. and J.v.S. gratefully acknowledge the financial support of the Deutsche Forschungsgemeinschaft, and A.M. additionally the Fonds der Chemischen Industrie, the German-Israeli Foundation for Scientific Research & Development (GIF), the Volkswagenstiftung as well as the European Union.

Notes and references

† In this context it is worthwhile to mention that different linkers in the Keplerates with approximately icosahedral symmetry span (distorted) Archimedean solids:^{3b,6} in the case of dinuclear metal linkers (a distorted) truncated icosahedron, $\{M_2\}_{30}$, and in the case of mononuclear linkers the unique icosidodecahedron $\{M\}_{30}$ with a highly “isotropic” surface (of importance for the magnetic behavior) due to the fact that all edges and dihedral angles are equal⁷ (Fig. 1). In the $\{M\}_{30}$ situation, a network of corner-shared triangles exists on the sphere surface (Fig. 1), which can cause in special spin situations like in the $\{Fe^{III}\}_{30}$ case a unique magnetic frustration.^{8,9a-c} These $\{Fe^{III}\}_{30}$ type clusters show furthermore a novel type of assembly process in solution.

‡ *Synthesis of 1*: $Na_4\{Mo_6O_{19}\}C\{Mo^{VI}_7Fe^{III}_{30}O_{252}(CH_3COO)_{20}(H_2O)_{92}\} \cdot ca. 120 H_2O \equiv Na_4 \cdot 1a \cdot ca. 120 H_2O$. 0.5 g $FeCl_3 \cdot 6H_2O$ (1.85 mmol) were added to a solution of 3.0 g $Na_2MoO_4 \cdot 2H_2O$ (12.4 mmol) in a mixture of 25 mL H_2O and 15 mL CH_3COOH 100%. After acidification with 12.5 mL 1 M hydrochloric acid the solution (pH \approx 2) was heated to 90–95 °C, stirred briefly and cooled to room temperature while after 6 h the yellow microcrystalline precipitate was filtered off. The yellow crystals of the pure compound precipitated from the filtrate after 5 days, were filtered off, washed with cold water and dried in air. Yield: 0.24 g (22% based on Fe). (The microcrystalline precipitate has approximately the same IR and Raman spectra but is much less soluble; it should contain the $\{Mo_7Fe_3\}$ type capsules linked in a non-ordered way, furthermore with different amounts of acetate ligands and without the hexamolybdate guest.)

Elemental analysis (%) calc.: Mo 40.26, C 2.58, H 2.62, Na 0.48%. Found: Mo 39.0, C 2.6, H 2.8, Na 0.5%. (The (not given) ESCA data obtained from Prof. M. Neumann (Osnabrück) correspond to the theoretical Mo to Fe ratio. There is a small error limit with respect to the charge/number of acetates.)

Characteristic IR bands: $\nu_{cm^{-1}}$ (KBr pellet): 1622m ($\delta(H_2O)$), 1541m ($\nu_{as}(COO)$), 1421w ($\nu_s(COO)$), 955m ($\nu(Mo=O)$), 854m, 778s, 627m, 573s, 445m.

Characteristic Raman bands: $\nu_{cm^{-1}}$ (solid state, KBr dilution, $\lambda_e = 1064$ nm): 950s, 908w ($\nu(Mo=O)$), 838s, 518m, 451w, 370m, 238 w-m.

§ *Crystal data for 1*: $C_{40}H_{484}Fe_{30}Mo_78Na_4O_{523}$, $M = 18587.05$ g mol⁻¹, rhombohedral, space group $R\bar{3}$, $a = 54.607(2)$, $c = 60.034(3)$ Å, $V = 155033(10)$ Å³, $Z = 12$, $\rho = 2.389$ g cm⁻³, $\mu = 2.763$ mm⁻¹, $F(000) = 108096$, crystal size = $0.25 \times 0.25 \times 0.20$ mm. Crystals of **1** were removed from the mother liquor and immediately cooled to 188(2) K on a Bruker AXS SMART diffractometer (three circle goniometer with 1 K CCD detector, Mo-K α radiation, graphite monochromator; hemisphere data collection in ω at 0.3° scan width in three runs with 606, 435 and 230 frames ($\phi = 0, 88$ and 180°) at a detector distance of 5.00 cm). A total of 173057 reflections ($1.59 < \theta < 22.49^\circ$) were collected of which 43683 reflections were unique ($R(int) = 0.0795$). An empirical absorption correction using equivalent reflections was performed with the program SADABS-2.10. The structure was solved with the program SHELXS-97 and refined using SHELXL-97 to $R = 0.0975$ for 23116 reflections with $I > 2\sigma(I)$, $R = 0.1851$ for all reflections; max./min. residual electron density 1.29 and -0.85 e Å⁻³ (SHELXS/L, SADABS from G. M. Sheldrick, University of Göttingen, 1997, 2003; structure graphics with DIAMOND 2.1 from K. Brandenburg, Crystal Impact GbR, 2001). CCDC 298078. For crystallographic data in CIF or other electronic format see DOI: 10.1039/b604977j. The $\{Mo_6\}$ type clusters are disordered over six positions while the sum of the occupancy factors for each Mo atom is, as expected, one. The situation is the same for the sites $\bar{1}$ and $\bar{3}$.

¶ Generally speaking, molybdenum oxide based building units—present as virtual ingredients in a dynamic library in aqueous solution—display a unique type of flexibility and can adjust their size and shape depending on the boundary conditions. This flexibility is especially nicely proven by the reaction of a solution of $[PMo_{12}O_{40}]^{3-}$ with Fe^{III} leading primarily to a fragmentation of the Keggin ions while the formed fragments and the Fe^{III} ions build up the spherical system $\{(Mo^{VI})_5(Mo^{VI})_3\}_{12}\{Fe^{III}\}_{30}$ with a non-decomposed Keggin ion encapsulated (A. Müller, S. K. Das, H. Bögge, M. Schmidtman, A. Botar and A. Patrut, *Chem. Commun.*, 2001, 657). This means in that case the intact rather stable Keggin ion is an educt, in contrast to the present investigation where the hexamolybdate is a “reaction product” (the formation of which again proves the flexibility of

the system). In the former case the number of acetate ligands inside the cavity is smaller than in **1a**, because the Keggin ion is larger than the hexamolybdate.

- (a) L. Cronin, in *Comprehensive Coordination Chemistry II*, ed. J. A. McCleverty and T. J. Meyer, Elsevier, Amsterdam, 2004, Vol. 7, pp. 1–56; (b) A. Müller and S. Roy, *Coord. Chem. Rev.*, 2003, **245**, 153; (c) N. Hall, *Chem. Commun.*, 2003, 803.
- A. Müller and S. Roy, in *The Chemistry of Nanomaterials: Synthesis, Properties and Applications*, ed. C. N. R. Rao, A. Müller and A. K. Cheetham, Wiley-VCH, Weinheim, 2004, Vol. II, pp. 452–475.
- (a) A. Müller, P. Kögerler and C. Kuhlmann, *Chem. Commun.*, 1999, 1347; (b) A. Müller, P. Kögerler and A. W. M. Dress, *Coord. Chem. Rev.*, 2001, **222**, 193.
- (a) A. Müller, A. M. Todea, J. van Slageren, M. Dressel, H. Bögge, M. Schmidtman, M. Luban, L. Engelhardt and M. Rusu, *Angew. Chem., Int. Ed.*, 2005, **44**, 3857; (b) for the synthesis of the same cluster with a different method, see: B. Botar, P. Kögerler and C. L. Hill, *Chem. Commun.*, 2005, 3138.
- A. Müller, E. Beckmann, H. Bögge, M. Schmidtman and A. Dress, *Angew. Chem., Int. Ed.*, 2002, **41**, 1162. But in this case reduced “species” are considered too, allowing further flexibility and growth.
- A. Müller, S. Sarkar, S. Q. N. Shah, H. Bögge, M. Schmidtman, Sh. Sarkar, P. Kögerler, B. Hauptfleisch, A. X. Trautwein and V. Schünemann, *Angew. Chem., Int. Ed.*, 1999, **38**, 3238.
- (a) M. O’Keeffe and B. G. Hyde, *Crystal Structures, I. Patterns and Symmetry*, Mineralogical Society of America, Washington, D.C., 1996; (b) H. S. M. Coxeter, *Introduction to Geometry*, Wiley, New York, 2nd edn, 1989; (c) H. S. M. Coxeter, *Regular Polytopes*, Dover, New York, 3rd edn, 1973.
- (a) D. Gatteschi, R. Sessoli, A. Müller and P. Kögerler, in *Polyoxometalate Chemistry: From Topology via Self-Assembly to Applications*, ed. M. T. Pope and A. Müller, Kluwer, Dordrecht, 2001, pp. 319–328; (b) D. Gatteschi, *Europhys. News*, 2003, **34**, 6 (Magnetism Special Issue), 214; (c) D. Gatteschi, in *Organic conductors, superconductors and magnets: from synthesis to molecular electronics*, ed. L. Ouahab and E. Yagubskii, Kluwer, Dordrecht, 2004, pp. 179–196; (d) D. Gatteschi, R. Sessoli and J. Villain, *Molecular Nanomagnets*, Oxford University Press, Oxford, 2006.
- (a) A. Müller, M. Luban, C. Schröder, R. Modler, P. Kögerler, M. Axenovich, J. Schnack, P. Canfield, S. Bud’ko and N. Harrison, *ChemPhysChem*, 2001, **2**, 517; (b) C. Schröder, H. Nojiri, J. Schnack, P. Hage, M. Luban and P. Kögerler, *Phys. Rev. Lett.*, 2005, **94**, 017205, 1–4; (c) O. Cépas and T. Ziman, *Prog. Theor. Phys. Suppl.*, 2005, **159**, 280 and literature cited therein; (d) G. Liu and T. Liu, *J. Am. Chem. Soc.*, 2005, **127**, 6942 and literature cited therein.
- (a) M. T. Pope, *Heteropoly and Isopoly Oxometalates*, Springer, Berlin, 1983; (b) M. T. Pope, in *Comprehensive Coordination Chemistry*, ed. G. Wilkinson, R. D. Gillard and J. A. McCleverty, Pergamon Press, Oxford, 1987, pp. 1023–1058.
- See e.g., (a) P. Kögerler and A. Müller, in *Polyoxometalate Molecular Science*, ed. J. J. Borrás-Almenar, E. Coronado, A. Müller and M. T. Pope, Kluwer, Dordrecht, 2003, pp. 297–323 and references cited therein; (b) A. Müller, F. Peters, M. T. Pope and D. Gatteschi, *Chem. Rev.*, 1998, **98**, 239; see also B. Krebs and I. Paulat-Bösch, *Acta Crystallogr., Sect. B*, 1982, **38**, 1710.
- A. Müller, S. K. Das, H. Bögge, M. Schmidtman, M. Dressel and J. van Slageren, unpublished work; see also B. Botar, P. Kögerler, A. Müller, R. Garcia-Serres and C. L. Hill, *Chem. Commun.*, 2005, 5621.
- A. Müller, *et al.*, unpublished work.
- (a) J. Greedan, *J. Mater. Chem.*, 2001, **11**, 37; (b) *Magnetic Systems with Competing Interactions*, ed. H. Diep, World Scientific, Singapore, 1994; (c) *Quantum Magnetism*, ed. U. Schollwöck, J. Richter, D. J. J. Farnell and R. F. Bishop, Springer, Berlin, 2004; (d) Y. Narumi, K. Katsumata, Z. Honda, J.-C. Domenge, P. Sindzingre, C. Lhuillier, Y. Shimaoka, T. C. Kobayashi and K. Kindo, *Europhys. Lett.*, 2004, **65**, 705.
- More details about this effect will be published in due course.
- G. A. Ozin and A. C. Arsenault, *Nanochemistry: A Chemical Approach to Nanomaterials*, Royal Society of Chemistry, Cambridge, UK, 2005.

Extending the $\{(Mo)Mo_5\}_{12}M_{30}$ Capsule Keplerate Sequence: A $\{Cr_{30}\}$ Cluster of $S = 3/2$ Metal Centers with a $\{Na(H_2O)_{12}\}$ Encapsulate**

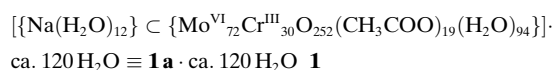
Ana Maria Todea, Alice Merca, Hartmut Bögge, Joris van Slageren, Martin Dressel, Larry Engelhardt, Marshall Luban, Thorsten Glaser, Marc Henry, and Achim Müller*

In memory of Abhilash Goplan Janardhan

In previous work it was shown that molybdenum oxide based spherical hollow clusters of the type $\{(Mo)Mo_5\}_{12}\{linker\}_{30}$ —which, because of their structural features, are also called Keplerates—can be directly synthesized by the addition of linkers, such as $V^{IV}O^{2+}$ and Fe^{III} , to a dynamic library containing (virtual) pentagonal units in solution^[1,2] (for general information see also refs. [3–5]). In the $\{linker\}_{30} = \{M_{30}\}$ situation, a network of corner-sharing triangles exists on the sphere surface,^[1,2a] and this gives rise, as in the $\{Mo_72Fe_{30}\}$ case, to a geometrically frustrated magnetic system which has received a lot of attention.^[4d–f,6] In fact, these zero-dimensional materials share topological features with the planar Kagomé lattices which also support geometrical frustration^[7] and are of interest for materials science.^[7a] The exploration of distinct yet related spin systems, which is an important aspect of the present work, is expected to provide a deeper understanding of basic aspects of geometrical frustration and especially the role played by varying the spin quantum number of the metal centers. Herein we report the synthesis (and new perspectives for the general synthetic principles leading to these types of capsules) of the spherical, hollow $\{(Mo)Mo_5\}_{12}\{Cr^{III}\}_{30}$ type cluster **1a** which contains an interesting encapsulated $\{Na(H_2O)_{12}\}$ type entity. This $\{Mo_{72}Cr_{30}\}$

cluster system exhibits, like the $\{Mo_{72}Fe_{30}\}$ and $\{Mo_{72}V_{30}\}$ systems, the unique Archimedean solid $\{M_{30}\}$ icosidodecahedron (see below and references [1a,2a]).

If an acidified aqueous solution of sodium molybdate containing a rather high concentration of acetic acid is treated with chromium(III) chloride, green crystals of **1** precipitate after some days (the basic differences to the preparation of the V_{30} and Fe_{30} systems are outlined in the Experimental Section). Compound **1**, which crystallizes in the space group $R\bar{3}$, was characterized by elemental analysis, thermogravimetry (to determine the actual water content based on the release of crystal water), spectroscopy (IR, Raman, UV/Vis), and single-crystal X-ray structure analysis.^[8a]



The cluster **1a** is of the expected spherical $\{(Mo)Mo_5\}_{12}\{Linker = Cr^{III}\}_{30}$ (Linker = Cr^{III}) type (Figure 1). Correspondingly, the heptacoordinate Mo centers of the 12 pentagonal $\{(Mo)Mo_5\}$ units describe an icosahedron, and the 30 Cr^{III} linkers the quasiregular icosidodecahedron. The latter Archimedean solid is a hybrid of the icosahedron and the dodecahedron and contains 20 triangular and 12 pentagonal faces. It comprises not only equivalent vertices but also equivalent edges and equal dihedral angles (see also refs. [1,2]). The 19 acetate ligands in **1a**, which are mainly disordered, are located inside the cavity and coordinate in a bidentate fashion to the metal centers, preferentially bridging Cr and Mo sites. In the $\{(Mo)Mo_5\}_{12}\{Cr^{III}\}_{30}$ cluster, the 30 Cr^{III} ions have their typical sixfold coordination, that is, with two bonds to the small ligands (either to two H_2O ligands or to one external H_2O and one to an internal acetate) and four bonds of the $Cr \cdots O(Mo)$ type to two pentagonal $\{(Mo)Mo_5\}$ units (Figure 1). This scenario can also be described as 30 Cr^{III} centers trapped in a matrix formed by the 12 pentagonal units/ligands. The Cr^{III} metal ions can be replaced by others, such as Fe^{III} and $V^{IV}O^{2+}$, in the typical way of coordination chemistry; this situation is of special interest for further syntheses and magnetic studies. The solution and solid-state electronic spectrum of **1** shows a band at approximately $15.6 \times 10^3 \text{ cm}^{-1}$ which arises from the presence of Cr^{III} and is assigned to the spin-allowed ${}^4A_{2g} \rightarrow {}^4T_{2g}$ transition.

One fascinating structural aspect is that a $\{Na(H_2O)_{12}\}$ cluster is encapsulated in the cavity of **1a**. The O atoms of the $\{Na(H_2O)_{12}\}$ cluster form an icosahedron, with its approximate C_5 axes coinciding with the C_5 axes of the metal oxide

[*] A. M. Todea, Dr. A. Merca, Dr. H. Bögge, Prof. Dr. T. Glaser, Prof. Dr. A. Müller
Fakultät für Chemie der Universität
Postfach 100131, 33501 Bielefeld (Germany)
Fax: (+49) 521-106-6003
E-mail: a.mueller@uni-bielefeld.de

Dr. J. van Slageren, Prof. Dr. M. Dressel
1. Physikalisches Institut
Universität Stuttgart
Pfaffenwaldring 57, 70550 Stuttgart (Germany)
L. Engelhardt, Prof. Dr. M. Luban
Ames Laboratory and
Department of Physics and Astronomy
Iowa State University, Ames, IA 50011 (USA)

Prof. Dr. M. Henry
Institut Le Bel
Université Louis Pasteur
4, Rue Blaise Pascal, 67070 Strasbourg (France)

[**] A.M., T.G., M.D., and J.v.S. gratefully acknowledge the financial support of the Deutsche Forschungsgemeinschaft, A.M. additionally the Fonds der Chemischen Industrie, the German-Israeli Foundation for Scientific Research & Development, the Volkswagenstiftung, and the European Union. Ames Laboratory is operated for the U.S. Department of Energy by Iowa State University under Contract No. W-7405-Eng-82.

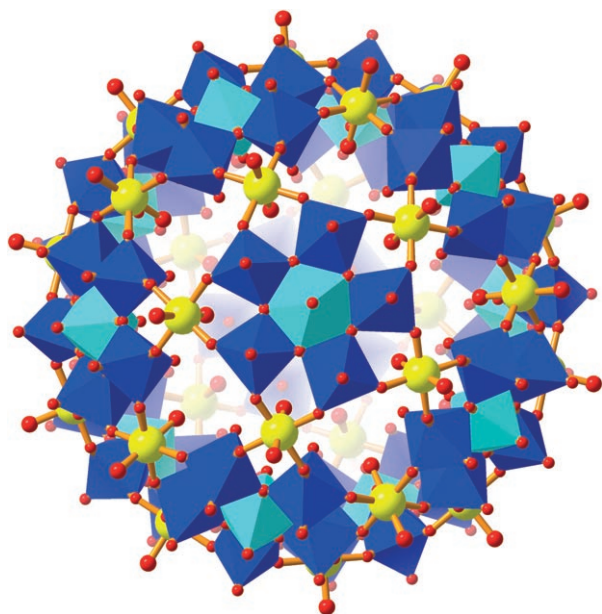


Figure 1. Structure of the spherical capsule $\{(\text{Mo})\text{Mo}_5\}_{12}\{\text{Cr}^{\text{III}}\}_{30}$ highlighting the basic pentagonal units (light and dark blue polyhedral representation; formula in text), which offer five coordination sites, and the 30 Cr^{III} linker centers (Cr yellow, O red). The Cr^{III} linker centers are in octahedral environments. Internal (disordered) acetate ligands are not shown.

based skeleton (the cluster is found not only at the $\bar{3}$ but also at the $\bar{1}$ site of the crystal lattice). The relatively small water cluster is protected by the hydrophobic shell built up by the acetate ligands and would otherwise not be formed within the cavities of the spherical capsules which have hydrophilic interiors.^[2] (Without the acetate ligands the hydrophilic groups would be expected to interact with the relatively small encapsulated water shell preventing the formation of the regular shape; in larger water aggregates, such as $\{\text{H}_2\text{O}\}_{100}$, many water molecules interact strongly with each other through hydrogen bonds, which has a stabilizing effect.^[8b]) A hydrogen-bond pattern for the icosahedral water cluster^[8c] was calculated according to a well established method^[8d] by considering electrostatic energy minimization using a combination of simulated thermal annealing and Powell's algorithms (see ref. [8e]). The result obtained corresponds to the minimum-energy structure when the coordinates of the sodium ion and of the 12 oxygen atoms are fixed (in the positions crystallographically determined at -90°C)^[8a] and all O–H bond lengths and H–O–H valence bond angles are fixed at 97 pm and 104.5° , respectively. (It is likely that other hydrogen-bond patterns of similar energy exist, which is in agreement with the comparably large vibrational ellipsoids of the O atoms.) Figure 2 shows the hydrogen-bond pattern, which can be described as a sandwich structure with two chair-shaped $\{\text{H}_2\text{O}\}_6$ rings and a sodium ion in between. The average binding energy between water molecules was found to be -59 kJ mol^{-1} , which reflects both the polarization effect by the central sodium cation and hydrogen-bonding interactions. Further details about the structure considering also the influence of the Na^+ ion will be published in a later paper.

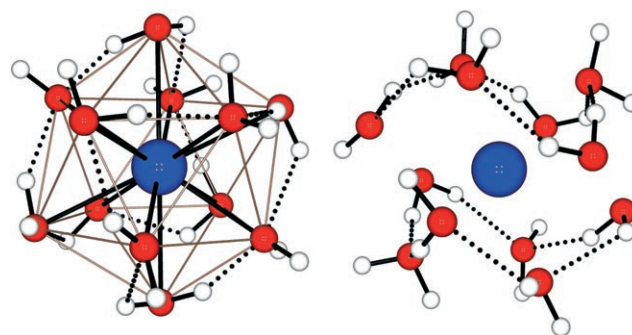


Figure 2. The $\{\text{Na}(\text{H}_2\text{O})_{12}\}$ cluster with a central Na^+ ion (blue). Left: H-bond pattern (black dots; H atoms white) and the 12 $\text{Na}\cdots\text{O}$ interactions (black) formally based on the icosahedron of 12 O atoms (red) with the 30 $\text{O}\cdots\text{O}$ edges (light brown), not referred to in right-hand picture. Right: Same H-bond pattern but shown as a sandwich structure with two chair-shaped water rings (average interatomic distances [Å] for the $\bar{3}$ site:^[8] $\text{O}\cdots\text{O}$ 2.72, $\text{Na}\cdots\text{O}$ 2.58).

Figure 3 shows the magnetic susceptibility temperature product χT and χ^{-1} as functions of temperature. The χT value is $47.17\text{ cm}^3\text{ K mol}^{-1}$ at $T=300\text{ K}$ decreasing with decreasing temperature, reaching $3.97\text{ cm}^3\text{ K mol}^{-1}$ at 1.8 K. The Curie–Weiss plot (Figure 3, bottom) is essentially a straight line above $T=100\text{ K}$, and a fit to the Curie–Weiss law yields a Curie constant of $54.8 \pm 0.1\text{ cm}^3\text{ K mol}^{-1}$ and a Weiss temperature of $\theta = -50 \pm 0.1\text{ K}$. The magnetization as a function of field at $T=1.8\text{ K}$ (not shown) increases rapidly with increasing field slowing down above $2T$, but it does not saturate. Preliminary X-band EPR measurements (not shown) show a broad line at high temperatures, which decreases on lowering the temperature and includes an evolving sharp feature. From these data the value $g = 1.966$ was obtained.

Both the decrease of the χT value with decreasing temperature and the substantial and negative Weiss temperature show that the predominant exchange interactions in **1** are antiferromagnetic which agrees with the fact that the room-temperature χT value is below that for 30 uncoupled spins $3/2$ with $g = 1.966$ ($54.35\text{ cm}^3\text{ K mol}^{-1}$). To quantify the magnetic behavior we performed quantum Monte Carlo (QMC) calculations^[9,10] of the weak-field susceptibility by adopting a Heisenberg model with isotropic exchange interaction of the form $-J \vec{S}_i \cdot \vec{S}_j$ for each pair of spins $3/2$ on nearest-neighbor sites i and j of an icosidodecahedron. The values of both J and g were optimized to fit the experimental data. The comparison between experimental and theoretical data was restricted to temperatures $T > 30\text{ K}$, because below that temperature the QMC method is not reliable for the icosidodecahedron structure owing to spin-frustration effects.^[9] The best fit was achieved for $J/k_B = -8.7 \pm 0.2\text{ K}$ and $g = 1.96 \pm 0.01$ (Figure 3, bottom). Note that also the weak upturn in χ^{-1} with decreasing T around 50 K is reproduced well by the calculations. In spite of the long superexchange pathway ($\text{Cr}^{\text{III}}\text{-O-Mo}^{\text{VI}}\text{-O-Cr}^{\text{III}}$) the interaction is quite strong. Literature values for exchange couplings along such a pathway range from about 1 K to about 21 K.^[11] The strength of the interaction is determined by the overlap of the Cr d orbitals with the empty d orbitals of the Mo^{VI} ion.

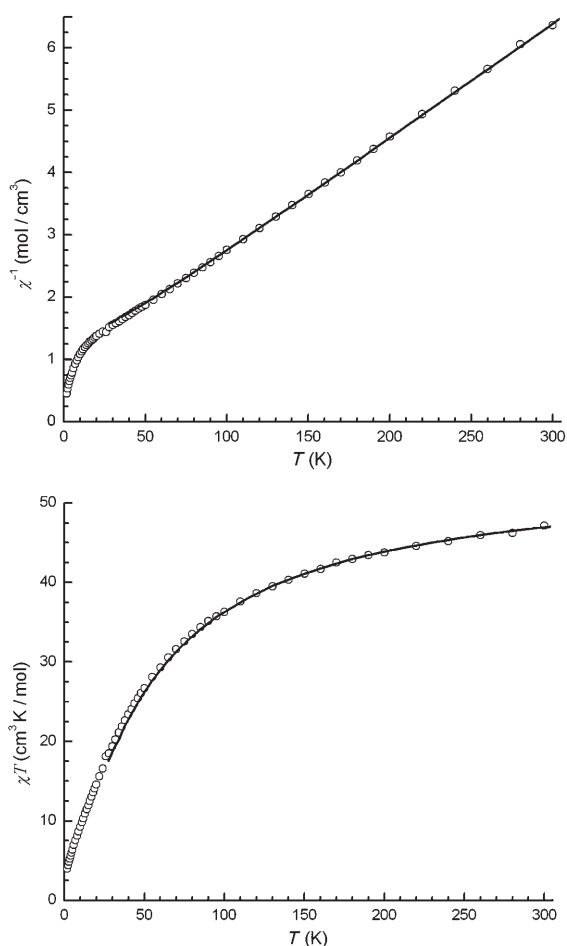


Figure 3. Experimental (symbols) χ^{-1} (top) and χT (bottom) versus temperature and quantum Monte Carlo result (continuous curve) for $J/k_B = -8.7$ K and $g = 1.96$ (see text and Experimental Section).

The moderate J value and the spin quantum number $3/2$ for the individual Cr^{III} centers makes compound **1** an interesting and experimentally convenient system for future physical, theoretical, and experimental studies and especially for the comparison of its magnetic properties with those of the corresponding Fe^{III} ^[2,3,6,12a] and V^{IV} ^[1] clusters (spins $5/2$ and $1/2$, respectively) as well as with the spin-related Kagomé systems.^[7] Of special interest is the possibility of observing a narrow minimum in the differential susceptibility dM/dH for $H \approx 20$ T (one-third of the saturation field) as has been seen in the Fe^{III} complex.^[6c] This minimum in dM/dH is associated with polytopes assembled from corner-sharing triangles and the Kagomé lattice. In addition, because of its convenient spin-state transition energies (see below), **1a** is excellently suited for experimental investigation (by inelastic neutron scattering) of the validity of the rotational band model^[6c] which has been developed for these clusters. In contrast, the V system is not suited for such investigations because of its very large exchange constant.

The three, practically isostructural, $\{(\text{Mo})\text{Mo}_5\}_{12}\{\text{M}\}_{30}$ clusters/skeletons have the sequence of spin values $S = 1/2$ ($\text{M} = \text{V}^{\text{IV}}$), $S = 3/2$ ($\text{M} = \text{Cr}^{\text{III}}$), and $S = 5/2$ ($\text{M} = \text{Fe}^{\text{III}}$) and

show quite different magnetic behavior. The capsule/Keplerate with $\text{M} = \text{Fe}^{\text{III}}$ behaves essentially classically because of the large $S = 5/2$ spin centered at 30 different corners of the icosidodecahedron and the weak superexchange interaction.^[12a] These factors and the weak exchange interaction are also responsible for the fact that quantum steps in the magnetization versus field have not been observed for accessible temperatures in contrast to other antiferromagnetically coupled systems. For $\text{M} = \text{V}^{\text{IV}}$, where the spin is small and delocalized, the system is called a “Quantum Keplerate”.^[1a] The electron delocalization creates a very strong spin coupling which has been shown by QMC calculations to be in the range of $J/k_B \approx -245$ K.^[1a] This spin coupling causes the excited spin states to be at very high energies, which makes, for example, spin-state crossings inaccessible in conventional laboratory magnetic fields. The spin system of **1a** is in between those of the other two compounds which results in correspondingly intermediate magnetic properties.

It should be possible to synthesize new related compounds with interesting and even new types of magnetic properties. These spherical cluster systems have other unique properties, as well. For example, the $\{\text{Fe}_{30}\}$ ^[12b] and $\{\text{Cr}_{30}\}$ clusters are “nanoacids” and show an unprecedented type of assembly processes leading to vesicles the size of which can be tuned by changing the pH value, a long-term goal in nanoscience. Future synthetic strategies will be determined by the general characteristics of the spherical clusters which can be compared with “coordination polymers” with spherical periodicity.^[13] Coordination polymers are considered as being based on metal ions and (organic) ligand building blocks assembling to infinite one-, two-, and three-dimensional networks, the properties of which depend in a characteristic way on the dimensionality.^[13] In our spherical clusters we can refer to metal–ligand interactions between the pentagonal units (the ligands) $\{(\text{Mo})\text{Mo}_5\text{O}_{21}(\text{H}_2\text{O})_6\}^{6-}$ (present in a dynamical library)^[1a] and the metal ions. These interactions are comparable to those between lacunary polyoxometalates and metal cations.^[4a]

The option of the planned syntheses of molecular spheres based on a careful selection of appropriate pentagonal ligands and metal ions with their specific coordination behavior^[14a] allows for the extension of this work to other 3d metal cations which can also lead to mixed-metal as well as mixed-valence clusters with different types of magnetic properties (see for instance ref. [14b]). The preparation of mixed-metal/mixed-valence clusters would correspond to symmetry breaking for the spherical systems which can also be brought about by choosing special cavity-internal ligands attached to the metal centers.^[1a] A spherical product is formed preferentially if the following condition is fulfilled: ligand-type pentagonal units with appropriate bonding sites are present, as are transition-metal cations which can coordinate to the pentagonal units (that is, assemble around them) maintaining the fivefold symmetry (see Figure 1). In the clusters discussed herein, the repeating unit is $\{(\text{Mo})\text{Mo}_5\text{M}_{5/2}\}$ ($\text{M} = \text{Cr}$, in the larger spherical system $\{(\text{Mo}^{\text{VI}})\text{Mo}^{\text{VI}}_{12}\{\text{Mo}^{\text{V}}_2\}_{30}$ which contains binuclear linkers the repeating unit is $\{(\text{Mo})\text{Mo}_5\text{Mo}_3\}$.^[5b] The repeating units occur 12 times in the spherical clusters corresponding to the icosahedral symmetry.

Experimental Section

CrCl₃·6H₂O (8.6 g, 32.27 mmol) was added to a solution of Na₂MoO₄·2H₂O (9.0 g, 37.2 mmol) in a H₂O (80 mL)/CH₃COOH (100%; 35 mL) mixture. After stirring for 5 min it was acidified with 1 M HCl (17 mL; resulting pH ≈ 2), and the solution was heated under reflux for 45 min. The resulting green solution was cooled to room temperature and the pale green precipitate (having a similar IR spectrum to the final product) was collected by filtration. Green crystals precipitated from the filtrate after 5 days, were collected by filtration, washed with cold water, and dried in air. Yield: 0.15 g (ca. 1% based on Cr, see also below); elemental analysis: calcd (%) for Na₁Mo₇₂Cr₃₀C₃₈O₅₁₆H₅₀₉: C 2.58, H 2.89, Na 0.13; found: C 2.6, H 2.5, Na 0.2%. (A small error for the number of Na⁺ and acetates has to be taken into account.) IR (KBr pellet): $\tilde{\nu}$ = 1622 (m, δ (H₂O)), 1547 (m, $\nu_{\text{as}}(\text{COO})$), 1423 (w, $\nu_{\text{s}}(\text{COO})$), 953 (m, $\nu(\text{Mo=O})$), 796 (s), 635 (w), 580 (s), 455 cm⁻¹ (w); FT-Raman (solid; $\lambda_{\text{c}} = 1064$ nm): $\tilde{\nu} = 948$ (w), 913 (s), $\nu(\text{Mo=O})$, 855 cm⁻¹ (s); UV/Vis (in H₂O): $\lambda = 642$ nm; UV/Vis (measured against cellulose as white standard) $\lambda = 645$ nm. Note: ratios of MoO₄²⁻:Cr³⁺ lower than 2:1 led to the formation of the Anderson type cluster [CrMo₆O₂₄H₆]³⁻[15] while a pH value higher than ca. 2.2 led to the formation of a trinuclear Cr^{III} cluster with acetate ligands.^[16] The reaction pathway leading to the V₃₀ and Fe₃₀ clusters is much simpler and the yields are higher. A major difference is that the residence time of H₂O ligands in the Cr^{III} aqua complex used as educt is very long with the consequence that a reactive cation/linker for the pentagonal units is not directly available as for example, in the Fe^{III} case.

Magnetic susceptibility and magnetization measurements were performed on a powder sample of **1** (18.52 mg) using a Quantum Design MPMS XL7 SQUID magnetometer. The data for the molar magnetic susceptibility were corrected for diamagnetic contributions using Pascal's constants (-7504×10^{-6} cm³ mol⁻¹).

Adopting a Heisenberg model of nearest-neighbor exchange interaction between spins $S=3/2$ on the sites of an icosidodecahedron, quantum Monte Carlo calculations of the susceptibility were performed using the stochastic series expansion^[17] of the partition function with directed loops.^[18] The detailed balance condition is satisfied by implementing the appropriate "directed-loop equations".^[18] The effectiveness of this technique for magnetic molecules has recently been demonstrated for antiferromagnetic Heisenberg spin rings^[10] and for a very large variety of finite quantum Heisenberg spin models.^[9] It should be noted that though the {Mo₇₂Cr₃₀} metal skeleton can be described as icosahedral (this is in fact an (excellent) approximation) the coordination of the internal water and acetate ligands destroys that symmetry to a minor extent as the metal centers (Cr...Cr: 6.32–6.45 Å) do not have the same environment. Thus the assumption of only one exchange coupling constant J is an approximation, but a very good one.

Received: February 21, 2007

Published online: July 12, 2007

Keywords: Kagomé lattice · magnetic properties · polyoxometalates · self-assembly · water cluster

- [1] a) A. Müller, A. M. Todea, J. van Slageren, M. Dressel, H. Bögge, M. Schmidtman, M. Luban, L. Engelhardt, M. Rusu, *Angew. Chem.* **2005**, *117*, 3925–3929; *Angew. Chem. Int. Ed.* **2005**, *44*, 3857–3861; b) for the synthesis of the same cluster by a different method, see: B. Botar, P. Kögerler, C. L. Hill, *Chem. Commun.* **2005**, 3138–3140.
- [2] a) A. Müller, A. M. Todea, H. Bögge, J. van Slageren, M. Dressel, A. Stammler, M. Rusu, *Chem. Commun.* **2006**, 3066–3068; b) All the present Kepleralates contain {Mo₁₂} icosahedra in addition to {Mo₃₀} icosidodecahedra (Kepleralate definition: A.

Müller, *Nature*, **2007**, *447*, 1035); a rather large number of (distorted) Platonic and Archimedean solids besides those mentioned exist in similar spherical polyoxomolybdate clusters (A. Müller, *Science*, **2003**, *300*, 749–750).

- [3] A. Müller, S. Sarkar, S. Q. N. Shah, H. Bögge, M. Schmidtman, Sh. Sarkar, P. Kögerler, B. Hauptfleisch, A. X. Trautwein, V. Schünemann, *Angew. Chem.* **1999**, *111*, 3435–3439; *Angew. Chem. Int. Ed.* **1999**, *38*, 3238–3241.
- [4] a) L. Cronin in *Comprehensive Coordination Chemistry II*, Vol. 7 (Eds.: J. A. McCleverty, T. J. Meyer), Elsevier, Amsterdam, **2004**, pp. 1–56; b) A. Müller, S. Roy, *Coord. Chem. Rev.* **2003**, *245*, 153–166; c) N. Hall, *Chem. Commun.* **2003**, 803–806; d) D. Gatteschi, R. Sessoli, J. Villain, *Molecular Nanomagnets: Mesoscopic Physics and Nanotechnology*, Oxford University Press, **2006**; e) D. Gatteschi, *Europhys. News* **2003**, *34*(6), 214–216 (Magnetism Special Issue); f) D. Gatteschi in *Organic Conductors, Superconductors and Magnets: From Synthesis to Molecular Electronics* (Eds.: L. Ouahab, E. Yagubskii), Kluwer, Dordrecht, **2004**, pp. 179–196; g) D.-L. Long, L. Cronin, *Chem. Eur. J.* **2006**, *12*, 3698–3706; h) P. Gouzerh, M. Che, *L'Actualité Chimique* June Issue, **2006**, No. 298, 9–22.
- [5] a) A. Müller, S. Roy in *The Chemistry of Nanomaterials: Synthesis, Properties and Applications*, Vol. II (Eds.: C. N. R. Rao, A. Müller, A. K. Cheetham), Wiley-VCH, Weinheim, **2004**, pp. 452–475; b) A. Müller, P. Kögerler, H. Bögge, *Struct. Bonding (Berlin)* **2000**, *96*, 203–236.
- [6] a) A. Müller, M. Luban, C. Schröder, R. Modler, P. Kögerler, M. Axenovich, J. Schnack, P. Canfield, S. Bud'ko, N. Harrison, *ChemPhysChem* **2001**, *2*, 517–521; b) M. Axenovich, M. Luban, *Phys. Rev. B* **2001**, *63*, 100407; c) C. Schröder, H. Nojiri, J. Schnack, P. Hage, M. Luban, P. Kögerler, *Phys. Rev. Lett.* **2005**, *94*, 017205; d) V. O. Garlea, S. E. Nagler, J. L. Zarestky, C. Stassis, D. Vaknin, P. Kögerler, D. F. McMorro, C. Niedermayer, D. A. Tennant, B. Lake, Y. Qiu, M. Exler, J. Schnack, M. Luban, *Phys. Rev. B* **2006**, *73*, 024414; e) J. Schnack, M. Luban, R. Modler, *Europhys. Lett.* **2001**, *56*, 863–869; f) for further magnetic properties see: A. S. Mischenko, A. S. Chernyshov, A. K. Zvezdin, *Europhys. Lett.* **2004**, *65*, 116–122; J. Schnack, M. Luban, *Phys. Rev. B* **2000**, *63*, 014418; J. Schnack, H.-J. Schmidt, J. Richter, J. Schulenburg, *Eur. Phys. J. B* **2001**, *24*, 475–481; M. Exler, J. Schnack, *Phys. Rev. B* **2003**, *67*, 094440; O. Cépas, T. Ziman, *Prog. Theor. Phys. Suppl.* **2005**, *159*, 280–291; R. Schmidt, J. Richter, J. Schnack, *J. Magn. Magn. Mater.* **2005**, *295*, 164–167; J. Schnack in *Lecture Notes in Physics*, Vol. 645, Springer, Berlin, **2004**, pp. 155–194.
- [7] a) J. E. Greedan, *J. Mater. Chem.* **2001**, *11*, 37–53; b) *Magnetic Systems with Competing Interactions* (Ed.: H. T. Diep), World Scientific, Singapore, **1994**; c) *Quantum Magnetism* (Eds.: U. Schollwöck, J. Richter, D. J. J. Farnell, R. F. Bishop), Springer, Berlin, **2004**; d) Y. Narumi, K. Katsumata, Z. Honda, J.-C. Domenge, P. Sindzingre, C. Lhuillier, Y. Shimaoka, T. C. Kobayashi, K. Kindo, *Europhys. Lett.* **2004**, *65*, 705–711.
- [8] a) Crystal data for **1**: C₃₈H₅₀₉Cr₃₀Mo₇₂NaO₅₁₆, $M_r = 17716.12$ g mol⁻¹, space group R $\bar{3}$, $a = 54.4434(14)$, $c = 59.767(2)$ Å, $V = 153420(8)$ Å³, $Z = 12$, $\rho = 2.301$ g cm⁻³, $\mu = 2.433$ mm⁻¹, $F(000) = 103440$, crystal size = $0.3 \times 0.2 \times 0.1$ mm³. A total of 196988 reflections ($1.59 < \theta < 22.49^\circ$) were collected of which 43996 reflections were unique ($R(\text{int}) = 0.1807$). An empirical absorption correction using equivalent reflections was performed with the program SADABS 2.03. The structure was solved with the program SHELXS-97 and refined using SHELXL-97 to $R = 0.1015$ for 15460 reflections with $I > 2\sigma(I)$, $R = 0.2471$ for all reflections; max./min. residual electron density 1.536 and -0.714 e Å⁻³. Crystals of **1** were removed from the mother liquor and immediately cooled to 188(2) K on a Bruker AXS SMART diffractometer (three circle goniometer with 1 K CCD detector, MoK α radiation, graphite monochromator; hemi-

sphere data collection in ω at 0.3° scan width in three runs with 606, 435, and 230 frames ($\varphi = 0, 88$ and 180°) at a detector distance of 5 cm). (SHELXS/L, SADABS from G. M. Sheldrick, University of Göttingen **1997/2001**; structure graphics with DIAMOND 2.1 from K. Brandenburg, Crystal Impact GbR, 2001). CCDC-637150 contains the supplementary crystallographic data for this paper. These data can be obtained free of charge from The Cambridge Crystallographic Data Centre via www.ccdc.cam.ac.uk/data_request/cif. The “icosahedral” water cluster appears on crystallographically independent sites $\bar{1}$ and $\bar{3}$, the distortion in the $\bar{1}$ case is more pronounced. b) See for instance M. Henry, H. Bögge, E. Diemann, A. Müller, *J. Mol. Liq.* **2005**, *118*, 155–162 and A. Müller, E. Krickemeyer, H. Bögge, M. Schmidtman, S. Roy, A. Berkle, *Angew. Chem.* **2002**, *114*, 3756–3761; *Angew. Chem. Int. Ed.* **2002**, *41*, 2805–2808. c) In the present case, a “water cluster” is encapsulated and not a polymolybdate as in ref. [2] where a higher concentration of molybdate was used in the synthesis. d) The method has been shown to be suitable to calculate the neutron diffraction crystallographic H-atom coordinates for water molecules in 13 ice polymorphs (M. Henry, *ChemPhysChem* **2002**, *3*, 607–616) as well as the X-ray diffraction crystallographic H-atom coordinates, for water molecules interacting with polyoxometalate species such as the decavanadate (M. Henry, *J. Cluster Sci.* **2002**, *13*, 437–458); the method is particularly well-suited for studying hydrogen bonding of water molecule assemblies (see for example, D. R. Turner, M. Henry, C. Wilkinson, G. J. McIntyre, S. A. Mason, A. E. Goeta, J. W. Steed, *J. Am. Chem. Soc.* **2005**, *127*, 11063–11074 where the calculation was supported by a single-crystal neutron structure analyses); e) W. H. Press, S. A. Teukolsky, W. T. Vetterling, B. P. Flannery, *Numerical Recipes in C, the Art of Scientific Computing*, 2nd ed, Cambridge University Press, Cambridge, **1992**, pp. 412–420.

- [9] L. Engelhardt, M. Luban, C. Schröder, *Phys. Rev. B* **2006**, *74*, 054413.
- [10] L. Engelhardt, M. Luban, *Phys. Rev. B* **2006**, *73*, 054430.
- [11] a) L. Xu, Z. Li, H. Liu, J. Huang, Q. Zhang, *Chem. Eur. J.* **1997**, *3*, 226–231; see also: J. Glerup, A. Hazell, K. Michelsen, H. Weihe, *Acta Chem. Scand.* **1994**, *48*, 618–627; b) J. Glerup, A. Hazell, K. Michelsen, *Acta Chem. Scand.* **1991**, *45*, 1025–1031.
- [12] a) The $S = 5/2$ (Fe^{III}) analogue of complex **1**, $\{\text{Fe}_{30}\text{Mo}_{72}\}$ has some very intriguing properties which has led to many experimental^[6a,c,d] and theoretical^[6a–f] studies. Briefly, it is well described by a simple picture of geometrical frustration whereby the $S = 0$ ground state corresponds to a spin topology of three coplanar spin sublattice vectors of length 25, each spin sublattice being associated with ten parallel $S = 5/2$ ion spins, with an angular separation of 120 degrees between the individual sublattice vectors. In the low-temperature regime, with increasing applied magnetic field, H , the three sublattice vectors cant and these may be pictured as a “uniformly folding umbrella”; the projections of the sublattice vectors in the plane normal to the external field maintain a frustration angle of 120 degrees and the magnetization grows linearly with H and ultimately saturates at a field $H_{\text{sat}} \approx 17.6$ T. Additionally, at low, nonzero temperatures the differential susceptibility $\partial M/\partial H$ versus H shows a characteristic minimum at $H_{\text{sat}}/3$ which has been explained^[6c] in terms of the competition between two spin configurations (the canted frustrated phase and a magnetically stiff configuration). Similar behavior can be expected for compound **1**, where, using our result $J/k_{\text{B}} = -8.7$ K, we estimate $H_{\text{sat}} \approx 60$ T. A drawback of the Fe^{III} analogue is that owing to the weak superexchange interaction of $J/k_{\text{B}} = -1.57$ K, the energy levels are very closely spaced, and thus the individual spin-state crossings and transitions have not been observed in experiments;^[6a,d] b) T. Liu, B. Imber, E. Diemann, G. Liu, K. Cokleski, H. Li, Z. Chen, A. Müller, *J. Am. Chem. Soc.* **2006**, *128*, 15914–15920 as well as unpublished work by the same authors.
- [13] a) R. J. Puddephatt, *Coord. Chem. Rev.* **2001**, *216–217*, 313–332; b) R. Robson, *J. Chem. Soc. Dalton Trans.* **2000**, 3735–3744 in which it was mentioned that in special cases parallels can exist between infinite arrays of coordination polymers and discrete supramolecules, as for example, Fujita’s $[\text{M}_6(\text{tpt})_4]$ (tpt corresponds to a complex triazine ligand), M. Fujita, D. Oguro, M. Miyazawa, H. Oka, K. Yamaguchi, K. Ogura, *Nature*, **1995**, *378*, 469–471. Interestingly, the pentagonal units discussed herein also occur in network structures (see refs. [22a,b] of ref. [5b]).
- [14] a) The present situation is formally comparable to the “poly-association” leading, for example, to the impressive helices of J.-M. Lehn. In both cases, polytopic ligands—either preorganized in the form of poly(bipyridine) ligand strands in the helices or existing as pentagonal units in a dynamic library in the spherical systems—interact with a larger number of directing metal cations showing the expected coordination type; in the former cases the copper (I) ions enforce the tetrahedral coordination geometry and in the latter cases the M^{III} ions the octahedral (see J.-M. Lehn, *Supramolecular Chemistry: Concepts and Perspectives*, Wiley-VCH, Weinheim, **1995**); b) B. Botar, P. Kögerler, A. Müller, R. Garcia-Serres, C. L. Hill, *Chem. Commun.* **2005**, 5621–5623; see also: A. Müller, B. Botar, H. Bögge, P. Kögerler, A. Berkle, *Chem. Commun.* **2002**, 2944–2945.
- [15] A. Perloff, *Inorg. Chem.* **1970**, *9*, 2228–2239.
- [16] R. D. Cannon, R. P. White, *Prog. Inorg. Chem.* **1988**, *36*, 195–298.
- [17] A. W. Sandvik, J. Kurkijarvi, *Phys. Rev. B* **1991**, *43*, 5950–5961.
- [18] O. F. Syljuåsen, A. W. Sandvik, *Phys. Rev. E* **2002**, *66*, 046701.

Unique Properties of $\text{Mo}_{72}\text{Fe}_{30}$ Cluster in Solution

Achim Müller, Ana Maria Todea*

Prof. Dr. A. Müller, A. M. Todea
Fakultät für Chemie der Universität
Postfach 100131, 33501 Bielefeld (Germany)
Fax: (+49)521-106-6003
E-mail: a.mueller@uni-bielefeld.de

Giant molecular spheres with the general formula $[(\text{pentagon})_{12}(\text{linker})_{30}]$ or $[\text{Mo}(\text{Mo})_5]_{12}(\text{Linker})_{30}$, due to their structural features also called Keplertes [1-3], with variable size can be generated by linking the fundamental pentagonal $\{(\text{Mo})\text{Mo}_5\}$ building block with various linkers, which can be of the dinuclear $(\{\text{Mo}^{\text{V}}_2\text{O}_4(\text{ligand})\})^{n+}$ (e.g. ligand = HCOO^- , CH_3COO^- , SO_4^{2-} , H_2PO_2^- , PO_4^{3-}) or mononuclear $(\{\text{Fe}^{\text{III}}(\text{H}_2\text{O})\}^{3+}$, $\{\text{Cr}^{\text{III}}(\text{H}_2\text{O})\}^{3+}$, $\{\text{Mo}^{\text{V}}\text{O}(\text{H}_2\text{O})\}^{3+}$, $\{\text{V}^{\text{IV}}\text{O}(\text{H}_2\text{O})\}^{2+})$ type.

Here we begin to study the replacement with D_2O of the crystal water and of the H_2O ligands attached to the Fe^{III} and Mo^{VI} centres of the cluster with the stoichiometry: $[\text{Mo}_{72}\text{Fe}_{30}\text{O}_{252}(\text{CH}_3\text{COO})_{12}[\text{Mo}_2\text{O}_7(\text{H}_2\text{O})]_2 [\text{H}_2\text{Mo}_2\text{O}_8(\text{H}_2\text{O})] (\text{H}_2\text{O})_{91}] \cdot \text{ca. } 150 \text{ H}_2\text{O}$ ($\text{Mo}_{72}\text{Fe}_{30}$), which is part this class of spherical systems. The 72 $\text{Mo}^{\text{VI}}\text{O}_n$ polyhedra are organized into twelve pentagonal $\{\text{Mo}(\text{Mo})_5\}$ type units (comprising a central MoO_7 pentagonal bipyramid linked via edges to five MoO_6 octahedra). The $\text{Mo}=\text{O}$ bonds are preferably directed outwards (ca. 80%), but according to a disorder also approximately 20% $\text{Mo}(\text{OH}_2)$ groups are directed outwards. The twelve pentagonal units are connected by 30 $\text{Fe}(\text{O})_6$ octahedra acting as linkers. Each of these linkers exposes a single terminal $\text{Fe}(\text{OH}_2)$ outwards. Inside the near-spherical capsule there are twelve additional water molecules bound to the Fe^{III} centers. The remaining 18 octahedral coordination sites on the Fe^{III} linkers are bridges to molybdate (two of $[\text{Mo}_2\text{O}_7(\text{H}_2\text{O})]$ type and one of $[\text{H}_2\text{Mo}_2\text{O}_8(\text{H}_2\text{O})]$ type) or to acetate ligands.

The $\text{Mo}_{72}\text{Fe}_{30}$ clusters exist as discrete, almost neutral molecules in aqueous solution at $\text{pH} < 2.9$, but get deprotonated and self-associate into single-layer blackberry-type structures at higher pH while the assembly process, i.e. the size of the final species can be controlled by the pH values. The average hydrodynamic radius (R_h) of the aggregates decreases monotonically with increasing number of charges on the $\text{Mo}_{72}\text{Fe}_{30}$ macroanions (from ~ 45 nm at $\text{pH} \sim 3.0$ to ~ 15 nm at $\text{pH} \sim 6.6$), as studied by laser light scattering and TEM techniques.

Standard ^{17}O -NMR investigations on 18.65mg/ml aqueous solutions of $\text{Mo}_{72}\text{Fe}_{30}$, limited to $2 < \text{pH} < 3$ because of the cluster stability as it dissociates slowly at $\text{pH} < 2$ and forms larger aggregates at $\text{pH} > 3$, showed that the rates of exchange of waters bound to the $\text{Fe}^{\text{III}}(\text{OH}_2)$ functional groups on the $\text{Mo}_{72}\text{Fe}_{30}$ cluster are $\sim 10^4$ more rapid than for the simple aqua ion, $\text{Fe}(\text{H}_2\text{O})_6^{3+}$, but slightly slower than the Fe^{III} -EDTA and its derivatives, but also that small changes in pH near the pK_a of the sites have little effect on the rates of exchange of bound waters [5].

That these molecules remain intact in the aqueous phase is well established through characteristic Raman spectrum (due to their high symmetry the free clusters exhibit only a few well-defined lines).

Two strategies were employed in order to replace the H_2O present by D_2O in the $\text{Mo}_{72}\text{Fe}_{30}$ -type cluster[‡]:

A) Recrystallization of $\text{Mo}_{72}\text{Fe}_{30}$ from heavy water

0.5 g $\text{Mo}_{72}\text{Fe}_{30}$ (prepared according to the method of Müller et al. [4]) were dissolved in 15 ml D_2O , leading to a 33.33mg/ml solution of $\text{Mo}_{72}\text{Fe}_{30}$. The solution was heated at $\sim 60^\circ\text{C}$, under argon 24h, 48h and 72h respectively. The resulting solution was cooled under 0°C and the

[‡] These investigations were done for quasi elastic neutron scattering experiments.

formed precipitate was filtered off and dried under argon. The identity of " $\text{Mo}_{72}\text{Fe}_{30}\text{-D}_2\text{O}$ ", where most of H_2O was replaced by D_2O , was established by IR.

Figures 2-4 show the IR spectra of the " $\text{Mo}_{72}\text{Fe}_{30}\text{-D}_2\text{O}$ " samples precipitated from the 33.33 mg/ml heavy water solutions after heating these solutions for 24h, 48h and 72h respectively at $\sim 60^\circ\text{C}$. In this case we can notice a decrease in the intensity of the bands at 3200 cm^{-1} and 1616 cm^{-1} and the appearance of the bands at $\sim 2200\text{ cm}^{-1}$ and $\sim 1194\text{ cm}^{-1}$ due to the replacement of H_2O by D_2O .

Stirring for 24h at 80°C leads to the decomposition of the cluster and subsequent precipitation of an "iron-polymolybdate".

- [1] A. Müller, P. Kögerler, C. Kuhlmann, *Chem. Commun.* **1999**, 1347-1358.
- [2] A. Müller, P. Kögerler, H. Bögge, *Structure and Bonding*, Berlin, **2000**, 96, 203-236
- [3] L. Cronin in *Comprehensive Coordination Chemistry II*, Vol. 7 (Eds.: J. A McCleverty, T. J. Meyer), Elsevier, Amsterdam, **2004**, pp. 1- 56.
- [4] A. Müller, S. Sarkar, S.Q.N. Shah, H. Bögge, M. Schmidtman, Sh. Sarkar, P. Kögerler, B. Hauptfleisch, A.X. Trautwein, V. Schünemann, *Angew. Chem. Int. Ed.* **1999**, 38, 3238-3241.
- [5] E. Balogh, A. M. Todea, A. Müller, W. H. Casey, *Inorg. Chem.*, **2007**, 46, 7087-7092 .

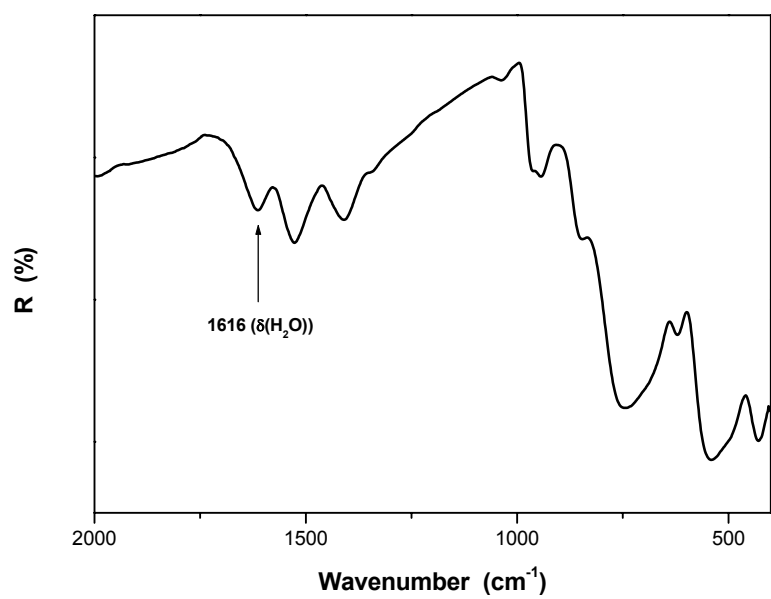
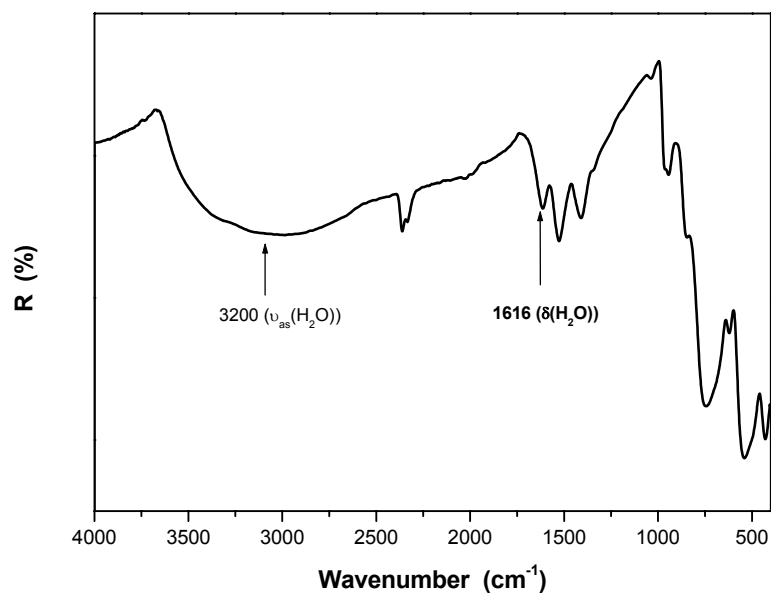


Figure 1. IR spectrum (diamond ATR) of $[\text{Mo}_{72}\text{Fe}_{30}\text{O}_{252}(\text{CH}_3\text{COO})_{12}[\text{Mo}_2\text{O}_7(\text{H}_2\text{O})]_2 [\text{H}_2\text{Mo}_2\text{O}_8(\text{H}_2\text{O})] (\text{H}_2\text{O})_{91}] \cdot \text{ca. } 150 \text{ H}_2\text{O} \equiv \text{Mo}_{72}\text{Fe}_{30}$.

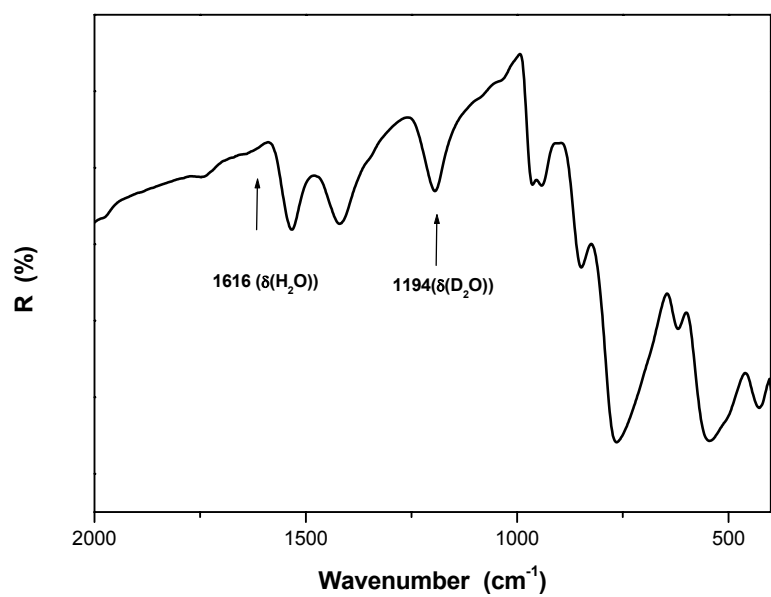
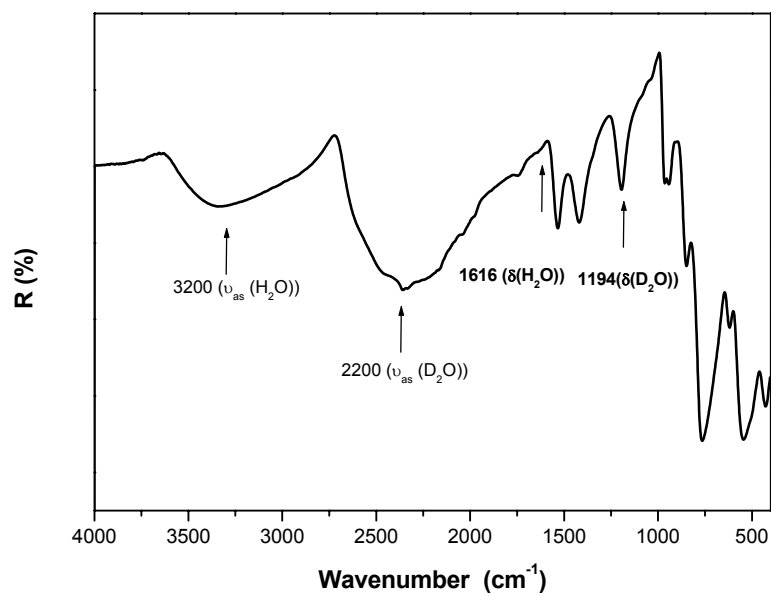


Figure 2. IR spectrum (diamond ATR) of " $\text{Mo}_{72}\text{Fe}_{30}\text{-D}_2\text{O}$ " precipitated from a heavy water solution after stirring for 24h at $\sim 60^\circ\text{C}$.

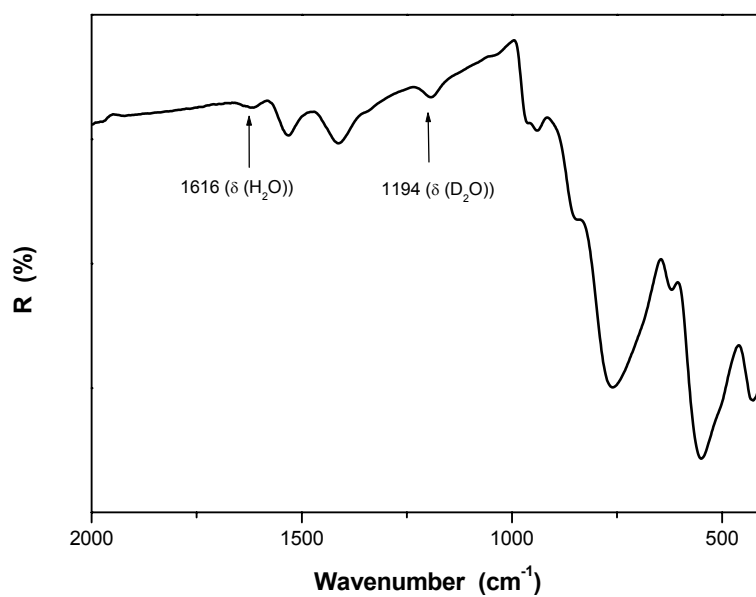
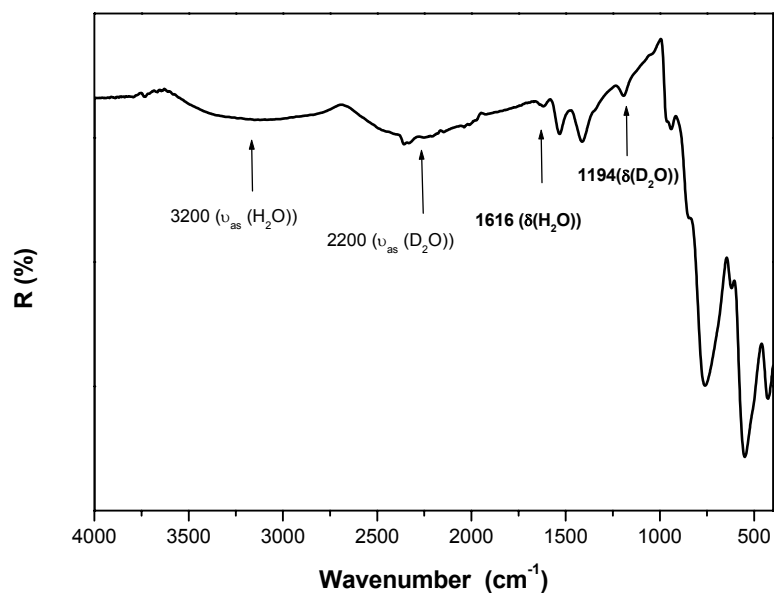


Figure 3. IR spectrum (diamond ATR) of " $\text{Mo}_{72}\text{Fe}_{30}\text{-D}_2\text{O}$ " precipitated from a heavy water solution after stirring for 48h at $\sim 60^\circ\text{C}$.

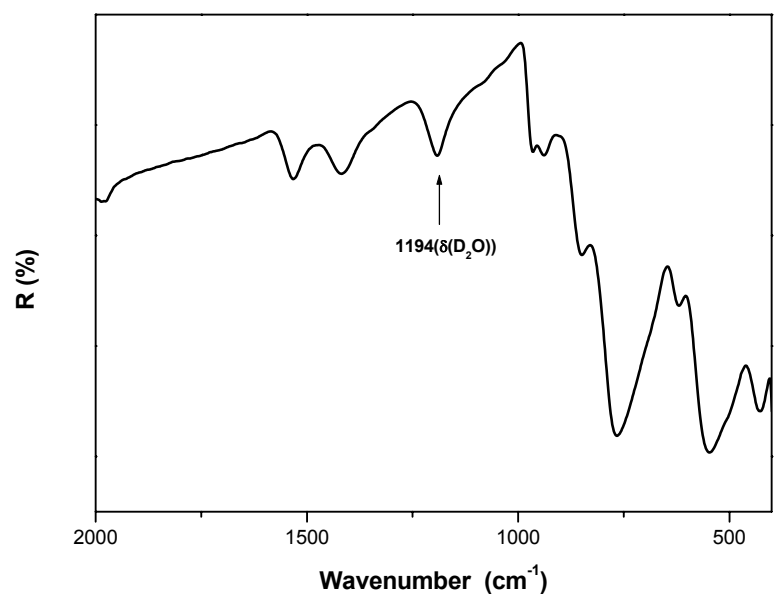
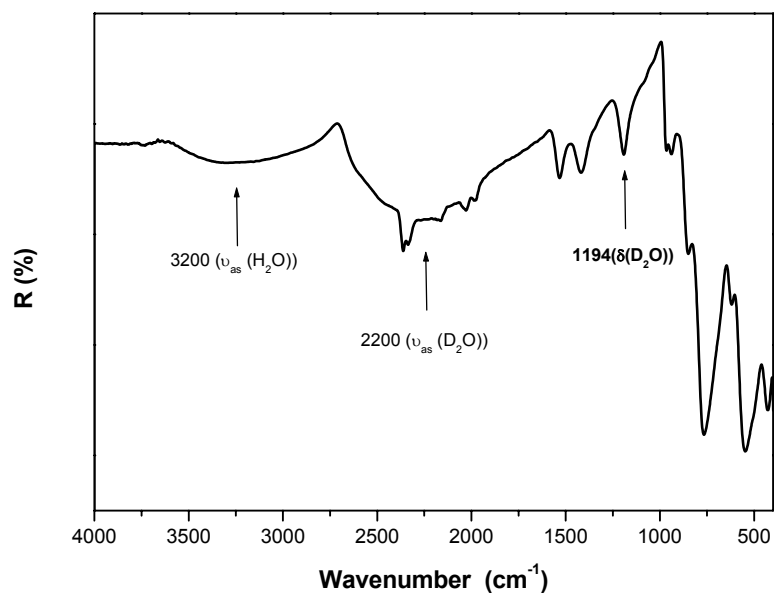


Figure 4. IR spectrum (diamond ATR) of " $\text{Mo}_{72}\text{Fe}_{30}\text{-D}_2\text{O}$ " precipitated from a heavy water solution after stirring for 72h at $\sim 60^\circ\text{C}$.

B) Starting with deuterated precursors

0.3g FeCl₃ (1.85mmol) were added to a solution of 1.78g MoO₃ (12.36 mmoli) (from Aldrich) in a mixture of 2.87g NaOD (40% in D₂O, 99 atom %D) (from Aldrich), 35g D₂O (99.8 atom %D, from Acros Organics) and 16.06g CH₃COOD 100% (98 atom %D, from Acros Organics). After acidification with 1.63g DCl (35% in D₂O, 99 atom %D) (from Aldrich) the solution (pH≈2) was heated to 90-95°C, stirred shortly and cooled to room temperature while after 6h the yellow microcrystalline precipitate was filtered off (under argon). The yellow crystals of the pure compound precipitated from the filtrate (kept under argon) after 5 days, were filtered off and dried under argon.

The attempts to prepare the "**Mo₇₂Fe₃₀-D₂O**" cluster starting from deuterated precursors lead to the precipitation of compounds in which the H₂O could be replaced only to a small extent (figure 5, 6, 7 and 8). The source of H₂O could be FeCl₃. The precipitation of the iron ball with water ligands could be due to the fact this is less soluble than the heavy water enriched iron ball or to an unusual type of isotope effect.

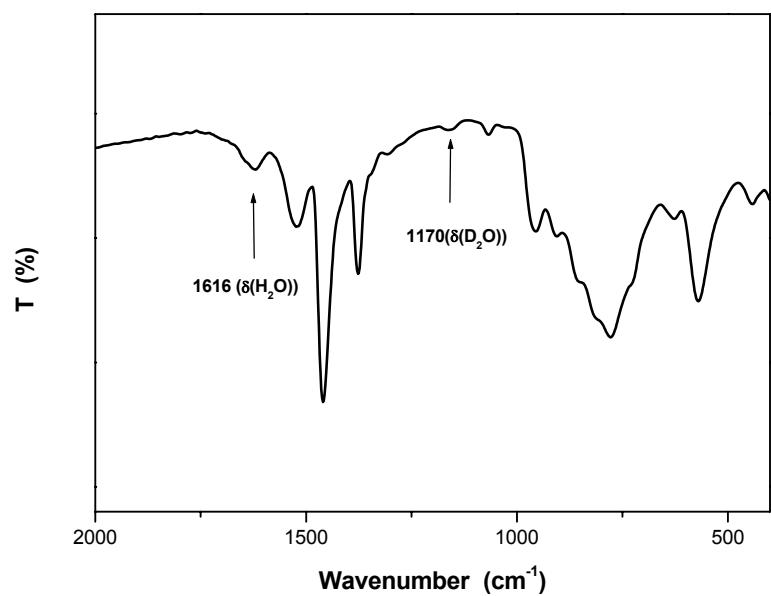
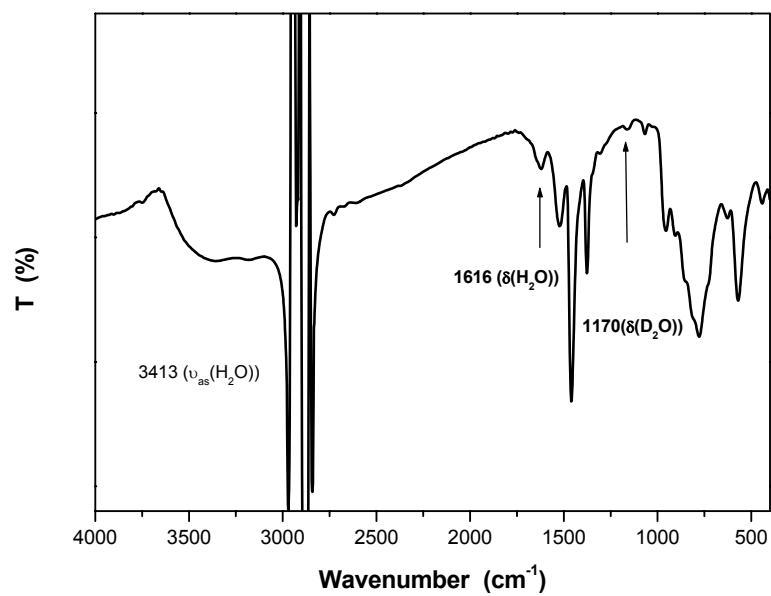


Figure 5. IR spectrum in nujol of "**Mo₇₂Fe₃₀-H₂O-D₂O**" prepared starting from deuterated precursors.

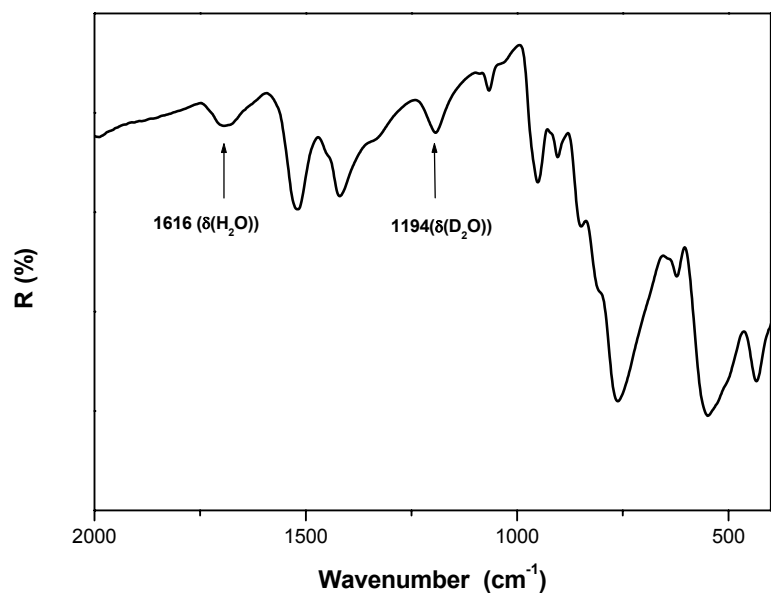
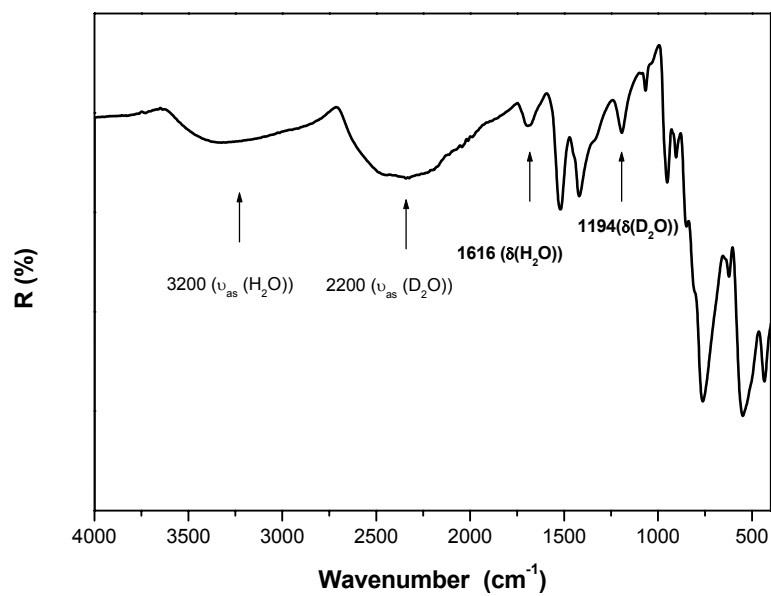


Figure 6. IR spectrum (diamond ATR) of " $\text{Mo}_{72}\text{Fe}_{30}\text{-H}_2\text{O-D}_2\text{O}$ " prepared starting from deuterated precursors.

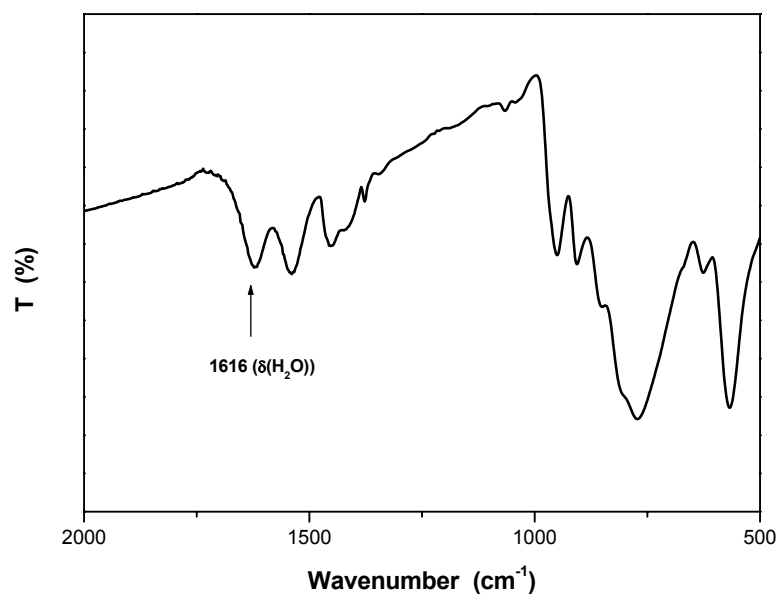
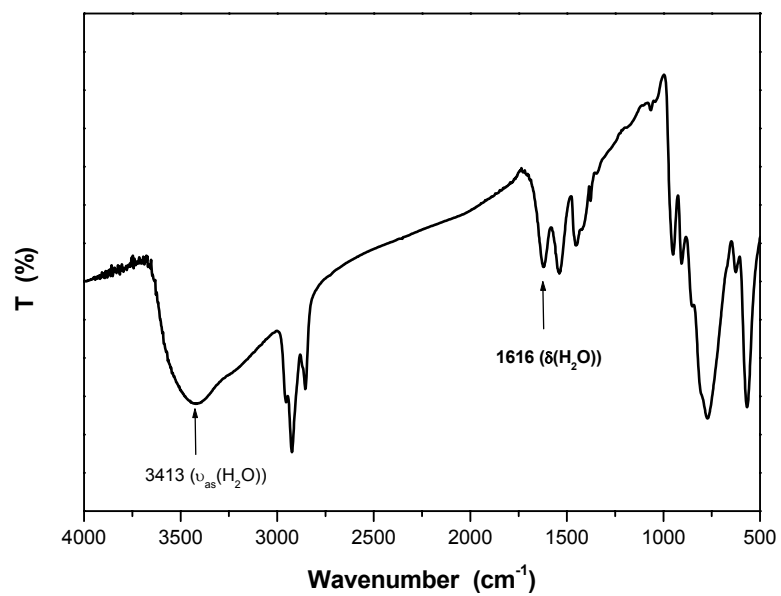


Figure 7. IR spectrum in nujol of " $\text{Mo}_{72}\text{Fe}_{30}\text{-H}_2\text{O}$ " prepared starting from deuterated precursors.

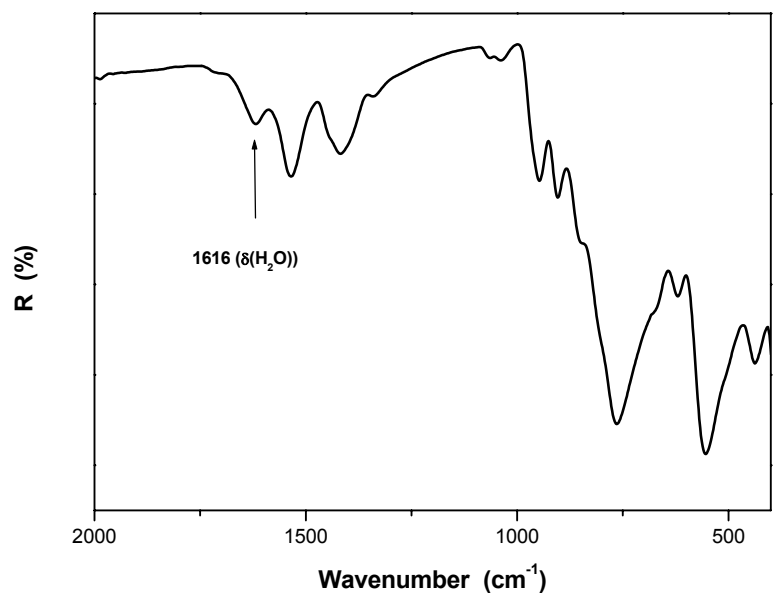
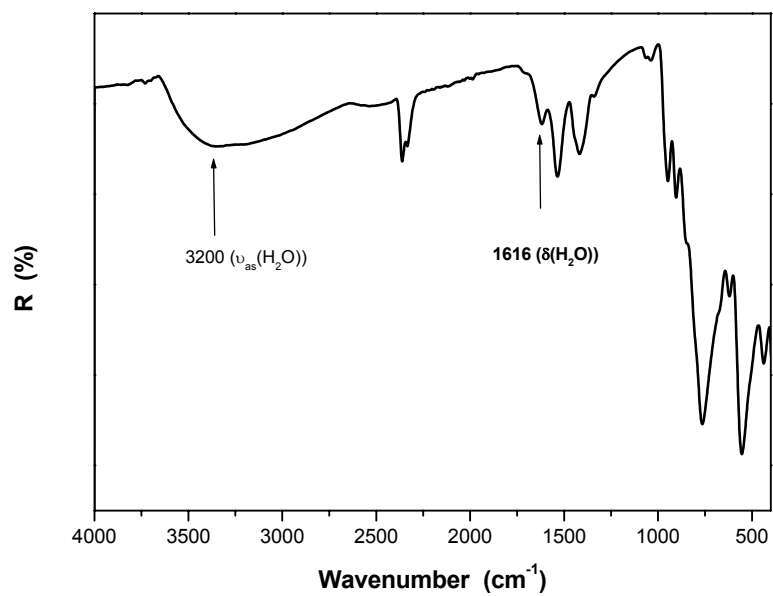


Figure 8. IR spectrum (diamond ATR) of "**Mo₇₂Fe₃₀-H₂O**" prepared starting from deuterated precursors.

Metal-Oxide-Based Nucleation Process under Confined Conditions: Two Mixed-Valence V_6 -Type Aggregates Closing the W_{48} Wheel-Type Cluster Cavities**

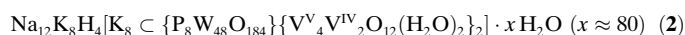
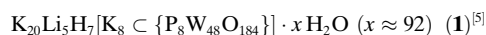
Achim Müller,* Michael T. Pope,* Ana Maria Todea, Hartmut Bögge, Joris van Slageren, Martin Dressel, Pierre Gouzerh, René Thouvenot, Boris Tsukerbat, and Aidan Bell

Dedicated to Professor C. N. R. Rao

Understanding assembly processes based on the linking of simple XY_n -type polyhedra has been of tremendous interdisciplinary interest since the time of Pauling's original statements referring especially to the silicates.^[1a] It seems to be of importance to distinguish between self-assembly and directed-assembly, terms used for elementary processes that probably occurred on the primordial earth.^[1b] In bulk solution one can mostly refer to self-assembly, but under confined conditions directed-assembly should be predominant because

of the probable influence of the "environment". In nearly all of these cases the elementary processes, especially the first related steps, are not known. The most studied system in this context is that of the polyoxometalates (POMs), in which MO_n -type species appear finally as polyhedra linked (mainly) through corners and edges.^[2] Regarding directed-assembly, two reports should be mentioned: a study on a giant wheel-type species in which molecular growth is observed inside the cavity^[3] and the discovery of an unprecedented stepwise molecular cascade type growth process based on nucleophilic/electrophilic interactions.^[4] Herein we report a process that occurs within the highly negatively charged wheel-shaped $\{P_8W_{48}\}$ -type species^[5] in which the formation of two mixed-valence $\{V_4^V V_2^{IV} O_{12}(H_2O)_2\}^{4+}$ assemblies with linked tetrahedra and octahedra is directed by the internal surface, thereby closing the cluster cavity.^[6] This type of process allows generation of a variety of magnetically interesting mixed-valence species by studying systematically the influence of the environment and internal wheel surface under variable redox conditions.

Reaction of a solution of **1** with vanadyl sulfate in aqueous medium yields crystals of **2** after some time. Compound **2**, which crystallizes in the triclinic space group $P\bar{1}$, was characterized by elemental analysis, thermogravimetry to determine the actual crystal water content, spectroscopic methods (IR, resonance Raman, UV/Vis, EPR, MAS-NMR), single-crystal X-ray structure analysis (including bond-valence-sum (BVS) calculations),^[7] and susceptibility measurements. A view of the structure of **2** in a mixed polyhedral and ball-and-stick representation is shown in Figure 1.



The "host" anion, $[K_8 \subset P_8W_{48}O_{184}]^{32-}$ (**1a**) with fourfold (D_{4h}) symmetry is derived from the linkage of four $\{P_2W_{12}O_{48}\}$ lacunary fragments of the Wells–Dawson anion $[P_2W_{18}O_{62}]^{6-}$; it encloses eight potassium cations in the positions shown in Figure 2a. The cations at the 3-, 6-, 9-, and 12-o'clock positions in the figure are disordered over two sites above and below the equatorial mirror plane; the remainder lie in that plane. Potassium cations occupy analogous positions within the new host–guest complex **2a** but they are now sandwiched between the two cyclic capping groups

[*] Prof. Dr. A. Müller, A. M. Todea, Dr. H. Bögge, Dr. A. Bell
Fakultät für Chemie der Universität
Postfach 100131, 33501 Bielefeld (Germany)
Fax: (+49) 521-106-6003
E-mail: a.mueller@uni-bielefeld.de

Prof. Dr. M. T. Pope
Department of Chemistry
Georgetown University
Box 571227, Washington, DC 20057 (USA)
Fax: (+1) 202-687-6209
E-mail: popem@georgetown.edu

Dr. J. van Slageren, Prof. Dr. M. Dressel
1. Physikalisches Institut
Universität Stuttgart
Pfaffenwaldring 57, 70550 Stuttgart (Germany)

Prof. Dr. P. Gouzerh, Dr. R. Thouvenot
Laboratoire de Chimie Inorganique et Matériaux Moléculaires
(UMR CNRS 7071)
Université Pierre et Marie Curie—Paris 6
4 place Jussieu, 75252 Paris (France)

Prof. Dr. B. Tsukerbat
Department of Chemistry
Ben-Gurion University of the Negev
Beer Sheva (Israel)

[**] A.M., J.S., and M.D. gratefully acknowledge the financial support of the Deutsche Forschungsgemeinschaft. A.M. further acknowledges the financial support of the Fonds der Chemischen Industrie, the Volkswagenstiftung, and the European Union (together with A.B.) (MRTN-CT-2003-504880). A.M. and B.T. gratefully acknowledge the financial support of the German–Israeli Foundation for Scientific Research and Development (GIF). M.T.P. acknowledges support from the Alexander von Humboldt Foundation and the Petroleum Research Fund administered by the American Chemical Society.

Supporting information for this article (UV/Vis, IR, and Raman spectra of **2**; ³¹P MAS-NMR spectra of **1** and **2**; and comments on valence localization/delocalization and the observation of intervalence transitions) is available on the WWW under <http://www.angewandte.org> or from the author.

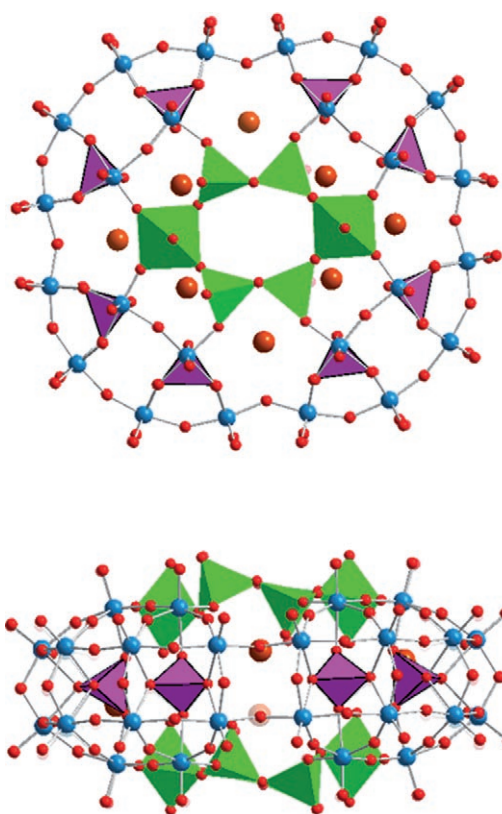


Figure 1. Two views of the structure of **2a** showing the capping V_6 groups and the positions of the K cations within the cavity. Color code: W blue, O small red spheres, K large brown-red spheres, PO_4 pink, VO_6 green.

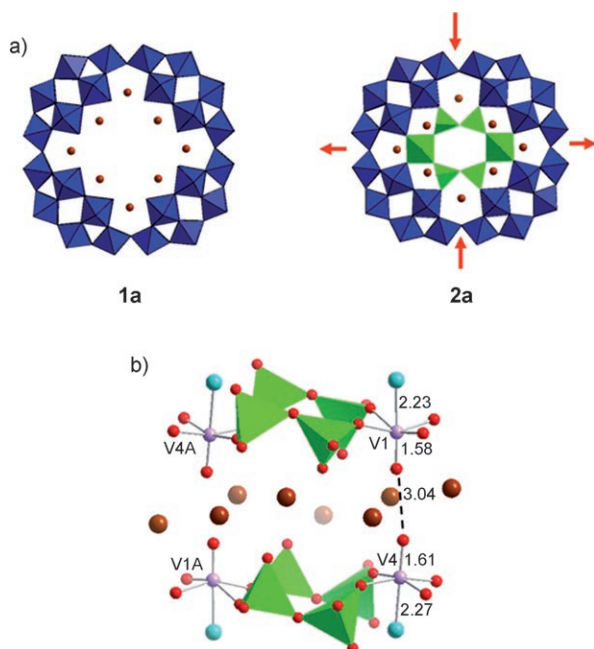


Figure 2. a) Comparison of the structures of **2a** and the host anion **1a** showing the distortion introduced by the $\{V_4V^{IV}_2O_{12}(H_2O)_2\}^{4+}$ capping groups **3a**. b) Some metrical details (in Å) of the capping groups **3a**. Color code as in Figure 1 plus V^{IV} lilac, H_2O ligands turquoise.

$\{V_4V^{IV}_2O_{12}(H_2O)_2\}^{4+}$ (**3a**), each with two octahedral V^{IV} and four tetrahedral V^V centers (Figure 2 a). **3a** can be considered formally as an interesting polycation exhibiting two different types of entities, namely, $\{O=V(H_2O)\}^{2+}$ [8a] and V_2O_5 [8b] which occur under well-defined conditions, the latter in the gas phase, the former in hydrated form in aqueous solution. The formation of **3a** is based on oxidation of V^{IV} by air and does not occur in absence of oxygen. As is evident from the figure the V_6 caps force a rhombic distortion of the square $\{P_8W_{48}\}$ perimeter observed in **1a**. [9] The internal angles of the rhombus in **2a** (of lines extended from the $P\cdots P$ vectors in each $\{P_2W_{12}\}$ unit) are close to 80° and 100° . The overall anion dimensions (measured by the separation between the oxygen atom “hinges” linking the corner-shared $\{WO_6\}$ octahedra at 6- and 12-o’clock positions in Figure 2 a versus those at 3- and 9-o’clock positions) are 15.27 and 17.94 Å. As shown in Figure 2 b the short terminal $V-O$ bonds of the four VO^{2+} centers are directed towards the interior of the structure and point towards the centroids of groups of three encapsulated potassium cations. The orientation of the VO^{2+} groups places four weakly bound water molecules ($V-OH_2 = 2.23$ and 2.27 Å) on the surface of the anion, and this leads to the possibility of attaching (albeit weakly) other ligands at these positions. The structure is a rare example of a polyoxometalate in which $M-O_{terminal}$ vectors point towards the interior of the anion. [10] Presumably space limitations (the $V\cdots V$ separation is 6.21 Å) preclude the enclosure of two water molecules.

Magnetic measurements were performed and Figure 3 shows the paramagnetic susceptibility–temperature product and the inverse of the susceptibility recorded on a fresh

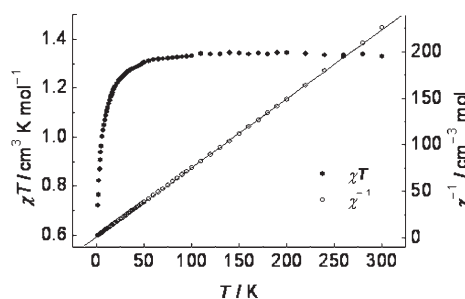


Figure 3. Temperature dependence of χT (filled circles) and χ^{-1} (open circles) recorded at 1 T. The drawn line is a fit to the Curie–Weiss law $\chi^{-1} = T/C - \theta/C$ ($T \geq 15$ K) with the parameters $C = 1.35 \text{ cm}^3 \text{ K mol}^{-1}$ and $\theta = -1.8 \pm 0.2$ K.

powder sample of **2** at an applied field of 1 T, both as a function of temperature. The high-temperature χT value of $1.34 \text{ cm}^3 \text{ K mol}^{-1}$ corresponds to the presence of 3.8 V^{IV} centers, which is in good agreement with the four $\{V^{IV}O(H_2O)\}$ units found in the crystallographic studies. From this result it can be immediately concluded that there are no additional $\{V^{IV}O\}^{2+}$ units in the lattice. The Curie–Weiss plot of the inverse of the susceptibility as a function of temperature (Figure 3) gives a Curie constant of $1.35 \text{ cm}^3 \text{ K mol}^{-1}$, which is in excellent agreement with the room-temperature value of χT . The small Weiss temperature of $\theta = -1.8 \pm 0.2$ K shows that the ions are only very weakly interacting, which is

not surprising in view of the orientation and separation of the magnetic (“ d_{xy} ”) orbitals of the V^{IV} centers. The decrease of the value of χT at lower temperatures is not an effect of magnetization saturation because the 0.1 T applied field susceptibility curve does not differ from that measured at an applied field of 1 T. This behavior is probably a consequence of small inter- or intramolecular exchange interactions.

The X-band EPR spectrum recorded on a powder sample exhibits a broad line with $g = 1.95$ at room temperature, but shows a hyperfine splitting from $I = 7/2$ V^{IV} nuclei of the order of $A = 200$ MHz ($67 \times 10^{-4} \text{ cm}^{-1}$) at 4.1 K (Figure 4). The

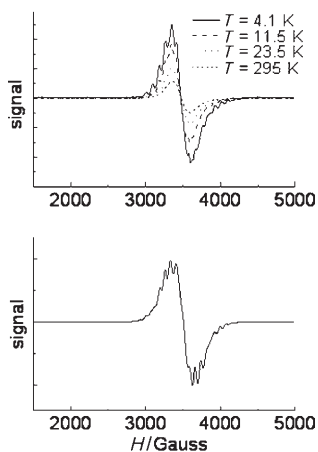


Figure 4. Top: EPR spectrum of **2** at various temperatures (hyperfine splitting only resolved for 4.1 K); bottom: simulation with g and A parameters from Table 1, $D = 0.008 \text{ cm}^{-1}$, and linewidths of 60 G.

magnitude of A and the pattern of hyperfine features are consistent with a triplet state arising from interactions between pairs of V^{IV} centers rather than a single VO^{2+} center, although the “forbidden” half-field line was not observed. Raising the temperature immediately leads to line broadening and disappearance of the hyperfine structure as a result of an increase in spin-lattice relaxation. Owing to the broadness of the spectrum even at 4.1 K it is not possible to obtain an unambiguous set of g and A parameters by simulation. The simulation depicted in Figure 4 corresponds to the parameters shown in Table 1, but these are by no means optimal. Nevertheless, the hyperfine parameters are similar to those reported for the vanadyl tartrate dimers shown in Table 1 and are quite distinct from those of a typical monovanadium(IV)polytungstate, also shown in the Table.

It seems plausible to assume that the “eclipsed” V^{IV} centers (V1 and V4, Figure 2b) account for the triplet state

Table 1: Selected EPR g and A [10^{-4} cm^{-1}] parameters.

Compound	$V^{IV} \dots V^{IV}$ [Å]	g_{\parallel}	g_{\perp}	A_{\parallel}	A_{\perp}	Reference
2	6.21	1.93	1.93	75	30	this work
VO- <i>dl</i> -tartrate dimer	4.08	1.953	1.982	72.3	21.3	[11]
VO- <i>dd</i> -tartrate dimer	4.35	1.950	1.984	73.2	24.6	[11]
$[PW_{11}V^{IV}O_{40}]^{5-}$		1.915	1.970	167.2	59.7	[14d]

EPR spectrum since the V1...V4A separation is 10.2 Å and would involve an unfavorable $V^{IV}(\text{oct.})\text{-O-V}^V(\text{tet.})\text{-O-V}^V(\text{tet.})\text{-V}^{IV}(\text{oct.})$ superexchange pathway. Superexchange between V1 and V4 involves multiple $V^{IV}\text{-O-W}^{VI}\text{-O-W}^{VI}\text{-O-W}^{VI}\text{-O-V}^{IV}$ pathways favored by the “mixed-valence” interaction between V^{IV} and W^{VI} (discussed below). Similar exchange involving multiple bond pathways has been demonstrated in $[KAs_4W_{40}(VO)_2O_{140}]^{23-}$.^[12] However, the adjacency of the two triplet states within the same anion is almost certainly responsible for the increased spin-lattice relaxation observed. A more detailed single-crystal EPR analysis is warranted for this interesting compound.

According to the Robin–Day classification^[13] **3a** is a Class I mixed-valence fragment/cation since the two valence states are clearly distinguished by their different coordination geometries, while the electron density is predominantly localized on the octahedral site, for which the crystal-field stabilization (here applicable only in a formal sense) is larger than that for the tetrahedral site ($10Dq_{\text{tet}} = -(4/9)10Dq_{\text{oct}}$). The electronic spectra of Class I mixed-valence compounds are a combination of the spectra of the individual oxidation states with no additional absorption (intervalence) bands. The situation is a little more complicated when the complete anion **2a** is considered because **3a** is embedded in the polytungstate matrix. In addition to the $V^{IV}V^V$ Class I mixed-valence situation, there is also adjacency of V^{IV} with W^{VI} . As has been well established for tungstovanadates(IV) (e.g., $[\text{SiW}_{11}\text{V}^{IV}\text{O}_{40}]^{6-}$), these can be treated as Class II systems with partial electron delocalization from “octahedral” V^{IV} to “octahedral” W^{VI} , which results in intensity-enhanced “d–d transitions” of V^{IV} as well as $V^{IV}\text{-W}^{VI}$ “intervalence” charge transfer at around 500 nm (see reference [14]). In contrast to the case of the $V^{IV}V^V$ situation, the enhancement of the electron-transfer rate for the $V^{IV}W^{VI}$ case should also be influenced by the vibrations that change the metal–metal distances and therefore modulate the transfer integrals (see the Supporting Information). The UV/Vis spectrum of a freshly prepared solution of **2** (Figure S1 in the Supporting Information) shows just such absorption features.^[15]

The slow decomposition of **2** in solution, together with the presence of four paramagnetic centers, precluded the observation of useful multinuclear NMR spectra. However, solid-state spectra could be recorded (see the Supporting Information).

Apart from the points that refer to general aspects of encapsulation chemistry,^[16] another interesting phenomenon was discovered. **3a** can be considered to be an interesting mixed-valent polycation that is formed by a nucleation process under confined conditions, and the specific geometric environment influences the type of electron distribution and exchange interactions, which are negligible in the present case. There is no doubt that other nucleation processes can be studied in the $\{P_8W_{48}\}$ cluster cavity under formally similar conditions such as those related to molybdenum oxide based aggregates, which were observed in larger cavities.^[3] The interesting aspect is that a variety of magnetically interesting mixed-valence species can be generated by changing the redox potentials.^[3]

Experimental Section

VOSO₄·5H₂O (0.35 g, 1.38 mmol) was added to a stirred solution of K₂₈Li₅[H₇P₈W₄₈O₁₈₄]-92H₂O (0.35 g, 0.024 mmol) in freshly prepared 1M NaCH₃COO/CH₃COOH buffer (30 mL, pH 4.4). The resulting solution was heated to 50°C for 4 h and then filtered, and the filtrate was allowed to evaporate at room temperature in an open 50-mL Erlenmeyer flask, during which period partial aerial oxidation of vanadium occurred. After 1 week the dark purple crystals were filtered, washed with cold water, and dried in air; yield: 0.2 g (54%); elemental analysis: calcd for Na₁₂K₁₆W₄₈P₈V₁₂O₂₉₂H₁₇₂: Na 1.79, K 4.05, V 3.96; found: Na 1.8, K 3.8, V 3.9%. Characteristic IR bands (KBr pellet): $\tilde{\nu}$ = 1622(m) [δ (H₂O)], 1144(m), 1092(m), 1020(w) [all ν_{as} (P-O)], 956(sh), 935(w), 912(s) [ν (W=O)/ ν (V=O)], 791(vs), 708(vs) [ν_{as} (W-O-W)/ ν_{as} (W-O-V)], 574(w), 536(w), 467(w) cm⁻¹; characteristic resonance Raman bands (solid/KBr dilution, λ_c = 1064 nm, cm⁻¹): ν = 950(sh), 923(s) [ν_s (W=O)/ ν_s (V=O)]; UV/Vis spectrum (in H₂O, nm): λ = 506 (ϵ = 7700 M⁻¹ cm⁻¹) (V^{IV} → W^{VI} (IVCT)), 680(sh), 890(w) (d-d (V^{IV})).

Magnetic susceptibility measurements were performed on a powder sample with a Quantum Design MPMS XL7 SQUID magnetometer. The underlying diamagnetic susceptibility was determined by susceptibility measurements on the diamagnetic [P₈W₄₈O₁₈₄]⁴⁰⁻ host ion, because standard procedures with Pascal's constants give values that are too low. X-band EPR spectra were recorded on a Bruker ESP300 X-band EPR spectrometer equipped with a continuous-flow Helium cryostat. The simulation was performed by using the Bruker WINEPR Simfonia program.

Received: January 31, 2007

Published online: May 8, 2007

Keywords: confined geometries · directed-assembly · electronic structure · mixed-valent compounds · polyoxometalates

- [1] a) L. Pauling, *The Nature of the Chemical Bond*, Ithaca, New York, **1948**; b) "Prebiotic Chemistry: From Simple Amphiphiles to Protocell Models": D. W. Deamer, J. P. Dworkin, *Top. Curr. Chem.* **2005**, 259 (Ed.: P. Walde).
- [2] M. T. Pope, *Heteropoly and Isopoly Oxometalates*, Springer, Berlin, **1983**.
- [3] A. Müller, S. Q. N. Shah, H. Bögge, M. Schmidtman, *Nature* **1999**, 397, 48–50.
- [4] From molybdate solutions under reducing conditions finally a Mo₃₇-type species is formed: A. Müller, J. Meyer, E. Krickemeyer, C. Beugholt, H. Bögge, F. Peters, M. Schmidtman, P. Kögerler, M. J. Koop, *Chem. Eur. J.* **1998**, 4, 1000–1006.
- [5] R. Contant, A. Tézé, *Inorg. Chem.* **1985**, 24, 4610–4614.
- [6] Examples of P₈W₄₈ complexes containing single-valence guests include [Cu₂₀Cl(OH)₂₄(H₂O)₁₂(P₈W₄₈O₁₈₄)]²⁵⁻ (S. S. Mal, U. Kortz, *Angew. Chem.* **2005**, 117, 3843–3846; *Angew. Chem. Int. Ed.* **2005**, 44, 3777–3780) and {Ln₄(H₂O)₂₈(H₂O)₂₈[KCP₈W₄₈O₁₈₄(H₄W₄O₁₂)₂Ln₂(H₂O)₁₀]¹³⁻}_x (Ln = La, Ce, Pr, Nd) (M. Zimmermann, N. Belai, R. J. Butcher, M. T. Pope, Symposium on "Nano-structures and Physicochemical Properties of Polyoxometalate Superclusters and Related Colloid Particles", Kanagawa, Japan, November 21–25, **2004**; M. Zimmermann, Diplomarbeit (supervised by M.T.P.), Bielefeld University, **2005**; M. Zimmermann, N. Belai, R. J. Butcher, M. T. Pope, E. V. Chubarova, M. H. Dickman, U. Kortz, *Inorg. Chem.* **2007**, 46, 1737–1740). Kortz has also reported other Cu₂₀-encapsulated anions as well as complexes incorporating four Ni²⁺, Co²⁺, and V^{VO}₂⁺ cations (German Research Foundation meeting on Molecular Magnetism, Bad Durkheim, Germany, January 15–17, **2006**).
- [7] Crystal data for **2**: H₁₇₂K₁₆Na₁₂O₂₉₂P₈V₁₂W₄₈, *M* = 15430.70 g mol⁻¹, triclinic, space group *P* $\bar{1}$, *a* = 19.7360(14), *b* = 20.7245(15), *c* = 21.1487(16) Å, α = 104.134(1), β = 117.561(1), γ = 104.410(1)°, *V* = 6745.6(9) Å³, *Z* = 1, ρ = 3.799 g cm⁻³, μ = 21.203 mm⁻¹, *F* (000) = 6892, Crystal size = 0.45 × 0.30 × 0.25 mm³. A total of 39426 reflections (1.64 < θ < 27.02°) were collected of which 28343 reflections were unique (*R*(int) = 0.0382). An empirical absorption correction using equivalent reflections was performed with the program SADABS 2.03. The structure was solved with the program SHELXS-97 and refined using SHELXL-97 to *R* = 0.0589 for 25047 reflections with *I* > 2 σ (*I*), *R* = 0.0665 for all reflections; Max/min residual electron density 3.177 and -3.875 e Å⁻³. Crystals of **2** were removed from the mother liquor and immediately cooled to 183(2) K on a Bruker AXS SMART diffractometer (three-circle goniometer with 1 K CCD detector, MoK α radiation, graphite monochromator; hemisphere data collection in ω at 0.3° scan width in three runs with 606, 435, and 230 frames (φ = 0, 88, and 180°) at a detector distance of 5 cm). (SHELXS/L, SADABS from G. M. Sheldrick, University of Göttingen **1997/2001**; structure graphics with DIAMOND 2.1 from K. Brandenburg, Crystal Impact GbR, **2001**). Further details on the crystal structure investigations may be obtained from the Fachinformationszentrum Karlsruhe, 76344 Eggenstein-Leopoldshafen, Germany (fax: (+49)7247-808-666; e-mail: crysdata@fiz-karlsruhe.de), on quoting the depository number CSD-417620.
- [8] a) F. A. Cotton, G. Wilkinson, C. A. Murillo, M. Bochmann, *Advanced Inorganic Chemistry*, 6th ed., Wiley, New York, **1999**; b) O. Glemser, A. Müller, *Z. Anorg. Allg. Chem.* **1963**, 325, 220–224 and references cited therein.
- [9] Although the nonrigidity of the [P₈W₄₈] assembly should not have been unexpected, the other reported derivatives^[6] retain the essentially "square" conformation.
- [10] Other examples include equatorial W centers in [As^{III}₂W₂₁O₆₉(H₂O)]⁶⁻ (Y. Jeannin, J. Martin-Frère, *J. Am. Chem. Soc.* **1981**, 103, 1664–1667) and [P^V₂W₂₁O₇₁(H₂O)₃]⁶⁻ (C. M. Tourné, G. F. Tourné, T. J. R. Weakley, *J. Chem. Soc. Dalton Trans.* **1986**, 2237–2242). The problem is of basic importance for larger species such as Mo₁₃₂, Mo₇₂Fe₃₀, and Mo₁₅₄. In the first two species, the Mo=O bonds are preferably directed outwards (ca. 80%), but according to a disorder also approximately 20% Mo(OH₂) groups are directed outwards. In the latter ring-type species, the situation is more complicated because of the presence of more (different) building units. In any case, there is a preference for H₂O ligands on the outer periphery (for compound types, see, for example: A. Müller, S. Roy, *J. Mater. Chem.* **2005**, 15, 4673–4677 and A. Müller, S. Roy, in *The Chemistry of Nanomaterials: Synthesis, Properties and Applications* (Eds.: C. N. R. Rao, A. Müller, A. K. Cheetham), Wiley-VCH, Weinheim, **2004**, 452–475).
- [11] R. L. Belford, N. D. Chasteen, H. So, R. E. Tapscott, *J. Am. Chem. Soc.* **1969**, 91, 4675–4680.
- [12] "Single crystal EPR studies on magnetic interactions in polyoxometalates containing several paramagnetic ions": Y. H. Cho, PhD Thesis, Sogang University, Seoul, Korea, **1996**.
- [13] M. B. Robin, P. Day, *Adv. Inorg. Chem. Radiochem.* **1967**, 10, 247–422.
- [14] a) H. So, M. T. Pope, *Inorg. Chem.* **1972**, 11, 1441–1443; b) D. P. Smith, H. So, J. Bender, M. T. Pope, *Inorg. Chem.* **1973**, 12, 685–688; c) H. So, C. M. Flynn, Jr., M. T. Pope, *J. Inorg. Nucl. Chem.* **1974**, 36, 329–332; d) J. J. Altenau, M. T. Pope, R. A. Prados, H. So, *Inorg. Chem.* **1975**, 14, 417–421.
- [15] The extinction coefficient per V^{IV} center (ca. 1900 M⁻¹ cm⁻¹) in **2** is approximately three times greater than that observed in other tungstovanadates (S. P. Harmaker, M. A. Leparulo, M. T. Pope, *J. Am. Chem. Soc.* **1983**, 105, 4286–4292). This is attributed to the larger V-O-W angles (162–164°) in **2**, which favor greater electron delocalization from V^{IV} to W^{VI}.
- [16] M. Gross, *Chem. Br.* **2003**, (8), 18.



Supporting Information

© Wiley-VCH 2007

69451 Weinheim, Germany

**Metal-Oxide-Based Nucleation Process under Confined Conditions:
Two Mixed-Valence V₆-Type Aggregates Closing the W₄₈ Wheel-Type
Cluster Cavities**

Achim Müller,* Michael T. Pope,* Ana Maria Todea, Hartmut Bögge, Joris van Slageren, Martin Dressel, Pierre Gouzerh, René Thouvenot, Boris Tsukerblat and Aidan Bell

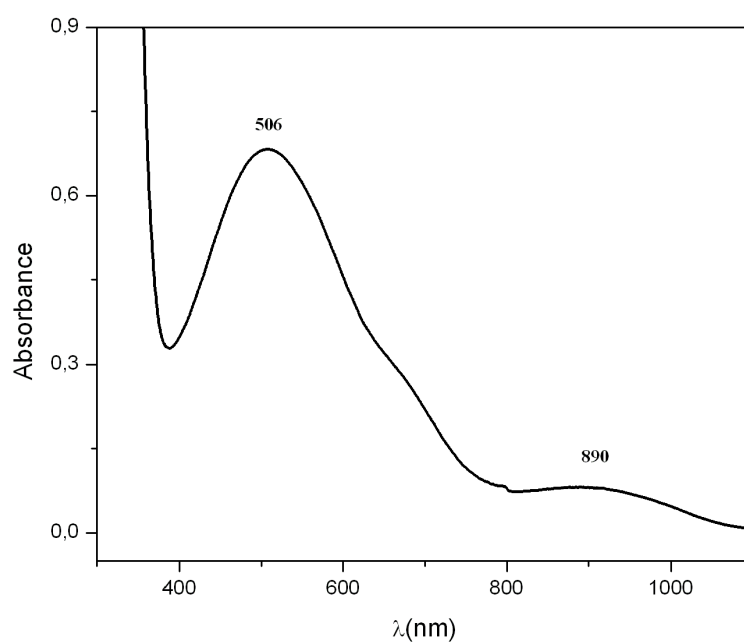


Figure S1. UV-Vis spectrum of a freshly-prepared solution of **2**.

Valence localization/delocalization and Intervalence Charge Transfer Transitions

An effect that contributes to the degree of electron localization which is important for Intervalence Charge Transfer Transitions arises – generally speaking – from the vibronic coupling with “breathing” modes of the local surroundings (Piepho-Kraus-Schatz (PKS) model; S.B. Piepho, *J. Am. Chem. Soc.* **1988**, *110*, 6319–6326, S. B. Piepho, *J. Am. Chem. Soc.* **1990**, *112*, 4197–4206 and J. J. Borrás-Almenar, E. Coronado, S. M. Ostrovsky, A. V. Palii, B. S. Tsukerblat, *Chem. Phys.* **1999**, *240*, 149–161) while the PKS coupling constants can be expressed in terms of the derivatives of Dq with respect to the metal-ligand distances R .

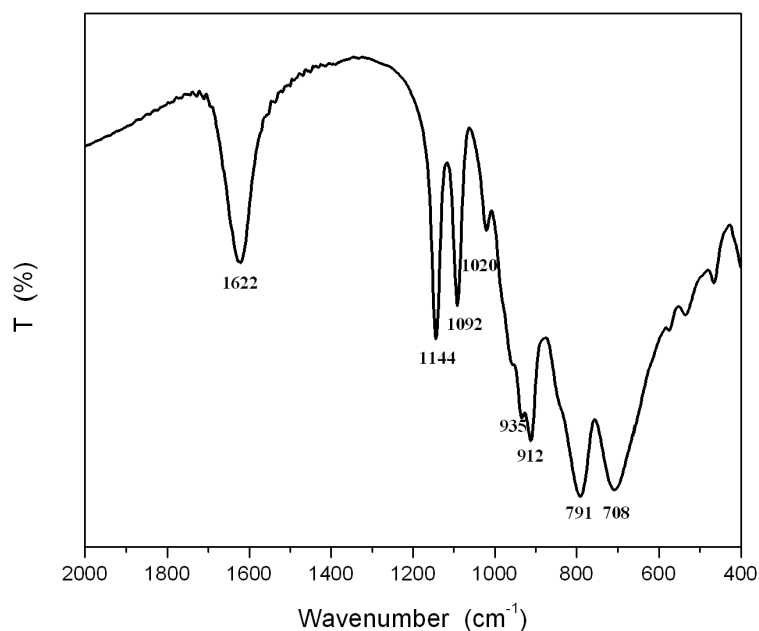


Figure S2. IR spectrum of **2**

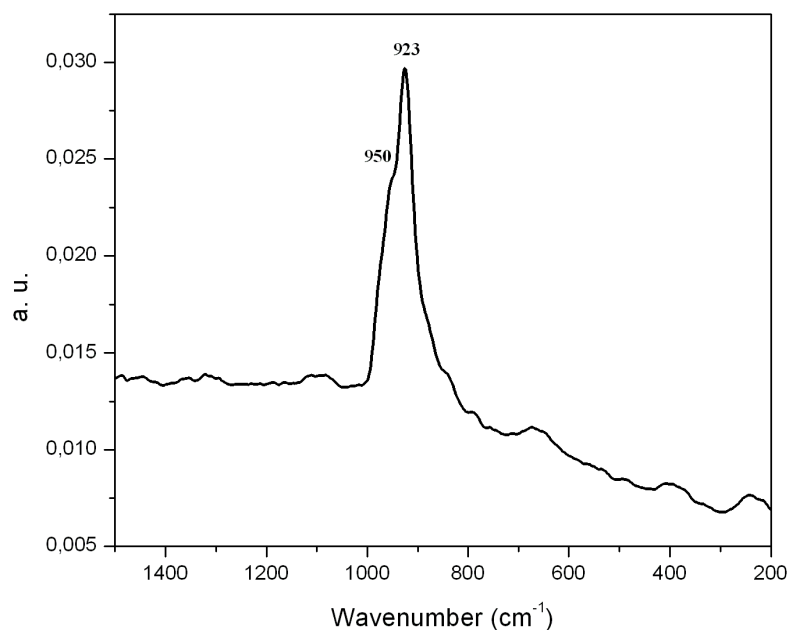


Figure S3. Raman spectrum of **2** (solid)

Phosphorus NMR Spectra

Room temperature ³¹P solid-state NMR spectra were recorded at 162 MHz in the single-pulse mode using a Bruker Avance 400 spectrometer equipped with a 4 mm MAS NMR probe. Owing to the small chemical shift anisotropy of the samples, relatively low spinning rates (= 10 kHz) were sufficient to obtain spectra free of spinning side bands. Data were acquired with 10° flip angle of 1 ms length with a repetition time of 1 s. Chemical shifts are given with respect to 85% H₃PO₄ as external standard.

The ³¹P MAS NMR spectrum of **1** (Figure S4) displays three partially overlapping isotropic signals at *ca.* -7.7, -7.3 and -7.1 ppm (fwhm *ca.* 160 Hz, *ca.* 1 ppm). This indicates the presence of at least three different phosphorus environments compatible

with the X-ray structural analysis showing the presence of four crystallographically-independent phosphorus atoms in the crystal.^[5] The ^{31}P MAS NMR spectrum of **2** (Figure S5) displays a very broad isotropic feature centered at *ca.* 0 ppm (fwhm *ca.* 2 kHz, *ca.* 12 ppm) which consists essentially of two overlapping signals with unequal width. According to the centrosymmetrical **2a**, there should be four inequivalent phosphorus atoms. Due to the vicinity of the paramagnetic V^{IV} centers the individual signals are broadened with respect to **1** and overlap each other.

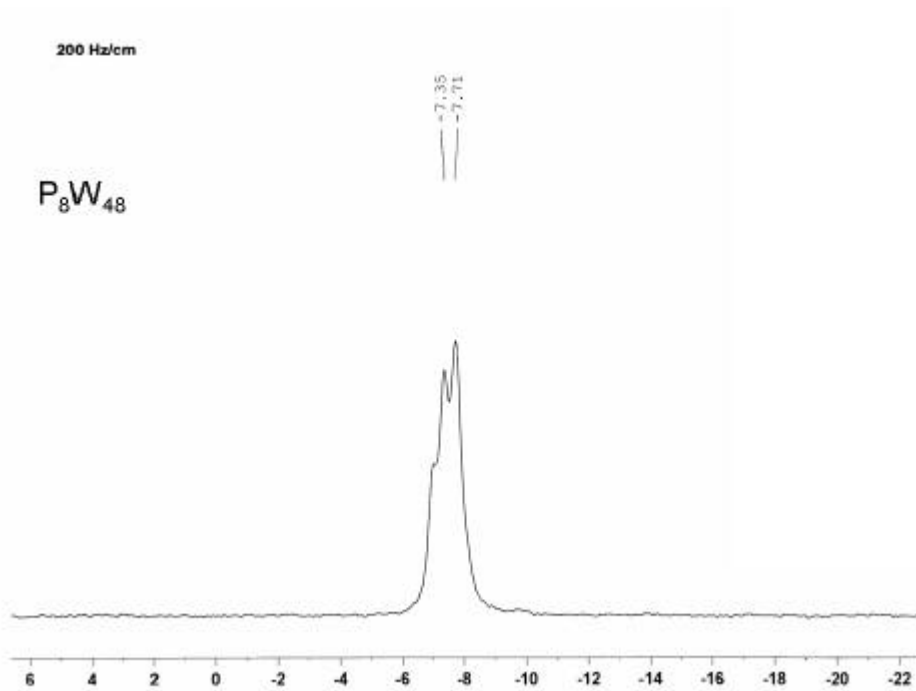


Figure S4. ^{31}P MAS-NMR spectrum of **1**

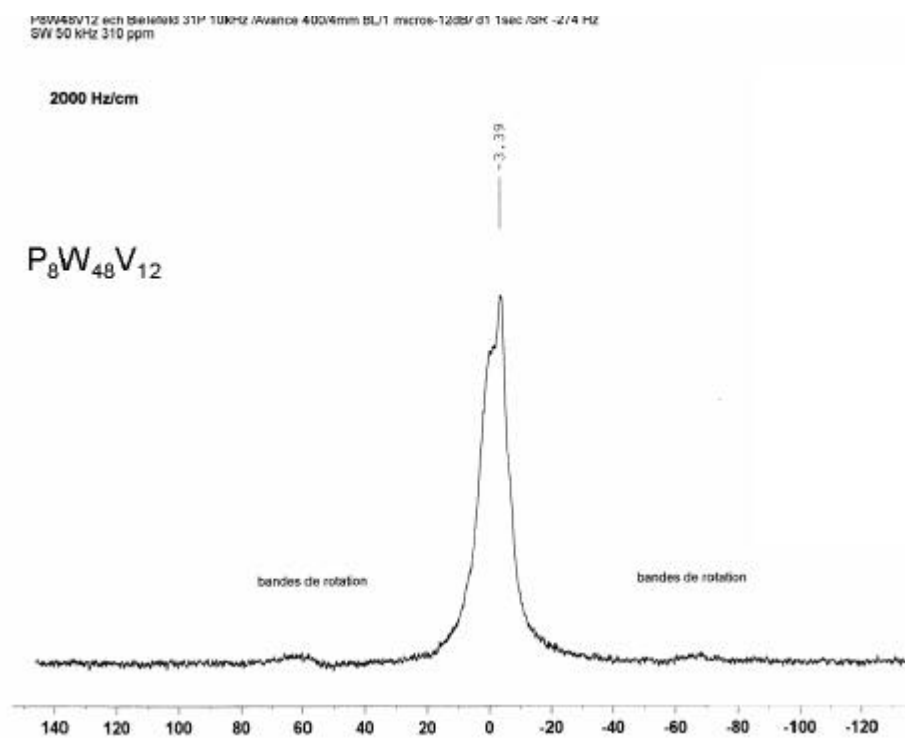


Figure S5. ^{31}P MAS-NMR spectrum of **2**

Nucleation Process in the Cavity of a 48-Tungstophosphate Wheel Resulting in a 16-Metal-Centre Iron Oxide Nanocluster

Sib Sankar Mal,^[a] Michael H. Dickman,^[a] Ulrich Kortz,^{*,[a]} Ana Maria Todea,^[b] Alice Merca,^[b] Hartmut Bögge,^[b] Thorsten Glaser,^[b] Achim Müller,^{*,[b]} Saritha Nellutla,^[c] Narpinder Kaur,^[c] Johan van Tol,^[c] Naresh S. Dalal,^{*,[c]} Bineta Keita,^[d] and Louis Nadjo^{*,[d]}

Dedicated to Professor Jerry Atwood on the occasion of his 65th birthday

Abstract: The 16-Fe^{III}-containing 48-tungsto-8-phosphate [P₈W₄₈O₁₈₄Fe₁₆(OH)₂₈(H₂O)₄]²⁰⁻ (**1**) has been synthesised and characterised by IR and ESR spectroscopy, TGA, elemental analyses, electrochemistry and susceptibility measurements. Single-crystal X-ray analyses were carried out on Li₄K₁₆[P₈W₄₈O₁₈₄Fe₁₆(OH)₂₈(H₂O)₄]-66H₂O·2KCl (**LiK-1**, orthorhombic space group *Pnmm*, *a* = 36.3777(9) Å, *b* = 13.9708(3) Å, *c* = 26.9140(7) Å, and *Z* = 2) and on the corresponding mixed sodium–potassium salt Na₉K₁₁[P₈W₄₈O₁₈₄Fe₁₆(OH)₂₈(H₂O)₄]-100H₂O (**NaK-1**, monoclinic space group *C2/c*, *a* = 46.552(4) Å, *b* = 20.8239(18) Å, *c* = 27.826(2) Å, *β* = 97.141(2)° and *Z* = 4). Polyanion **1** contains—in the form of a

cyclic arrangement—the unprecedented {Fe₁₆(OH)₂₈(H₂O)₄}²⁰⁺ nanocluster, with 16 edge- and corner-sharing FeO₆ octahedra, grafted on the inner surface of the crown-shaped [H₇P₈W₄₈O₁₈₄]³³⁻ (**P₈W₄₈**) precursor. The synthesis of **1** was accomplished by reaction of different iron species containing Fe^{II} (in presence of O₂) or Fe^{III} ions with the **P₈W₄₈** anion in aqueous, acidic medium (pH ≈ 4), which can be regarded as an assembly process under confined geometries. One fascinating aspect is the possibility to model the uptake and re-

lease of iron in ferritin. The electrochemical study of **1**, which is stable from pH 1 through 7, offers an interesting example of a highly iron-rich cluster. The reduction wave associated with the Fe^{III} centres could not be split in distinct steps independent of the potential scan rate from 2 to 1000 mV s⁻¹; this is in full agreement with the structure showing that all 16 iron centres are equivalent. Polyanion **1** proved to be efficient for the electrocatalytic reduction of NO_x, including nitrate. Magnetic and variable frequency EPR measurements on **1** suggest that the Fe^{III} ions are strongly antiferromagnetically coupled and that the ground state is tentatively spin *S* = 2.

Keywords: electrochemistry • iron • magnetic properties • polyoxometalates • self-assembly

[a] S. S. Mal, Dr. M. H. Dickman, Prof. Dr. U. Kortz
Jacobs University Bremen
School of Engineering and Science
P.O. Box 750 561, 28725 Bremen (Germany)
Fax: (+49) 421-200-3229
E-mail: u.kortz@jacobs-university.de

[b] A. M. Todea, Dr. A. Merca, Dr. H. Bögge, Prof. Dr. T. Glaser,
Prof. Dr. A. Müller
Fakultät für Chemie der Universität, Postfach 100131
33501 Bielefeld (Germany)
Fax: (+49) 521-106-6003
E-mail: a.mueller@uni-bielefeld.de

[c] Dr. S. Nellutla, N. Kaur, Dr. J. van Tol, Prof. Dr. N. S. Dalal
Department of Chemistry and Biochemistry
Florida State University and
National High Magnetic Field Laboratory and
Centre for Interdisciplinary Magnetic Resonance

Tallahassee, FL 32306-4390 (USA)
Fax: (+1) 850-644-8281
E-mail: dalal@chem.fsu.edu

[d] Dr. B. Keita, Prof. Dr. L. Nadjo
Laboratoire de Chimie Physique, UMR 8000, CNRS
Equipe d'Electrochimie et Photoelectrochimie
Université Paris-Sud, Bâtiment 350
91405 Orsay Cedex (France)
Fax: (+33) 169-154-328
E-mail: nadjo@lcp.u-psud.fr

Supporting information for this article is available on the WWW under <http://www.chemeurj.org/> or from the author. It contains detailed electrochemical characterisation of **1**, with Figure S1. Figures S2–S4 show cyclic voltammograms of **1** and **P₈W₄₈** in the presence of nitrate and NO, and Figure S5 shows the thermogram of **LiK-1** from room temperature to 900 °C.

Introduction

Chemistry under confined geometries—and this in a general sense—has attractive aspects which may be related to special topics of surface,^[1a] geo-^[1b] and especially biosciences.^[2,3] One may ask general questions, such as: what is it like for molecules/ions to “live” inside a nanosized molecular container (or generally under constrained/shielded environmental conditions) with respect to the interactions between them? In this context we can refer to two scenarios: 1) such interactions take place (nearly) independent of the cavity-internal shell functionalities (as in a nano-test-tube) or 2) they are influenced by the shell functionalities. Whereas in the first case the situation allows the spectroscopic identification/characterisation of the species under consideration more easily than under bulk conditions, in the second case one can study template-directed syntheses leading to unprecedented nanospecies. Such a process occurs in nature in different types of compartments.^[3] In the case of biomineralisation we can refer to the imposition of (biological) directionality on the chemistry of growth processes (vectorial regulation).^[3] In the present study we consider templated nucleation processes based on hydrate complexes of Fe^{II} (in presence of O₂) and Fe^{III} in the cavity of the cyclic 48-tungstophosphate **P₈W₄₈** leading to an unprecedented 16-metal-centre iron oxide formed by linking FeO₆ octahedra. This type of nucleation is based on a breaking of symmetry during the assembly process caused by the template effect of the cavity internal WO groups. The mentioned reaction of Fe^{II} in the presence of dioxygen shows an important feature: it played a key role on the early earth leading to iron-banded ores and is—regarding the confinement conditions—the basis for the formation of the iron oxide core of the metal-storage protein ferritin.^[4a] In context with the present vectorial growth process, we should refer also to the bacterial Mo storage proteins, in which different specific pockets of the protein cavity direct in unique nucleation processes the formation of different polyoxometalates (POMs).^[4b] The type of procedure/nucleation process described in this paper, which has several important interdisciplinary aspects, could in principle be extended to POMs with much larger cavities, for example, wheel-shaped polyoxomolybdates of the type Mo₁₇₆.^[4c]

Results and Discussion

Synthesis and structure: Although the **P₈W₄₈** cluster has been known for more than 20 years,^[5] only recently the first examples of metal-containing derivatives have been reported. Pope's group prepared the first lanthanide derivative, {Ln₄(H₂O)₂₈[K₂C₈P₈W₄₈O₁₈₄(H₄W₄O₁₂)₂Ln₂(H₂O)₁₀]¹³⁻}_x (Ln = La, Ce, Pr, Nd),^[6] and Körtz and co-workers isolated the first transition-metal derivative, the 20-copper(II)-containing [Cu₂₀Cl(OH)₂₄(H₂O)₁₂(P₈W₄₈O₁₈₄)]²⁵⁻^[7] (see also the report on the Cu₂₀-azide derivative [P₈W₄₈O₁₈₄Cu₂₀(N₃)₆(OH)₁₈]²⁴⁻^[8]), while Müller et al. discovered

[K₈C₈{P₈W₄₈O₁₈₄}[V^V₄V^{IV}₂O₁₂(H₂O)₂]₂]²⁴⁻, containing two cationic V₆-type mixed-valence clusters and formed by an unprecedented nucleation process.^[9] Very recently Körtz et al. reported [K(H₂O)₃{Ru(*p*-cymene)(H₂O)₄}{P₈W₄₉O₁₈₆(H₂O)₂}]²⁷⁻, which represents the first organometallic derivative of **P₈W₄₈**.^[10] Here we report on the iron derivative [P₈W₄₈O₁₈₄Fe₁₆(OH)₂₈(H₂O)₄]²⁰⁻ (**1**), which was identified independently in Bremen^[11] and Bielefeld.

Polyanion **1** was isolated as the mixed cation salts Li₄K₁₆[P₈W₄₈O₁₈₄Fe₁₆(OH)₂₈(H₂O)₄]·66 H₂O·2 KCl (**LiK-1**) and Na₉K₁₁[P₈W₄₈O₁₈₄Fe₁₆(OH)₂₈(H₂O)₄]·100 H₂O (**NaK-1**), see Experimental Section. Polyanion **1** contains an unprecedented {Fe₁₆(OH)₂₈(H₂O)₄}²⁰⁺ cluster in the cavity of **P₈W₄₈** with 16 edge- and corner-sharing FeO₆ octahedra being grafted to the inner surface of the “host” (see Figures 1 and 2).

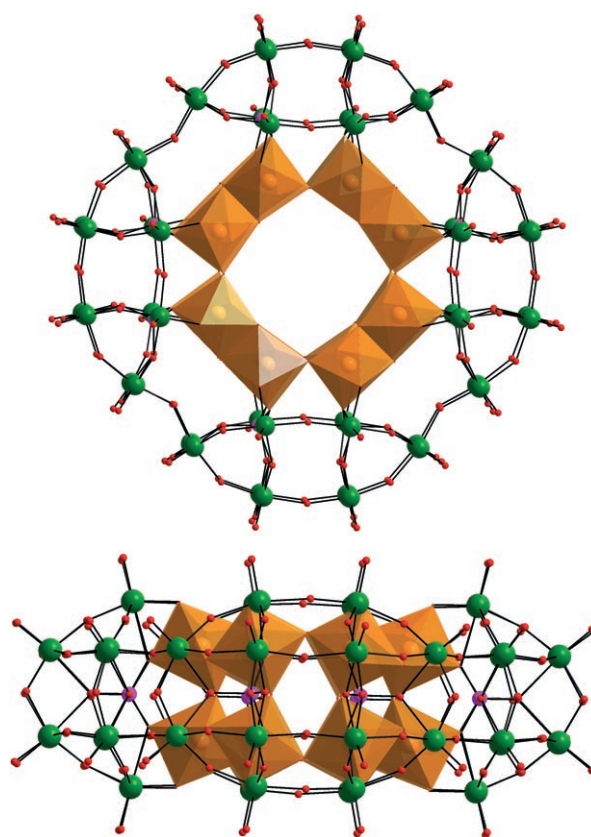


Figure 1. Front and side view of the structure of **1** emphasising the FeO₆ octahedra (brown) in polyhedral representation. Colour code: W (green), O (red), P (pink).

Polyanion **1** was generated by rather different synthetic procedures with respect to the type of iron precursors and the solvents (see Experimental Section). The Bremen group developed three slightly different synthesis procedures for **1** versus two of the Bielefeld group. For example, **1** can be prepared by reaction of a solution of **P₈W₄₈** with 1) FeCl₃ in 0.5 M LiCH₃COO/CH₃COOH buffer, pH 4.0 and a few drops of 30% H₂O₂, 2) Fe(ClO₄)₃ in 0.5 M LiCH₃COO/

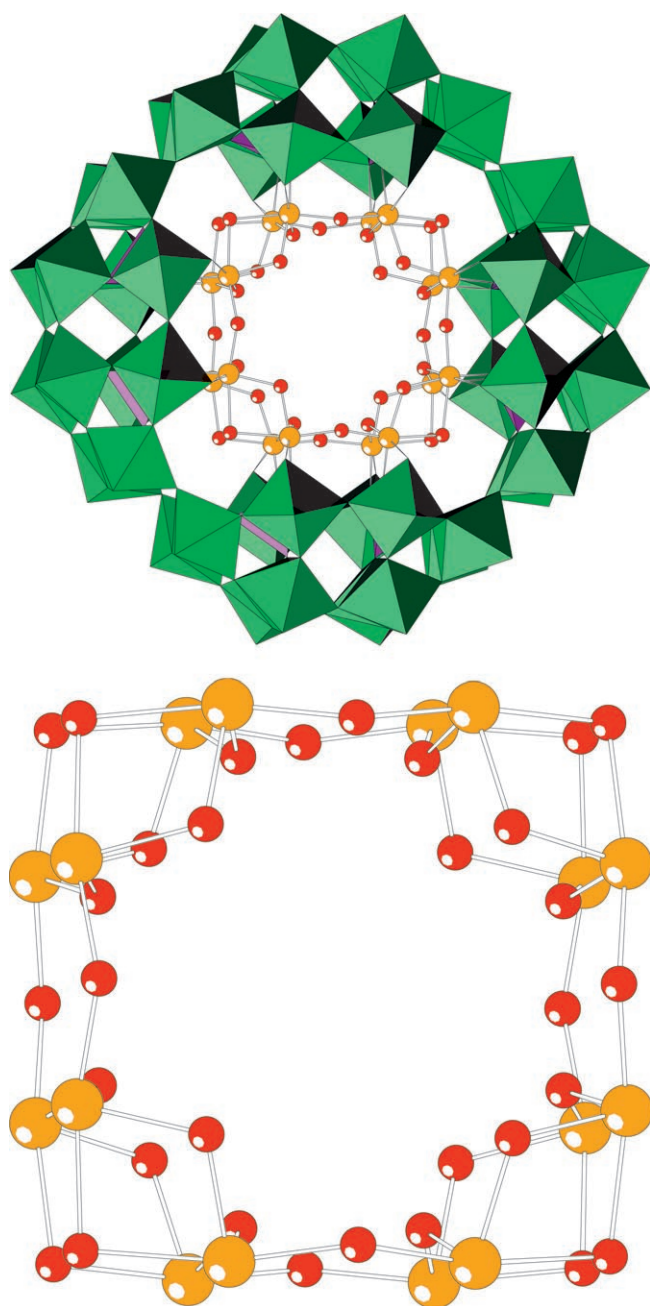


Figure 2. Top: Combined polyhedral/ball-and-stick representation of **1** emphasizing the connectivity of the central $[\text{Fe}_{16}(\text{OH})_{28}(\text{H}_2\text{O})_4]^{20+}$ cluster. Bottom: Ball-and-stick representation of the 16-iron-hydroxo cluster alone. Colour code: Fe (brown), O (red), PO_4 tetrahedra (pink), WO_6 octahedra (green).

CH_3COOH buffer, pH 4.0, 3) FeSO_4 in 0.5 M $\text{LiCH}_3\text{COO}/\text{CH}_3\text{COOH}$ buffer, pH 4.0 and a few drops of 30% H_2O_2 , 4) $[\text{Fe}_3\text{O}(\text{CH}_3\text{COO})_6(\text{H}_2\text{O})_3]\text{Cl}\cdot\text{H}_2\text{O}$ (**Fe₃Ac₆**) in 1 M $\text{NaCH}_3\text{COO}/\text{CH}_3\text{COOH}$ buffer, pH 4.2 and 5) FeCl_2 in 1 M $\text{NaCH}_3\text{COO}/\text{CH}_3\text{COOH}$ buffer, pH 4.2 in presence of O_2 . Interestingly, the last reaction can be considered as a model for the formation of the iron(III) oxide nucleus of ferritin.

It became apparent that, as expected, the pH is a crucial parameter besides the acetate medium. On the other hand,

it is possible to use a large variety of iron salts as starting materials, ranging from mononuclear iron(II) and iron(III) complexes (the former requires addition of an oxidant) to trinuclear iron(III) carboxylates. These observations support earlier knowledge that POM syntheses in general depend very much on the boundary conditions in the reaction vessel (e.g., pH and solvent).

Polyanion **1** exhibits a highly attractive symmetrical D_{4h} structure (see Figures 1 and 2). The large cavity (roughly $9 \times 9 \times 7 = 567 \text{ \AA}^3$) of the “cyclic template/host” **P₈W₄₈** has been “decorated” with a cationic nanocluster built up by 16 FeO_6 octahedra, resulting in a smaller, central cavity (roughly $6 \times 6 \times 5 = 180 \text{ \AA}^3$). The related “ Fe_{16} ring” is composed of eight pairs of structurally equivalent, edge-shared FeO_6 octahedra that are connected to each other through corners. While most of the Fe–O–Fe bridges are monoprotonated, four are diprotonated (presence of H_2O ligands). This can be confirmed by looking at the related bond valence sums (BVS) of these oxygen atoms.^[12] For example, the protonated oxygens (with the corresponding BVS values) of the polyanion in the mixed lithium–potassium salt **LiK-1** are O14F (0.69), O23F (0.71), O13F (1.08), O24F (1.11), O14G (1.17), O23G (1.27), O1FE (1.31), O2FE (1.32), and O4FE (1.34), see Figure 3. The rather low, but “intermediate” (between mono- and diprotonation) BVS values of 0.69 and 0.71 for O14F and O23F, respectively, led us to believe that we are looking at a water and a hydroxo ligand disordered over these two sites. Hence, we should have a total of 28 hydroxo and 4 aqua ligands associated with **1**.

These results confirm that we have indeed grafted an unprecedented, cyclic $[\text{Fe}_{16}(\text{OH})_{28}(\text{H}_2\text{O})_4]^{20+}$ iron nanocluster with hydroxo and aqua ligands inside the cavity of **P₈W₄₈** (see Figures 1 and 2). Selected bond lengths and angles of the $[\text{Fe}_{16}(\text{OH})_{28}(\text{H}_2\text{O})_4]^{20+}$ unit are shown in Figure 3. The FeO_6 octahedra are only slightly distorted with Fe–O distances ranging from 1.985(12) to 2.153(12) Å.

It is of interest to compare the structure of **1** with **P₈W₄₈**-type analogues containing other transition-metal centres. For example, we notice that the grafting mode of the 16 Fe^{III} centres in **1** is different from that of the 20 Cu^{II} centres in $[\text{Cu}_{20}\text{Cl}(\text{OH})_{24}(\text{H}_2\text{O})_{12}(\text{P}_8\text{W}_{48}\text{O}_{184})]^{25-}$.^[7a] In **1** each of the 16 equivalent Fe^{III} centres is bound to **P₈W₄₈** by a Fe–O(W) and a Fe–O(P) bond, resulting in a tight anchoring of the 16-iron–hydroxo core. In the Cu_{20} -POM, only eight of the 20 Cu^{II} ions form two covalent Cu–O(W) bonds each to the **P₈W₄₈** host. Hence, the eight phosphate groups of **P₈W₄₈** are not involved in the binding to the cationic $[\text{Cu}_{20}(\text{OH})_{24}]^{16+}$ cluster guest. In fact, **1** is structurally most closely related to Mialane’s Cu_{20} -azide derivative $[\text{P}_8\text{W}_{48}\text{O}_{184}\text{Cu}_{20}(\text{N}_3)_6(\text{OH})_{18}]^{24-}$.^[8] In the latter, 16 of the 20 Cu^{II} ions are bound to the inner rim of **P₈W₄₈** in exactly the same fashion as the Fe^{III} centres in **1**. The sites of the remaining four unique, Jahn–Teller distorted Cu^{II} ions in Mialane’s POM remain empty in **1**. However, we believe that in principle these four sites could be filled in **1** as well; for example, by Cu^{II} ions. In other words, there is a good chance that a mixed-metal (e.g., 16-iron-4-copper) derivative of **1** can be prepared.

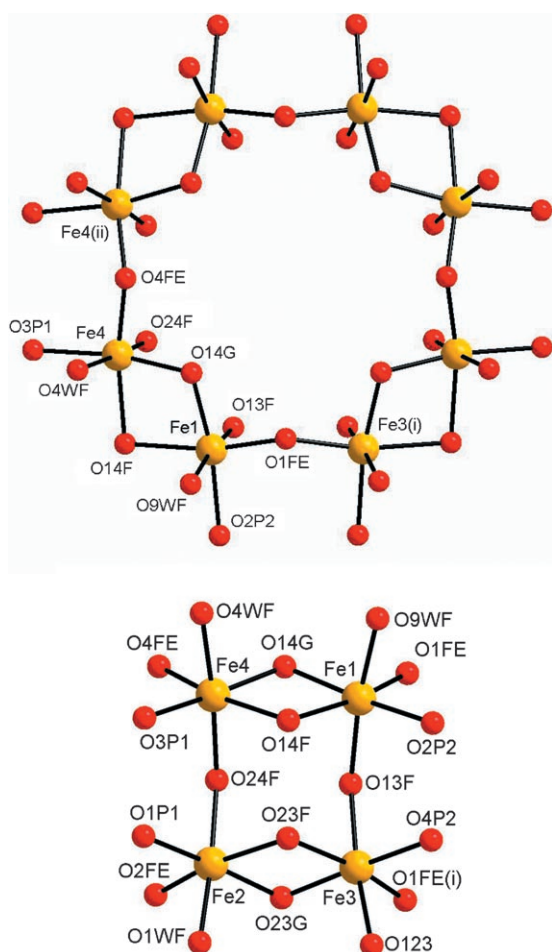


Figure 3. Top: Ball-and-stick view of a segment of **1**. Bottom: Side view including four independent Fe^{III} centres. Oxygen atoms O9WF, O4WF, O1WF, and O123 bridge to atoms W9, W4, W1, and W12, respectively. Atoms O1P1, O3P1, O2P2, and O4P2 bridge to atoms P1 and P2. Selected distances (Å) and angles (°): Fe1–O1FE, 1.895(12); Fe1–O14G, 1.959(12); Fe1–O9WF, 1.964(12); Fe1–O13F, 1.972(12); Fe1–O2P2, 2.086(12); Fe1–O14F, 2.145(12); Fe2–O2FE, 1.905(6); Fe2–O23G, 1.942(12); Fe2–O1WF, 1.975(12); Fe2–O24F, 1.985(12); Fe2–O1P1, 2.067(11); Fe2–O23F, 2.140(13); Fe3–O1FE, 1.924(12); Fe3–O23G, 1.933(12); Fe3–O123, 1.964(12); Fe3–O13F, 1.975(12); Fe3–O4P2, 2.093(12); Fe3–O23F, 2.126(12); Fe4–O4FE, 1.903(6); Fe4–O14G, 1.950(12); Fe4–O24F, 1.951(12); Fe4–O4WF, 1.986(12); Fe4–O3P1, 2.103(11); Fe4–O14F, 2.153(12); Fe1–O14G–Fe4, 107.3(6); Fe1–O14F–Fe4, 94.2(5); Fe2–O23F–Fe3, 94.8(5); Fe2–O23G–Fe3, 108.3(6); Fe1–O13F–Fe3, 135.1(7); Fe2–O24F–Fe4, 136.1(6); Fe1–O1FE–Fe3(i), 139.6(7); Fe2–O2FE–Fe2(ii), 139.2(9); Fe4–O4FE–Fe4(ii), 137.5(9). All O–Fe–O angles are within 12.5(6)° of 90 or 180. Symmetry operations: (i), $-x, -1-y, z$; (ii), $x, y, -z$.

Electrochemistry

Stability studies: UV/Vis spectroscopy and cyclic voltammetry (CV) were used to assess the stability of the title polyanion **1** by redissolving **LiK-1** in several aqueous media classically used as supporting electrolytes in electrochemical studies of POMs. Both techniques demonstrate that **1** is stable from pH 0.3 through 7. In this pH domain, its electronic spectra are characterised by an absorption peak located

roughly at 350 nm and assigned to the Fe^{III} centres in the structure and a second peak around 265 nm due to the tungstophosphate ligand framework **P₈W₄₈**. The locations of these peaks depend on the pH. CV experiments, the duration of which can last up to 10 h, confirm also that **1** is stable in this pH domain.

Voltammetric studies: UV/Vis spectroscopy and CV studies indicate that **1** is stable from pH 0.3 through 7 and also its precursor **P₈W₄₈**.^[13] Figure 4 shows the CVs of **1** and **P₈W₄₈**

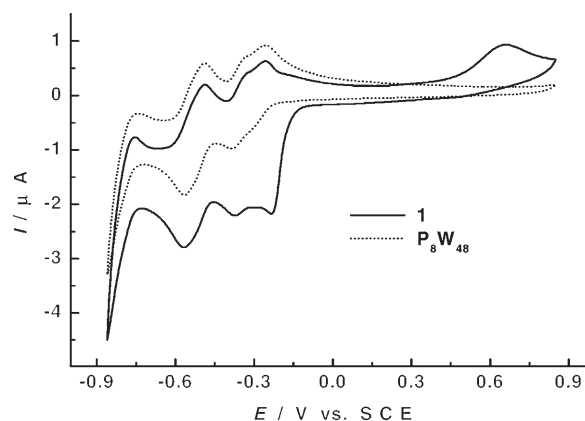


Figure 4. Superposition of the cyclic voltammograms of 4×10^{-5} M **1** (full line curve) and 4×10^{-5} M **P₈W₄₈** (dotted line curve) in pH 2 medium (0.5 M Li₂SO₄/H⁺). The working electrode was glassy carbon and the reference electrode was SCE. The scan rate was 10 mV s⁻¹. For further details, see text.

in superposition. In the cathodic branch of the CV of **1**, is observed a reduction peak located at -0.220 V versus SCE, which does not exist in the pattern of the lacunary species **P₈W₄₈**. This wave is assigned to the reduction of the Fe^{III} centres. As a matter of fact, the Fe^{III} centres are known to be more easily reduced than the W^{VI} centres as seen in several iron-containing polytungstates.^[14–16] For potential scan rates from 1000 down to 2 mV s⁻¹, no splitting of the single Fe-wave of **1** was observed. Controlled potential coulometry with the potential set at -0.230 V versus SCE indicates the consumption of 16 electrons per molecule. In addition, the characteristic blue colour of reduced W centres of most POMs was not observed during such reduction. These observations together confirm that this wave features the simultaneous one-electron reduction of the 16 Fe^{III} centres in **1**. Reduction of all the 16 structurally equivalent Fe centres of **1** in a single step suggests that they are relatively independent, a feature that is reminiscent of the reduction process of certain polymers or dendrimers. Analogous examples can be found in POM electrochemistry.^[16]

A detailed electrochemical study of **1** is provided in the Supporting Information (see Figures S1 and S2). These results underscore, at least, two important characteristics of **1**, which render this molecule a potential candidate for triggering electrocatalytic processes. Firstly, accumulation of several metallic centres associated with simultaneous electron

transfer and fairly fast kinetics is a necessary condition for reactions that require multiple electron transfers carried to completion and high efficiency. Secondly, the proximity of the Fe^{III} and W^{VI} waves of **1** can bring about beneficial effects.

To our knowledge, **1** constitutes the first example of multi-iron-containing POMs with such a small separation between the Fe^{III} and the first W waves. The benefit of this property was demonstrated in the electrocatalytic reduction of nitrite by Fe^{III}-monosubstituted Wells–Dawson-type tungstates or molybdates.^[17] Further examples were encountered in the electrocatalytic reduction of dioxygen and nitrogen oxides by Cu²⁺-substituted tungstomolybdates.^[18]

Electrocatalytic behaviour of 1 towards NO_x: The electrocatalytic reduction of nitrate remains a challenge in the NO_x series because very few POMs are active in such electrocatalytic reduction.^[19] The positive results observed with **1** are described in the Supporting Information. An exciting observation is described in the following.

Reversible binding of NO to 1: The interest in NO has grown considerably ever since its important role in biology, environment and industry was unveiled.

Very recently, we have demonstrated by CV that the following two POMs, [Co(H₂O)₂](B-β-SiW₉O₃₃(OH))(β-SiW₈O₂₉(OH)₂Co₃H₂O)₂]²⁰⁻^[19b] and [[Sn(CH₃)₂(H₂O)]₂₄[Sn(CH₃)₂]₁₂(A-PW₉O₃₄)₁₂]³⁶⁻,^[19c] interact reversibly with NO or related species. A similar, but much weaker interaction was detected for the plenary Wells–Dawson type tungstophosphate [P₂W₁₈O₆₂]⁶⁻ and the plenary Keggin type tungstosilicate [SiW₁₂O₄₀]⁴⁻. These observations suggest that the combination of large POM size and/or incorporation of Co^{II} or diorganotin moieties favours interaction with NO, followed by efficient electrocatalytic reduction of NO.^[19b,c]

With this prior knowledge in mind, we decided to study the interaction of **1** with NO, hoping for an associated catalytic activity of the polyanion towards the reduction of NO. For these experiments solutions of **1** at pH 1 were saturated in an alternating fashion with argon and NO, respectively. The main observations are illustrated in Figure 5; the potential domain is restricted to that of the composite wave recorded on a solution of **1** saturated with argon; it is composed of the Fe^{III} reduction wave and the first W^{VI} reduction wave of **1**. In the presence of NO an important catalytic current is observed that sets in at a more positive potential than that of the composite wave of **1**. In addition, the intensity of this catalytic wave increases strongly with time (Figure 5A). The cell was checked for leakage as explained in the Experimental Section.

An analogous behaviour is observed for P₈W₄₈ in the presence of NO (Figure S3 in the Supporting Information), albeit with a roughly seven times weaker intensity than for **1** (Figure S4). However, this example permits to highlight details of the catalytic process. Figure 5B shows in superposition this catalytic process with its current scaled down to make its peak current match that observed in the presence

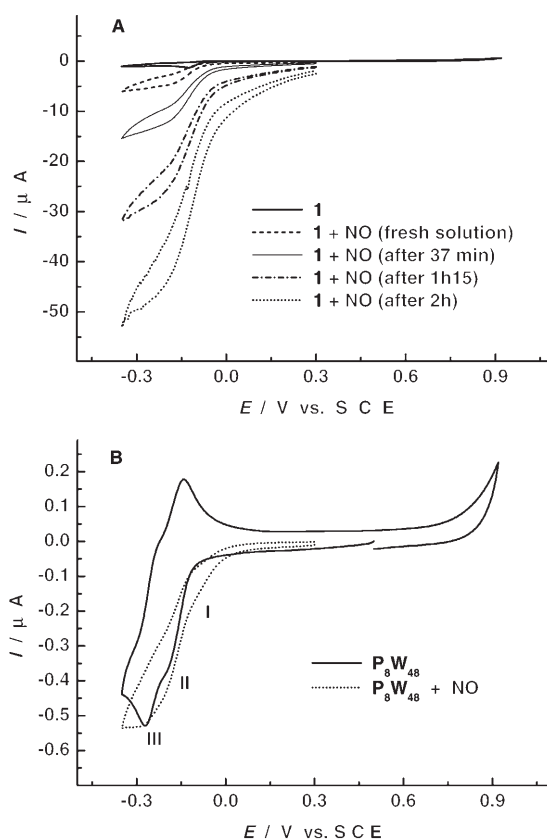


Figure 5. A) Cyclic voltammograms of 4×10^{-5} M **1** at pH 1 in the presence of NO. The CVs are restricted to the potential domain of the composite wave recorded on a solution saturated with argon and comprising the Fe^{III} reduction wave and the first W^{VI}-reduction wave of **1**, and at several time intervals after saturation with NO ([NO]=1 to 2 mM). The working electrode was glassy carbon and the reference electrode was SCE. The scan rate was 2 mV s^{-1} . For further details, see text. B) Cyclic voltammograms of 4×10^{-5} M P₈W₄₈ at pH 1 saturated with argon or with NO, respectively. The current in the presence of NO was scaled down to make its peak current match that observed in the presence of argon. The working electrode was glassy carbon and the reference electrode was SCE. The scan rate was 2 mV s^{-1} . For further details, see text.

of argon. Three closely spaced waves can be distinguished, with the peak potential of the first one located roughly 0.1 V positive of the first wave of P₈W₄₈. In short, this positive wave should be associated with a complex between NO and P₈W₄₈. The same kind of complex is probably also present for **1**, but obscured by the Fe^{III}-wave, thus leaving only the overall positive shift of the catalytic wave. It must be noted that such shift is larger for **1** than for P₈W₄₈. We found that NO can be eliminated by bubbling argon through the solutions and then voltammograms virtually identical to the original ones are restored for **1** and P₈W₄₈.

Together, these observations indicate a reversible interaction between NO and **1** or P₈W₄₈, followed by electrocatalytic reduction of NO.

Magnetic susceptibility and EPR studies: The molar magnetic susceptibility (χ_m) and $\chi_m T$ of LiK-**1** as a function of temperature, T , are displayed in Figure 6. The observed

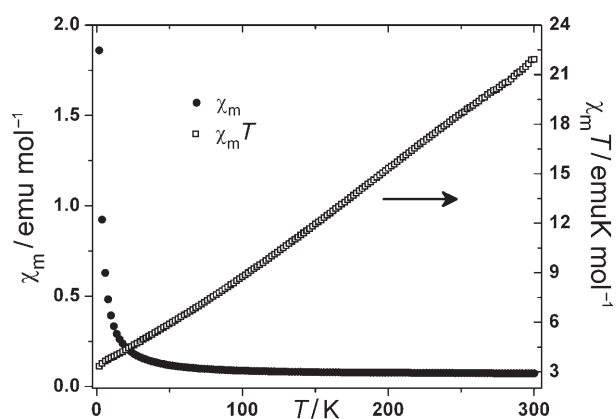


Figure 6. Magnetic susceptibility plotted as χ_m (●), $\chi_m T$ (□) versus T for **LiK-1** powder.

room-temperature $\chi_m T$ value of 21.9 emu K mol, when compared with that expected (70 emu K mol) for 16 non-interacting Fe^{III} ($S=5/2$, $g=2$) ions, indicates that antiferromagnetic interactions play a dominant role in the title polyanion **1**. At 1.8 K, a $\chi_m T$ value of 3.3 emu K mol⁻¹ suggests that the ground state is $S_T=2$ (expected is 3 emu K mol⁻¹ with $g=2$).

The highly symmetrical $\{\text{Fe}_{16}(\text{OH})_{28}(\text{H}_2\text{O})_4\}^{20+}$ magnetic cluster incorporated in **1** is composed of 16 equivalent Fe^{III} centres (see Figure 2). There are three types of Fe-O-Fe bridges (see Figure 3) that require three exchange coupling constants J_1 (e.g., Fe1-O1Fe-Fe3(i)), J_2 (e.g., Fe1-O14F/O14G-Fe4) and J_3 (e.g., Fe2-O24F-Fe4) and the interplay between them determines the ground state of **LiK-1**. The presence of 163 112 472 594 spin states with a total spin S_T ranging from 0 to 40 renders the detailed analysis of the magnetic susceptibility data of **LiK-1** complicated and is beyond the scope of the present study. However, a comparison of the Fe-O bond lengths and Fe-O-Fe bond angles of **1** with the literature values for μ_2 -hydroxo-bridged Fe^{III} dimers and oligomers suggests that the magnitudes of J_1 , J_2 and J_3 should be in the range of 20–25 cm⁻¹.^[20,21] We hypothesise that the exchange couplings might be very similar in magnitude resulting in closely spaced spin levels and therefore the ground-state $S_T=2$ assignment can only be tentative. Although the absence of a plateau at around 3.3 emu K mol⁻¹ in the χT profile supports our hypothesis, susceptibility measurements below 1.8 K are needed for confirmation.

Magnetisation ($M/N\beta$) versus field H for **LiK-1** at various temperatures is plotted in Figure 7. At 1.8 K, as the field increases from 0 to 7 T, $M/N\beta$ tends to reach 4, as expected for an $S=2$ spin system with $g=2$. The decrease in magnetisation as the temperature increases from 1.8 to 20 K could be due to the expected H/T dependence of the magnetisation.^[22]

In a further attempt to understand the magnetism of polyanion **1**, electron paramagnetic resonance (EPR) spectra were collected for various frequencies (9.65–319.2 GHz) and temperatures (5–300 K) for a powder sample of **LiK-1**. Only one broad peak ($\Delta H_{\text{pp}}=70 \pm 3$ mT) at $g=2.002 \pm 0.001$ is ob-

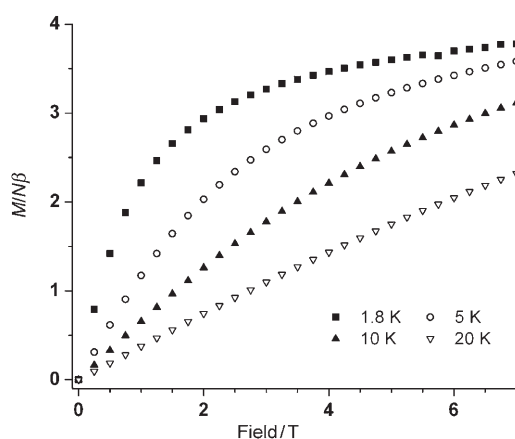


Figure 7. Magnetisation ($M/N\beta$) as a function of field for **LiK-1** powder plotted for various temperatures.

served at room temperature for all experimental frequencies (see Figure 8). This is reminiscent of our earlier results on the hexa- Fe^{II} -substituted Keggin dimer $[\text{Fe}(\text{OH})_3(A-\alpha\text{-GeW}_9\text{O}_{34}(\text{OH})_3)_2]^{11-}$.^[23] Figure 9 shows some typical X-band

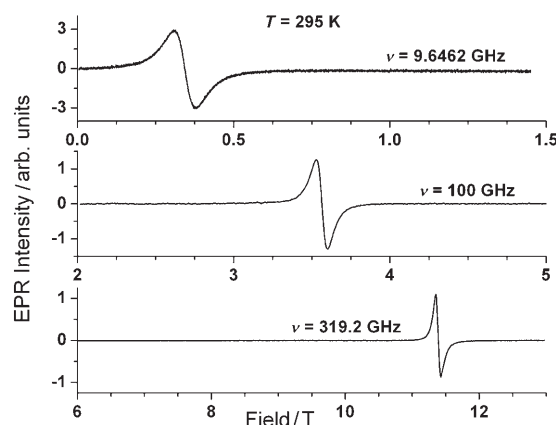


Figure 8. Room-temperature powder EPR spectra of **LiK-1** for 9.65, 100 and 319.2 GHz, respectively. Only one broad peak at $g=2.002$ is observed for all experimental frequencies.

(~9.65 GHz) and ~319 GHz spectra at a few temperatures. At least three features are evident: 1) a strong decrease in the signal intensity with decreasing temperatures, 2) signal broadening with decreasing temperatures and 3) absence of any additional splitting of the main peak. The intensity decrease is consistent with a similar trend in the magnetic susceptibility (Figure 6), and can thus be attributed to the population of states with smaller S_T values at lower temperatures. On the other hand, signal broadening could be due to dipolar broadening and/or shorter relaxation times. The lack of any fine structure at all frequencies and temperatures studied renders it meaningless to derive any conclusions about the single-ion anisotropy of the overall S_T value. The low temperature $g\sim 4.3$ peak observed at X-band (indicated by * in Figure 9 top) is a Fe^{III} impurity signal from the

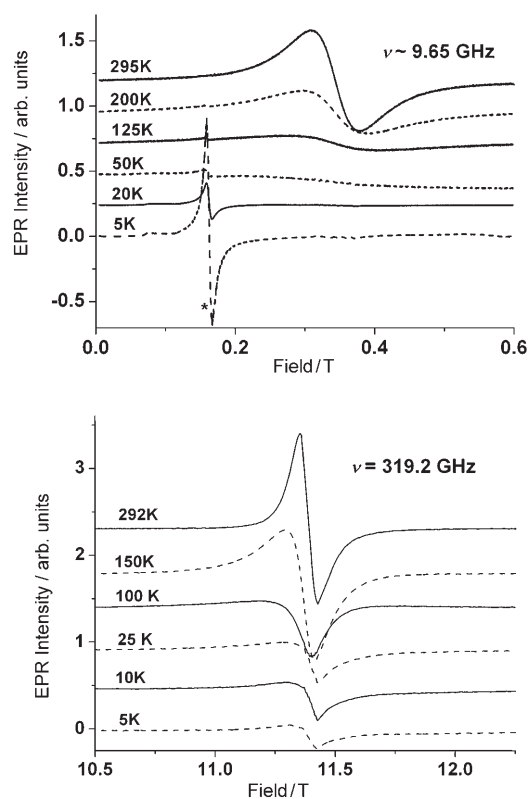


Figure 9. Temperature dependence of EPR spectra on **LiK-1** powder at ~ 9.65 GHz (top) and 319.2 GHz (bottom). The steady decrease of the signal intensity with decreasing temperature indicates the presence of excited states. The peak indicated by “*” at ~ 0.16 T in the top spectra is from a Fe^{III} impurity in the sample.

sample. Finally, the small remnant signal observed at 319.2 GHz (see Figure 9 bottom) is attributed to a minor $g \sim 2$ impurity in the system and is not considered significant to the overall focus of the present study.

Conclusion

We have prepared the $16\text{-Fe}^{\text{III}}$ containing 48-tungsto-8-phosphate $[\text{P}_8\text{W}_{48}\text{O}_{184}\text{Fe}_{16}(\text{OH})_{28}(\text{H}_2\text{O})_4]^{20-}$ (**1**) as the mixed cation salts $\text{Li}_4\text{K}_{16}[\text{P}_8\text{W}_{48}\text{O}_{184}\text{Fe}_{16}(\text{OH})_{28}(\text{H}_2\text{O})_4] \cdot 66\text{H}_2\text{O} \cdot 2\text{KCl}$ (**LiK-1**) and $\text{Na}_9\text{K}_{11}[\text{P}_8\text{W}_{48}\text{O}_{184}\text{Fe}_{16}(\text{OH})_{28}(\text{H}_2\text{O})_4] \cdot 100\text{H}_2\text{O}$ (**NaK-1**). Polyanion **1** contains 16 edge- and corner-sharing FeO_6 octahedra in the form of a cyclic, unprecedented $\{\text{Fe}_{16}(\text{OH})_{28}(\text{H}_2\text{O})_4\}^{20+}$ iron-hydroxo-aqua nanocluster, grafted on the inner surface of the crown-shaped $[\text{H}_7\text{P}_8\text{W}_{48}\text{O}_{184}]^{33-}$ (**P₈W₄₈**) precursor. The synthesis of **1** was accomplished by reaction of hydrate complexes of Fe^{II} (in presence of O_2), Fe^{III} and $[\text{Fe}_3\text{O}(\text{CH}_3\text{COO})_6(\text{H}_2\text{O})_3]^+$ with **P₈W₄₈** in aqueous, acidic medium ($\text{pH} \approx 4$).

Besides the unprecedented $\{\text{Fe}_{16}(\text{OH})_{28}(\text{H}_2\text{O})_4\}^{20+}$ iron-hydroxo-aqua nanocluster, the central (empty) cavity of the polyanion **1** has another highly interesting feature. Access of an oxidant/substrate to the “iron active site” is easily possible and therefore **1** is very attractive for catalytic applica-

tions. In fact, initial oxidation catalysis studies with air-oxygen as oxidant are highly promising.^[11]

Furthermore, it is very likely that the cavity in **1** can be filled with additional metal centres, for example, those different from iron(III). We are currently engaged in the process of preparing mixed-metal derivatives of **1** (e.g., “ $\text{Fe}_{16-x}\text{M}_x\text{P}_8\text{W}_{48}$ ”) with one or more of the iron centres substituted by other transition-metal ions (e.g. Mn^{II} , Co^{II} , Zn^{II}). Such derivatives could lead to interesting magnetic as well as catalytic properties.^[24]

The electrochemistry of **1** is characterised by a single 16-electron Fe-wave featuring the simultaneous reduction of all the Fe^{III} centres, in full agreement with their structural equivalence. This wave could not be split into distinct steps whatever the potential scan rate from 2 to 1000 mV s^{-1} . Its potential location is very close to that of the first W^{VI} wave of the lacunary precursor **P₈W₄₈**. Polyanion **1** shows efficient electrocatalytic properties regarding the reduction of NO_x , including nitrate. In addition, a remarkable reversible interaction between **1** and NO is observed. Such an interaction might justify investigating the biomimetic properties of this new POM.

The magnetic characterisation of **LiK-1** indicates that the ground state is made up of spin $S_T=2$, based on the data at 1.8 K . Even though we are unable to provide a quantitative estimate of the exchange interactions J_1 , J_2 and J_3 we hypothesise that $J_1 \approx J_2 \approx J_3$ and the observed $S_T=2$ could be regarded as a tentative ground state of **1**. Additional measurements in the low-temperature range ($< 1.8\text{ K}$) are needed to ascertain this prediction.

The study of a reaction of a solution of **P₈W₄₈** with metal cations offers the possibility to obtain basic information about principles of directed assembly processes under geometrically confined conditions. This can also lead, as in the present case, to cationic nanoclusters not obtainable under bulk conditions (see also reference [9]). One specific reaction described here refers to the “uptake of iron” under oxidative conditions and “release” under reducing conditions (the related simple reactions can be done under different reducing conditions) thereby mimicking the process occurring in the cavity of the protein ferritin. In this context one may also think about the option to study in a nanocavity the important reaction steps occurring during the reduction of O_2 with Fe^{II} , leading to O_2^- and $\text{OH}^{\text{[4a]}}$ even under simple “single-molecule type” conditions.

Experimental Section

Synthesis: The precursor salt $\text{K}_{28}\text{Li}_5[\text{H}_7\text{P}_8\text{W}_{48}\text{O}_{184}] \cdot 92\text{H}_2\text{O}$ was synthesised according to the published procedure of Contant^[25] and the purity was confirmed by infrared spectroscopy. All other reagents were used as purchased without further purification.

Li₄K₁₆[P₈W₄₈O₁₈₄Fe₁₆(OH)₂₈(H₂O)₄] · 66H₂O · 2 KCl (LiK-1)

Method 1 (Bremen): A sample of $\text{K}_{28}\text{Li}_5[\text{H}_7\text{P}_8\text{W}_{48}\text{O}_{184}] \cdot 92\text{H}_2\text{O}$ (0.370 g , 0.025 mmol) was dissolved in $\text{LiCH}_3\text{COO}/\text{CH}_3\text{COOH}$ buffer (0.5 M , 20 mL) at $\text{pH } 4.0$. Then $\text{FeCl}_3 \cdot 6\text{H}_2\text{O}$ (0.169 g , 0.625 mmol) was added and after complete dissolution, 30% H_2O_2 ($10\text{--}20$ drops) was added. Then

the solution was heated to 80 °C for 1 h and filtered while hot. After cooling to room temperature the filtrate was layered with around of KCl (1 M, 1 mL) solution. Slow evaporation in an open beaker at room temperature resulted in dark yellowish crystals after about one week. Evaporation was allowed to continue until the solution level had almost approached the solid product **LiK-1**, which was then collected by filtration, washed with cold water and air dried. Yield: 0.083 g (22%). IR: $\tilde{\nu}$ = 1119 (sh), 1064 (s), 1019 (m; all $\nu_{\text{as}}(\text{P-O})$), 951 (s), 927 (s, $\nu(\text{W=O})$), 793 (s), 752 (s), 687 (s), 647 (sh) ($\nu_{\text{as}}(\text{W-O-W})$), 559 (w), 526 (w), 473 cm^{-1} (w); elemental analysis calcd (%) for **LiK-1**: Li 0.18, K 4.56, Fe 5.78, W 57.1, P 1.60, Cl 0.46; found: Li 0.24, K 4.73, Fe 5.35, W 58.1, P 1.60, Cl 0.28. The degree of hydration of **LiK-1** was determined by TGA (see Figure S5). Elemental analysis was performed by Mikroanalytisches Labor Egmont Pascher, An der Pulvermühle 3, 53424 Remagen, Germany.

Method 2 (Bremen): A sample of $\text{K}_{28}\text{Li}_5[\text{H}_7\text{P}_8\text{W}_{48}\text{O}_{184}]\cdot 92\text{H}_2\text{O}$ (0.185 g, 0.0125 mmol) was dissolved in $\text{LiCH}_3\text{COO}/\text{CH}_3\text{COOH}$ buffer (0.5 M, 20 mL) at pH 4.0. Then $\text{Fe}(\text{ClO}_4)_3\cdot x\text{H}_2\text{O}$ (0.0974 g, 0.275 mmol) was added and the solution was heated to 80 °C for 1 h and filtered while hot. The following steps were identical to those of Method 1. The identity of **LiK-1** (isolated in very low yield, <10%) was established by XRD and IR.

Method 3 (Bremen): A sample of $\text{K}_{28}\text{Li}_5[\text{H}_7\text{P}_8\text{W}_{48}\text{O}_{184}]\cdot 92\text{H}_2\text{O}$ (0.185 g, 0.0125 mmol) was dissolved in $\text{LiCH}_3\text{COO}/\text{CH}_3\text{COOH}$ buffer (0.5 M, 20 mL) at pH 4.0. Then $\text{FeSO}_4\cdot 7\text{H}_2\text{O}$ (0.0868 g, 0.313 mmol) was added and after complete dissolution, 30% H_2O_2 (10–20 drops) was added. The colour of the solution changed to yellow. Then the solution was heated to 80 °C for 1 h and filtered while hot. The following steps were identical to those of Method 1. The identity of **LiK-1** (isolated in very low yield, <10%) was established by XRD and IR.

$\text{Na}_9\text{K}_{11}[\text{P}_8\text{W}_{48}\text{O}_{184}\text{Fe}_{16}(\text{OH})_{28}(\text{H}_2\text{O})_4]\cdot 100\text{H}_2\text{O}$ (NaK-1)

Method 4 (Bielefeld): $\text{K}_{28}\text{Li}_5[\text{H}_7\text{P}_8\text{W}_{48}\text{O}_{184}]\cdot 92\text{H}_2\text{O}$ (0.67 g, 0.046 mmol) was dissolved in $\text{NaCH}_3\text{COO}/\text{CH}_3\text{COOH}$ buffer (1 M, 30 mL, pH 4.2). After $[\text{Fe}_3\text{O}(\text{CH}_3\text{COO})_6(\text{H}_2\text{O})_3]\text{Cl}\cdot \text{H}_2\text{O}$ ($\{\text{Fe}_3\text{Ac}_6\}$) (0.2 g, 0.31 mmol) was added, the solution was heated to 60 °C for 30 h and filtered after cooling it to room temperature. Slow evaporation in an open Erlenmeyer flask at room temperature resulted in the precipitation of dark yellowish crystals that were filtered off after 3 days; these crystals were washed with a small amount of cold water and dried in air. Yield: 0.09 g, 13% (based on P_8W_{48}); elemental analysis calcd (%) for **NaK-1**: Na 1.30, K 2.71; found: Na 1.3, K 2.8. The identity of **NaK-1** was established by elemental analysis (in part done by Mikroanalytisches Labor Egmont Pascher, see above), IR spectroscopy and complete single-crystal X-ray structure analysis.

Method 5 (Bielefeld): $\text{K}_{28}\text{Li}_5[\text{H}_7\text{P}_8\text{W}_{48}\text{O}_{184}]\cdot 92\text{H}_2\text{O}$ (0.35 g, 0.024 mmol) was dissolved in $\text{NaCH}_3\text{COO}/\text{CH}_3\text{COOH}$ buffer (1 M, 20 mL, pH 4.2). After $\text{FeCl}_2\cdot 4\text{H}_2\text{O}$ (0.1 g, 0.5 mmol) was added, the resulting solution was heated to 65 °C for 12 h and filtered after cooling to room temperature. Slow evaporation in an open Erlenmeyer flask at room temperature resulted in the precipitation of dark yellowish crystals that were filtered off after 7 days; these crystals were washed with a small amount of cold water and dried in air. Yield: 0.03 g, 8%; elemental analysis calcd (%) for **NaK-1**: Na 1.30, K 2.71; found: Na 1.3, K 2.8. The identity of **NaK-1** was established by elemental analysis, XRD and IR spectroscopy.

X-ray crystallography

Crystal data for $\text{Li}_4\text{K}_{16}[\text{P}_8\text{W}_{48}\text{O}_{184}\text{Fe}_{16}(\text{OH})_{28}(\text{H}_2\text{O})_4]\cdot 66\text{H}_2\text{O}\cdot 2\text{KCl}$ (LiK-1**):** A yellow crystal of **LiK-1** with dimensions $0.06\times 0.12\times 0.33\text{ mm}^3$ was mounted in oil on a Hampton cryoloop for indexing and intensity data collection at 173 K on a Bruker D8 APEX II CCD single-crystal diffractometer with $\text{MoK}\alpha$ radiation ($\lambda = 0.71073\text{ \AA}$). Of the 335706 reflections collected ($2\theta_{\text{max}} = 52.8^\circ$, 99.7% complete), 14333 were unique ($R_{\text{int}} = 0.153$) and 10468 reflections were considered observed [$I > 2\sigma(I)$]. The data were processed using SAINT (from Bruker AXS) and an absorption correction was performed using the SADABS program (G. M. Sheldrick, Bruker AXS). Direct methods were used to locate the tungsten atoms (SHELXS-97), and the remaining atoms were found from successive Fourier maps (SHELXL-97). No H or Li atoms were located. The final cycles of refinement on F^2 over all data included the atomic coordinates, anisotropic thermal parameters (W, Fe, P, Cl and non-disordered K

atoms) and isotropic thermal parameters (O and disordered K atoms), converging to $R = 0.059$ [$I > 2\sigma(I)$] and $R_w = 0.183$ (all data). In the final difference map the deepest hole was -3.48 e \AA^{-3} (0.94 Å from W5) and the highest peak 4.20 e \AA^{-3} (0.73 Å from K4). The crystallographic data are provided in Table 1.

Table 1. Crystal data and structure refinement for $\text{Li}_4\text{K}_{16}[\text{P}_8\text{W}_{48}\text{O}_{184}\text{Fe}_{16}(\text{OH})_{28}(\text{H}_2\text{O})_4]\cdot 66\text{H}_2\text{O}\cdot 2\text{KCl}$ (**LiK-1**) and $\text{Na}_9\text{K}_{11}[\text{P}_8\text{W}_{48}\text{O}_{184}\text{Fe}_{16}(\text{OH})_{28}(\text{H}_2\text{O})_4]\cdot 100\text{H}_2\text{O}$ (**NaK-1**).

	LiK-1	NaK-1
formula	$\text{H}_{164}\text{Cl}_2\text{Fe}_{16}\text{K}_{18}$ $\text{Li}_8\text{O}_{382}\text{P}_8\text{W}_{48}$	$\text{H}_{236}\text{Fe}_{16}\text{K}_{11}\text{Na}_9$ $\text{O}_{316}\text{P}_8\text{W}_{48}$
M_r (g mol^{-1})	15473.7	15897.1
crystal system	orthorhombic	monoclinic
space group (No.)	<i>Pnmm</i> (58)	<i>C2/c</i> (15)
<i>a</i> [\AA]	36.3777(9)	46.5522(4)
<i>b</i> [\AA]	13.9708(3)	20.8239(18)
<i>c</i> [\AA]	26.9140(7)	27.8261(2)
<i>V</i> [\AA^3]	13678.4(6)	26765.34(4)
<i>Z</i>	2	4
<i>T</i> [$^\circ\text{C}$]	−73	−90
ρ_{calcd} [Mg m^{-3}]	3.76	3.945
μ [mm^{-1}]	21.37	21.74
max/min transmission	0.381/0.128	0.355/0.220
data/parameters	14333/492	29084/1584
goodness-of-fit on F^2	1.02	1.08
R [$I > 2\sigma(I)$] ^[a]	0.059	0.109
R_w (all data) ^[b]	0.183	0.303

$$[a] R = \sum |F_o| - |F_c| / \sum F_o. [b] R_w = [\sum w(F_o^2 - F_c^2)^2 / \sum w(F_c^2)]^{1/2}.$$

Crystal data for $\text{Na}_9\text{K}_{11}[\text{P}_8\text{W}_{48}\text{O}_{184}\text{Fe}_{16}(\text{OH})_{28}(\text{H}_2\text{O})_4]\cdot 100\text{H}_2\text{O}$ (NaK-1**):**

A yellow crystal of **NaK-1** with dimensions $0.06\times 0.1\times 0.1\text{ mm}^3$ was removed from the mother liquor and immediately cooled to 183(2) K on a Bruker AXS SMART diffractometer (three-circle goniometer with 1 K CCD detector, $\text{MoK}\alpha$ radiation, graphite monochromator; hemisphere data collection in ω at 0.3° scan width in three runs with 606, 435 and 230 frames ($\varphi = 0, 88$ and 180°) at a detector distance of 5 cm). A total of 78576 reflections ($1.48 < \theta < 27.05^\circ$) were collected of which 29084 reflections were unique ($R_{\text{int}} = 0.1127$). An empirical absorption correction using equivalent reflections was performed with the program SADABS 2.03. The structure was solved with the program SHELXS-97 and refined using SHELXL-97 to $R = 0.1088$ for 14786 reflections with $I > 2\sigma(I)$, $R = 0.1935$ for all reflections; max/min residual electron density 5.573 and -2.272 e \AA^{-3} . (SHELXS/L, SADABS from G. M. Sheldrick, University of Göttingen 1997/2003; structure graphics with DIAMOND 2.1 from K.Brandenburg, Crystal Impact GbR, 2001.)

Further details of the crystal structure investigations may be obtained from the Fachinformationszentrum Karlsruhe, 76344 Eggenstein-Leopoldshafen, Germany (Fax: (+49)7247-808-666; e-mail: crysdata@fiz-karlsruhe.de) on quoting the depository number CSD-418194 (**LiK-1**) and CSD-418527 (**NaK-1**).

UV/Vis spectroscopy: Pure water was used as solvent throughout, which was obtained by passing through a RiOs 8 unit followed by a Millipore-Q Academic purification set. All reagents were of high-purity grade and were used as purchased without further purification. The UV/Vis spectra were recorded on a Perkin-Elmer Lambda 19 spectrophotometer on $1.6\times 10^{-5}\text{ M}$ solutions of **LiK-1**. Matched 1.000 cm optical path quartz cuvettes were used. The following media proved useful for the present study: 0.5 M H_2SO_4 pH 0.30; 1 M LiCl/HCl , pH 1 to 3; 1 M $\text{CH}_3\text{CO}_2\text{Li}/\text{CH}_3\text{CO}_2\text{H}$, pH 5 to 7.

Electrochemical experiments: The solutions were deaerated thoroughly for at least 30 min with pure argon and kept under a positive pressure of this gas during the experiments. NO was introduced in an oxygen-free electrochemical cell through a catheter connected to a sealed purging system previously filled with argon, which excluded oxygen and allowed

contaminants such as NO_x to be scavenged in 9 M KOH. NO was bubbled through the electrolyte in the electrochemical cell for 30 min, resulting in a NO-saturated solution (1–2 mm). The electrochemical cell was checked for leaks in the following way: solutions saturated with NO were kept for several hours and used for electrocatalytic reduction of this substrate; after removing NO by bubbling pure argon, no electroactivity of NO or a related species could be detected in the potential range from +0.920 V to –0.730 V at pH 1.

The source, mounting and polishing of the glassy carbon (GC) electrodes have been described previously.^[26] The glassy carbon samples had a diameter of 3 mm. The electrochemical set-up was an EG & G 273 A driven by a PC with the M270 software. Potentials are quoted against a saturated calomel electrode (SCE). The counter electrode was a platinum gauze of large surface area. All experiments were performed at room temperature.

Magnetic measurements: Magnetic susceptibility and magnetisation measurements were carried out on powder samples of **LiK-1** using a Quantum Design MPMS SQUID magnetometer in the temperature range of 1.8–300 K and field range of 0–7 T. The data were corrected for the sample holder, TIP of Fe³⁺, W⁶⁺ ions, and molecular diamagnetism which was estimated from Klemm constants.^[27]

EPR measurements: Polycrystalline powder EPR spectra of **LiK-1** were recorded at frequencies ranging from 9.64 to 320 GHz at the high-field electron magnetic resonance facility at the National High Magnetic Field Laboratory in Tallahassee, FL, as described elsewhere.^[28] Temperature variation was carried out from room temperature to 5 K. An Oxford Instruments Teslatron superconducting magnet sweepable between 0 and 17 T was used to apply the Zeeman field. In all experiments the modulation amplitudes and microwave power were adjusted for optimal signal intensity and resolution.

Acknowledgements

U.K. acknowledges support from Jacobs University, the German Science Foundation (DFG-KO-2288/3-2) and the Fonds der Chemischen Industrie. A.M. thanks the German Science Foundation as well as the Fonds der Chemischen Industrie for continuous support over the years, furthermore the German-Israeli Foundation for Scientific Research & Development (GIF), and the European Union (MRTN-CT-2003-504880). This work was also supported by the CNRS and the University Paris-Sud 11 (UMR 8000). The help of Dr. Pedro de Oliveira in setting up experiments with NO is thankfully acknowledged. N.S. and J.v.T. would like to acknowledge the State of Florida and the NSF Core Operative Agreement grants DMR-0084173 and DMR-0520481 for financial support. Figures 1–3 were generated by Diamond Version 3.1e (copyright Crystal Impact GbR).

- [1] a) This refers in a general sense to scenarios where “materials” grow with preferred orientations on surfaces influenced/directed by the surfaces’ geometry: V. E. Henrich, P. A. Cox, *The Surface Science of Metal Oxides*, Cambridge University Press, Cambridge **1994**, p. 384; b) The process is quite common in the geosphere. This leads to situations where spaces with larger scale sizes (bulk condition comparable), but also up to smaller scales, are filled with minerals or water; the well-known geodes are objects of that type (see textbooks of mineralogy). The confinement induced changes in the water structure and dynamics, which are commonly substrate specific, play a key-role in the geosphere regarding the reactivity of mineral surfaces (see J. Wang, A. G. Kalinichev, R. J. Kirkpatrick, *J. Phys. Chem. B* **2005**, *109*, 14308–14313). Important information about that topic can be obtained from POM chemistry (see: A. Oleinikova, H. Weingärtner, M. Chaplin, E. Diemann, H. Bögge, A. Müller, *ChemPhys-Chem* **2007**, *8*, 646–649).
- [2] Phospholipid vesicles are for instance the reaction vessels for many biomineralisation processes: in the spatially confined environments

the biological systems can control the reaction conditions to achieve extraordinary morphologies (T. Douglas, in *Biomimetic Materials Chemistry* (Ed.: S. Mann), VCH, Weinheim, **1996**, p. 91).

- [3] S. Mann, *Biomineralisation: Principles and Concepts in Bioinorganic Materials Chemistry*, Oxford University Press, Oxford, **2001**.
- [4] a) W. Kaim, B. Schwederski, *Bioinorganic Chemistry: Inorganic Elements in the Chemistry of Life*, Wiley, Chichester, **1994**; see also L.-O. Essen, S. Offermann, D. Oesterheld, K. Zeth, in *Biomineralisation: Progress in Biology, Molecular Biology and Application* (Ed.: E. Baeuerlein), Wiley-VCH, Weinheim, **2004**, p. 119; in this context the authors refer to the toxicity of Fe^{II} for aerobic organisms in the sense that it reduces O₂ to the reactive superoxide anion O₂^{•-} and reacts with the peroxide in the Fenton reaction to form the highly reactive OH[•] radical; b) J. Schemberg, K. Schneider, U. Demmer, E. Warkentin, A. Müller, U. Ermler, *Angew. Chem.* **2007**, *119*, 2460–2465; *Angew. Chem. Int. Ed.* **2007**, *46*, 2408–2413; c) A. Müller, S. Q. N. Shah, H. Bögge, M. Schmidtman, *Nature* **1999**, *397*, 48–50.
- [5] R. Contant, A. Tézé, *Inorg. Chem.* **1985**, *24*, 4610–4614.
- [6] M. Zimmermann, N. Belai, R. J. Butcher, M. T. Pope, E. V. Chubarova, M. H. Dickman, U. Kortz, *Inorg. Chem.* **2007**, *46*, 1737–1740.
- [7] a) S. S. Mal, U. Kortz, *Angew. Chem.* **2005**, *117*, 3843–3846; *Angew. Chem. Int. Ed.* **2005**, *44*, 3777–3780; b) D. Jabbour, B. Keita, L. Nadjo, U. Kortz, S. S. Mal, *Electrochem. Commun.* **2005**, *7*, 841–847; c) M. S. Alam, V. Dremov, P. Müller, A. V. Postnikov, S. S. Mal, F. Hussain, U. Kortz, *Inorg. Chem.* **2006**, *45*, 2866–2872; d) G. Liu, T. Liu, S. S. Mal, U. Kortz, *J. Am. Chem. Soc.* **2006**, *128*, 10103–10110; corrigendum: G. Liu, T. Liu, S. S. Mal, U. Kortz, *J. Am. Chem. Soc.* **2007**, *129*, 2408.
- [8] C. Pichon, P. Mialane, A. Dolbecq, J. Marrot, E. Rivière, B. Keita, L. Nadjo, F. Sécheresse, *Inorg. Chem.* **2007**, *46*, 5292–5301.
- [9] A. Müller, M. T. Pope, A. M. Todea, H. Bögge, J. van Slageren, M. Dressel, P. Gouzerh, R. Thouvenot, B. Tsukerblat, A. Bell, *Angew. Chem.* **2007**, *119*, 4561–4564; *Angew. Chem. Int. Ed.* **2007**, *46*, 4477–4480.
- [10] S. S. Mal, N. H. Nsouli, M. H. Dickman, U. Kortz, *Dalton Trans.* **2007**, 2627–2630.
- [11] Novel iron-substituted polyoxometalates and processes for their preparation: U. Kortz, S. S. Mal, USSN 11/728,142, patent filed on 23 March 2007.
- [12] I. D. Brown, D. Altermatt, *Acta Crystallogr. Sect. A* **1985**, *41*, 244–247.
- [13] B. Keita, Y. W. Lu, L. Nadjo, R. Contant, *Electrochem. Commun.* **2000**, *2*, 720–726.
- [14] J. E. Toth, F. C. Anson, *J. Electroanal. Chem.* **1989**, 256,361–370.
- [15] B. Keita, A. Belhouari, L. Nadjo, R. Contant, *J. Electroanal. Chem.* **1998**, *442*, 49–57.
- [16] B. Keita, L. Nadjo, *Electrochemistry of Polyoxometalates, Encyclopedia of Electrochemistry, Vol 7* (Eds.: A. J. Bard, M. Stratmann), Wiley-VCH, **2006**, pp. 607–700.
- [17] B. Keita, F. Girard, L. Nadjo, R. Contant, R. Belghiche, M. Abbessi, *J. Electroanal. Chem.* **2001**, *508*, 70–80.
- [18] B. Keita, A. Abdeljalil, L. Nadjo, R. Contant, R. Belghiche, *Langmuir* **2006**, *22*, 10416–10425.
- [19] a) B. Keita, L. Nadjo, *J. Mol. Catal. A* **2007**, *262*, 190–215; b) L. Lissnard, P. Mialane, A. Dolbecq, J. Marrot, J. M. Clemente-Juan, E. Coronado, B. Keita, P. de Oliveira, L. Nadjo, F. Sécheresse, *Chem. Eur. J.* **2007**, *13*, 3525–3536; c) B. Keita, P. de Oliveira, U. Kortz, *Chem. Eur. J.* **2007**, *13*, 5480–5491.
- [20] a) S. M. Gorun, S. J. Lippard, *Inorg. Chem.* **1991**, *30*, 1625–1630; b) R. Werner, S. Ostrovsky, K. Griesar, W. Haase, *Inorg. Chim. Acta* **2001**, *326*, 78–88; c) C. Cañada-Vilalta, T. A. O’Brien, E. K. Brechin, M. Pink, E. R. Davidson, G. Christou, *Inorg. Chem.* **2004**, *43*, 5505–5521.
- [21] a) J. K. McCusker, C. A. Christmas, P. M. Hagen, R. K. Chadha, D. F. Harvey, D. N. Hendrickson, *J. Am. Chem. Soc.* **1991**, *113*, 6114–6124; b) C. Delfs, D. Gatteschi, L. Pardi, R. Sessoli, K. Wieghardt, D. Hanke, *Inorg. Chem.* **1993**, *32*, 3099–3103; c) A. Ozarowski, B. R. McGarvey, J. E. Drake, *Inorg. Chem.* **1995**, *34*, 5558–5566.

- [22] a) *Magnetochemistry* (Ed.: R. L. Carlin), Springer, Berlin, **1986**.
b) *Molecular Magnetism* (Ed.: O. Kahn), VCH, Weinheim, **1993**.
- [23] L.-H. Bi, U. Kortz, S. Nellutla, A. C. Stowe, J. van Tol, N. S. Dalal, B. Keita, L. Nadjjo, *Inorg. Chem.* **2005**, *44*, 896–903.
- [24] a) U. Kortz, S. Nellutla, A. C. Stowe, N. S. Dalal, J. van Tol, B. S. Bassil, *Inorg. Chem.* **2004**, *43*, 144–154; b) U. Kortz, S. Nellutla, A. C. Stowe, N. S. Dalal, U. Rauwald, W. Danquah, D. Ravot, *Inorg. Chem.* **2004**, *43*, 2308–2317; c) B. S. Bassil, S. Nellutla, U. Kortz, A. C. Stowe, J. van Tol, N. S. Dalal, B. Keita, L. Nadjjo, *Inorg. Chem.* **2005**, *44*, 2659–2665; d) S. Nellutla, J. van Tol, N. S. Dalal, L.-H. Bi, U. Kortz, B. Keita, L. Nadjjo, G. Khitrov, A. G. Marshall, *Inorg. Chem.* **2005**, *44*, 9795–9806.
- [25] R. Contant, *Inorg. Synth.* **1990**, *27*, 110.
- [26] B. Keita, L. Nadjjo, *J. Electroanal. Chem. Interfacial Electrochem.* **1988**, *243*, 87–103.
- [27] S. G. Vulfson, *Molecular Magnetochemistry*, Gordon and Breach Science: Amsterdam, **1998**, p. 241.
- [28] a) B. Cage, A. K. Hassan, L. Pardi, J. Krzystek, L. C. Brunel, N. S. Dalal *J. Magn. Reson.* **1997**, *124*, 495–498; b) A. K. Hassan, L. A. Pardi, J. Krzystek, A. Sienkiewicz, P. Goy, M. Rohrer, L. C. Brunel, *J. Magn. Reson.* **2000**, *142*, 300–312.

Received: September 10, 2007
Published online: December 28, 2007

Chapter 3

Summary

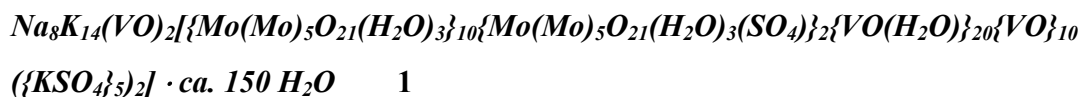
The thesis refers mainly to the synthesis of unique polyoxometalates having interesting magnetic properties. The compounds **1-5** which were obtained are described below.

The classical/historical polyoxometalates are diamagnetic, however they are currently receiving much attention in the field molecular magnetism due to the fact that: (i) they can act as ligands for the coordination of paramagnetic ions, like V(IV), Fe(III), Cr(III), Fe(II), Mn(II), Co(II), Ni(II) and Cu(II), leading to well-defined magnetic clusters of controlled nuclearities and topologies, (ii) they offer the opportunity to investigate both experimentally and theoretically the nature of the magnetic exchange interactions, and (iii) they stimulate the development of new theories to account for the interplay between electron delocalization and exchange interactions in high-nuclearity mixed valence clusters. In this dissertation we investigated the utility of the pentagonal $\{(Mo)Mo_5\}$ -type unit in constructing spherical systems with interesting magnetic properties.

Molybdenum-oxide based spherical, hollow clusters of the type $\{(Mo)Mo_5\}_{12}\{linker\}_{30}$ – because of their structural features also called Keplerates – can for instance be directly synthesized by the addition of linkers such as $V^{IV}O^{2+}$, Fe^{III} and Cr^{III} to a dynamic library containing (virtual) pentagonal units in solution.

In the $\{Mo_{72}V_{30}\}$ **1** cluster the 30 V^{IV} centers – acting as linkers for the pentagonal $\{(Mo^{VI})Mo_5^{VI}\}$ type units – describe a (slightly distorted) icosidodecahedron, the distortion is in agreement with the fact that 20 V^{IV} in the equatorial region have octahedral coordination and the two sets of five V^{IV} centers in the polar area have square pyramidal coordination. Ten of the twelve SO_4^{2-} ligands are coordinated by three oxygen atoms to three adjacent Mo^{VI} centers of the

$\{(\text{Mo}^{\text{VI}})\text{Mo}^{\text{VI}}\}_5$ groups such that two $\{\text{KSO}_4\}_5$ rings parallel to the equator result with the K^+ cations (formally) bridging the SO_4^{2-} anions.



We know that practically neutral spherical molybdenum-oxide based capsules – but positively charged without the organic ligands – have a high affinity for integration of different guest species. In the cavity of the $\{\text{Mo}_{72}\text{Fe}_{30}\}$ capsule a hexamolybdate Lindqvist type anion $[\text{Mo}_6\text{O}_{19}]^{2-}$ got encapsulated, noncovalently bonded. Such hexamolybdate polyanion cannot be obtained as other polymolybdates simply in aqueous medium and it is preferably formed in organic solvents while crystallizing together with organic cations. In the present system it is stabilized/protected by the comparably large number of acetates inside the cavity forming a hydrophobic protecting environment. As the skeleton of **2a** is nearly neutral and the pure inorganic part, *i.e.* without the acetate ligands, is even positively charged, this allows the attraction of small anionic fragments with the consequence that the stepwise formation of the $[\text{Mo}_6\text{O}_{19}]^{2-}$ occurs parallel to the growth of the capsule, *i.e.* on its internal electrophilic surface.

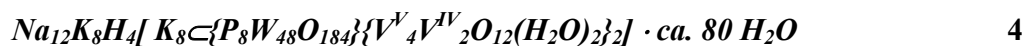


In the cavity of $\{\text{Mo}_{72}\text{Cr}_{30}\}$ **3a** cluster an $\{\text{Na}(\text{H}_2\text{O})_{12}\}$ cluster is encapsulated where the O atoms form an icosahedron, with its approximate C_5 axes coinciding with the C_5 axes of the metal-oxide based skeleton. The relatively small water cluster is protected by the hydrophobic shell built up by the acetate ligands and should therefore not be formed within the cavities of the present type of capsules which contain hydrophilic interiors.



The three practically isostructural clusters/skeletons of the type $\{(Mo)Mo_5\}_{12}\{M\}_{30}$ with a sequence of spin values $S=1/2$ (V^{IV}), $S=3/2$ (Cr^{III}) and $S=5/2$ (Fe^{III}) show quite different magnetic behavior. The capsule/Keplerate with $M=Fe^{III}$ has essentially a classical behavior with weak superexchange interaction due to the large spin 5/2 centred at 30 different corners of the $\{M_{30}\}$ icosidodecahedron. By contrast, in the case of $M=V^{IV}$ where the spin is small and the electrons delocalized, the system is called a “Quantum Keplerate”. The capsule with $M=Cr^{III}$ is just in between that of the two other ones with the correspondingly intermediate magnetic properties.

The wheel-shaped $\{P_8W_{48}\}$ polyoxotungstate provides a reaction chamber for the directed-assembly process leading to **4a**, where two unprecedented mixed-valence vanadium oxide $\{V^V_4V^{IV}_2O_{12}(H_2O)_2\}^{4+}$ cavity-capping groups based on linked octahedra and tetrahedra with V^{IV} and V^V centers, respectively are encapsulated and to **5a**, which contains – in the form of a cyclic arrangement – the unprecedented $\{Fe_{16}(OH)_{28}(H_2O)_4\}^{20+}$ nanocluster, with 16 edge- and corner-sharing FeO_6 octahedra, grafted on the inner surface of the crown-shaped $\{P_8W_{48}\}$ precursor.



In **4a** the terminal $V^{IV}O$ bonds are directed towards the interior of the composite anion and towards the corresponding bonds of the opposite capping group ($V...V$ separation *ca* 6.2Å). Potassium cations occupy analogous positions within the new host-guest complex but they are now sandwiched between the two cyclic capping groups $\{V^V_4V^{IV}_2O_{12}(H_2O)_2\}^{4+}$. There is no doubt that other nucleation processes can be studied in the $\{P_8W_{48}\}$ cluster cavity under formally similar conditions.

Appendix

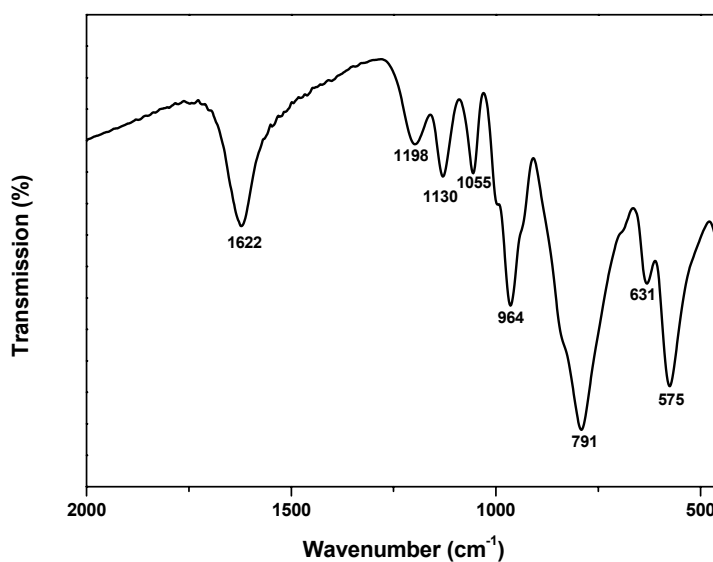
Spectroscopic data

Infrared and Raman spectroscopy

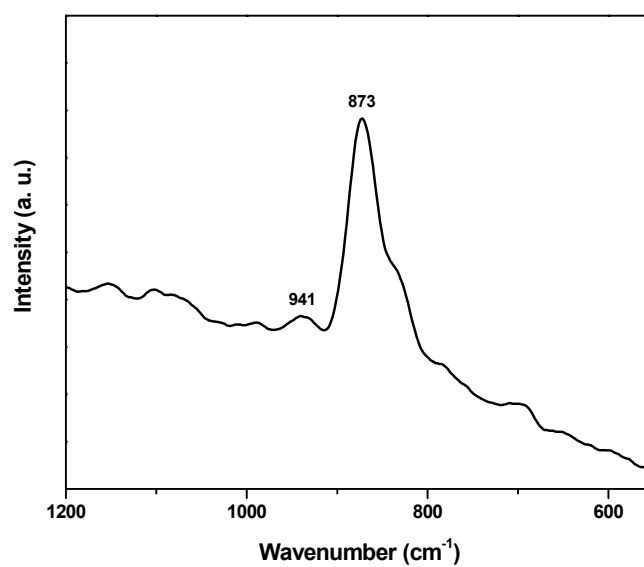
Vibrational spectra were recorded with a Bruker IFS 66 / FRAU 106 spectrometer. FT-IR: KBr pellet, recorded in the range 4000-400 cm^{-1} ; FT-Raman: KBr matrix, excitation with a Nd: YAG-laser; $\lambda_e = 1064 \text{ nm}$.

UV-Vis spectroscopy

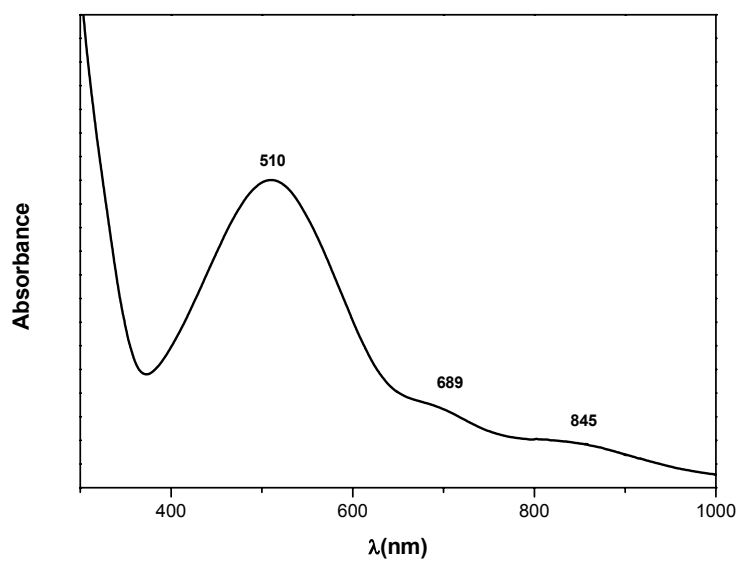
UV-Vis spectra were recorded from degassed solutions in the range 1200-200 nm with a Shimadzu UV-160A spectrophotometer and evaluated with a program associated with the spectrometer.



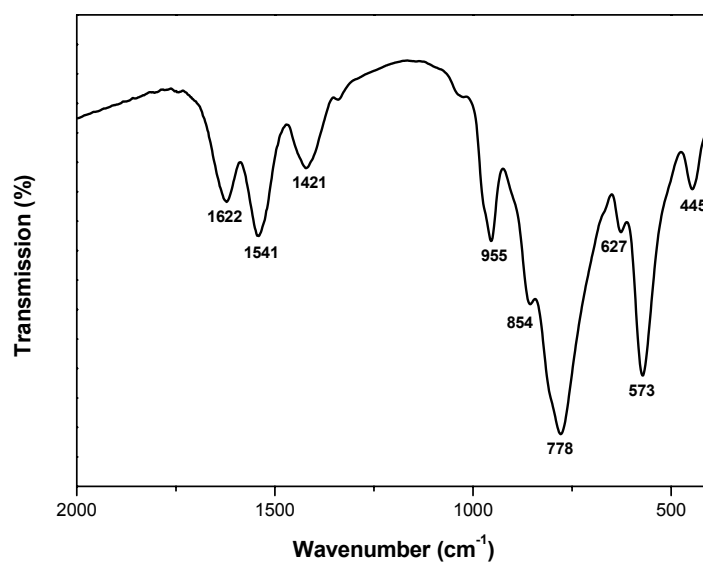
IR spectrum of $\text{Na}_8\text{K}_{14}(\text{VO})_2[\{\text{Mo}(\text{Mo})_5\text{O}_{21}(\text{H}_2\text{O})_3\}_{10}\{\text{Mo}(\text{Mo})_5\text{O}_{21}(\text{H}_2\text{O})_3(\text{SO}_4)\}_2\{\text{VO}(\text{H}_2\text{O})\}_{20}\{\text{VO}\}_{10}(\{\text{KSO}_4\}_5)_2] \cdot \text{ca. } 150 \text{ H}_2\text{O}$



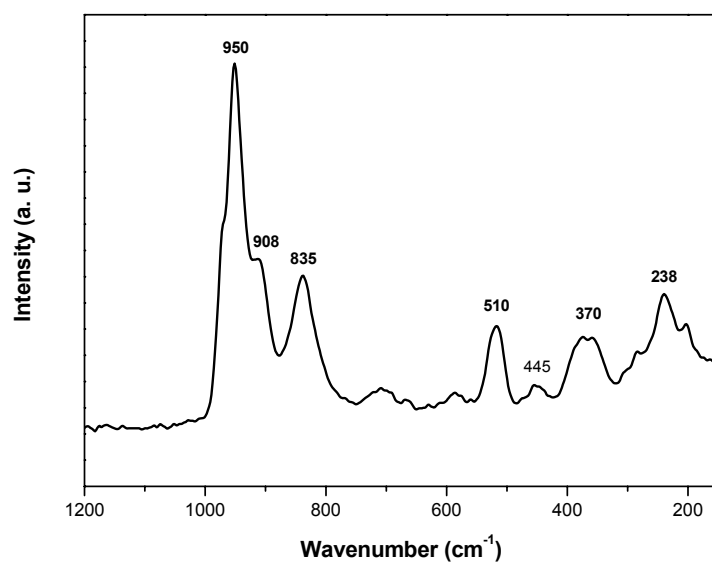
Solid state Raman spectrum of $\text{Na}_8\text{K}_{14}(\text{VO})_2[\{\text{Mo}(\text{Mo})_5\text{O}_{21}(\text{H}_2\text{O})_3\}_{10}\{\text{Mo}(\text{Mo})_5\text{O}_{21}(\text{H}_2\text{O})_3(\text{SO}_4)\}_2\{\text{VO}(\text{H}_2\text{O})\}_{20}\{\text{VO}\}_{10}(\{\text{KSO}_4\}_5)_2] \cdot \text{ca. } 150 \text{ H}_2\text{O}$



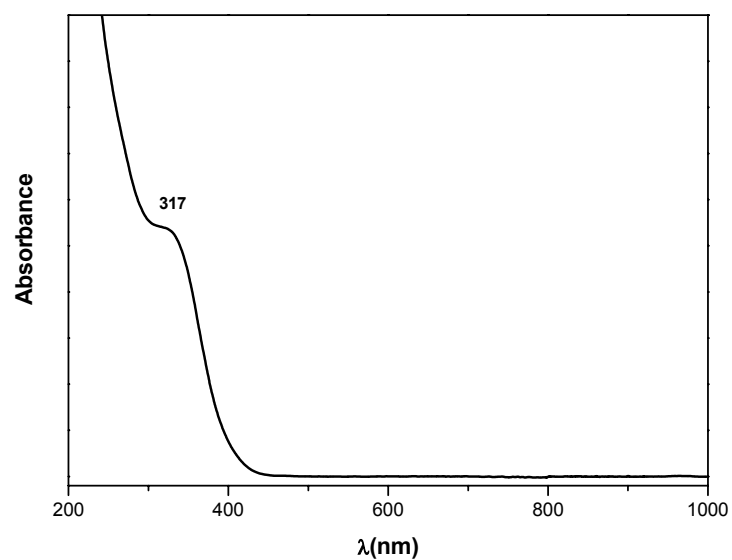
UV-Vis spectrum of $\text{Na}_8\text{K}_{14}(\text{VO})_2[\{\text{Mo}(\text{Mo})_5\text{O}_{21}(\text{H}_2\text{O})_3\}_{10}\{\text{Mo}(\text{Mo})_5\text{O}_{21}(\text{H}_2\text{O})_3(\text{SO}_4)\}_2\{\text{VO}(\text{H}_2\text{O})\}_{20}\{\text{VO}\}_{10}(\{\text{KSO}_4\}_5)_2] \cdot \text{ca. } 150 \text{ H}_2\text{O}$



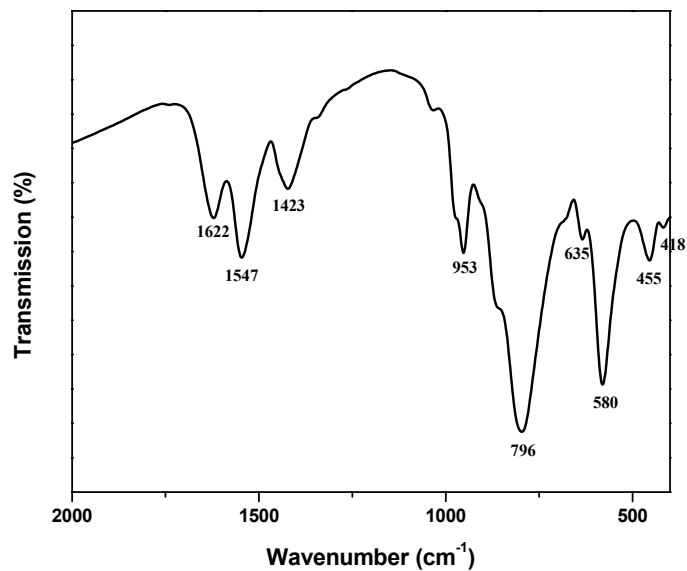
IR spectrum of $\text{Na}_4[\{\text{Mo}_6\text{O}_{19}\}^{2-} \subset \{\text{Mo}^{\text{VI}}_{72}\text{Fe}^{\text{III}}_{30}\text{O}_{252}(\text{CH}_3\text{COO})_{20}(\text{H}_2\text{O})_{92}\}] \cdot \text{ca. } 120 \text{ H}_2\text{O}$



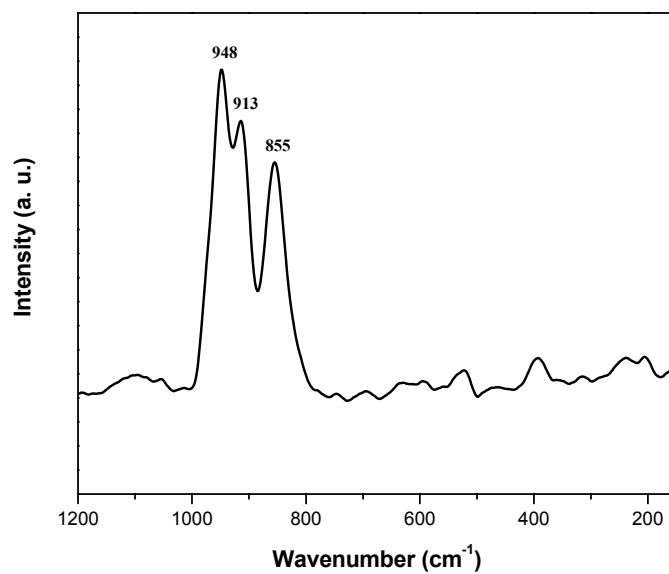
Solid state Raman spectrum of $\text{Na}_4[\{\text{Mo}_6\text{O}_{19}\}^{2-} \subset \{\text{Mo}^{\text{VI}}_{72}\text{Fe}^{\text{III}}_{30}\text{O}_{252} (\text{CH}_3\text{COO})_{20} (\text{H}_2\text{O})_{92}\}] \cdot \text{ca. } 120 \text{ H}_2\text{O}$



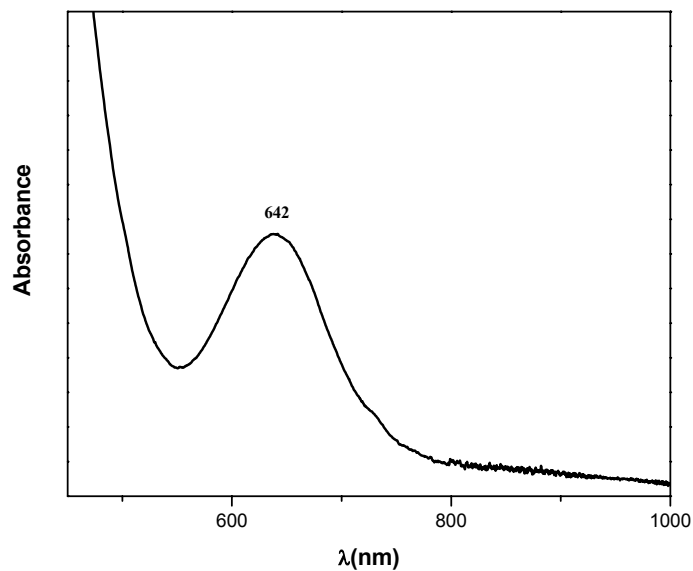
UV-Vis spectrum of $\text{Na}_4[\{\text{Mo}_6\text{O}_{19}\}^{2-} \subset \{\text{Mo}^{\text{VI}}_{72}\text{Fe}^{\text{III}}_{30}\text{O}_{252} (\text{CH}_3\text{COO})_{20} (\text{H}_2\text{O})_{92}\}] \cdot \text{ca. } 120 \text{ H}_2\text{O}$



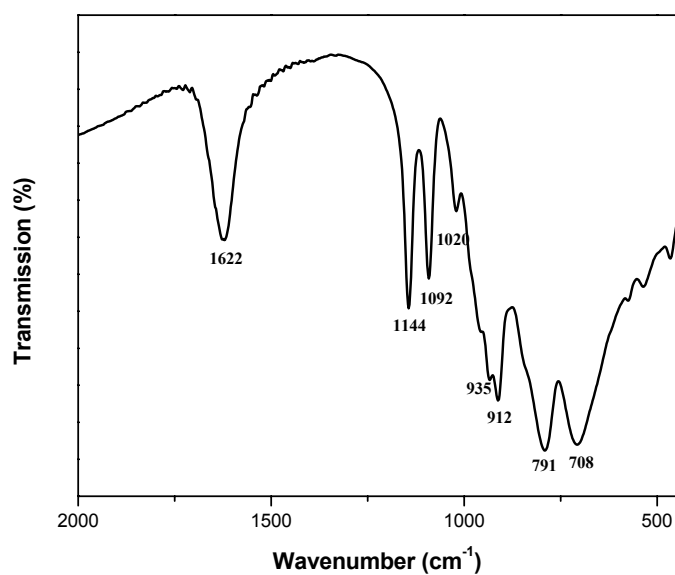
IR spectrum of $[\{Na(H_2O)_{12}\} \subset \{Mo^{VI}_{72}Cr^{III}_{30}O_{252}(CH_3COO)_{19}(H_2O)_{94}\}] \cdot ca. 120 H_2O$



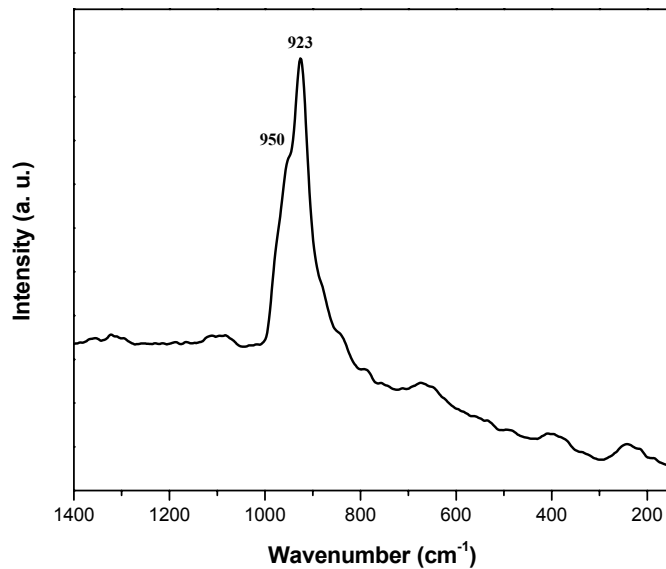
Solid state Raman spectrum of $[\{Na(H_2O)_{12}\} \subset \{Mo^{VI}_{72}Cr^{III}_{30}O_{252}(CH_3COO)_{19}(H_2O)_{94}\}] \cdot ca. 120 H_2O$



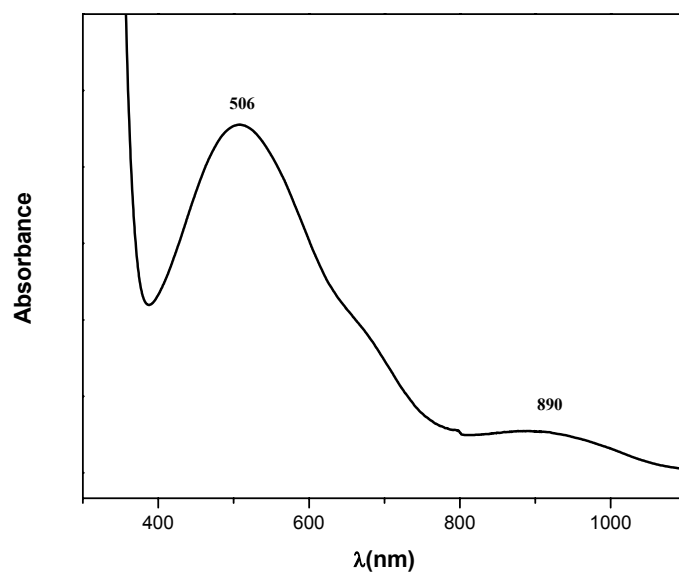
UV-Vis spectrum of $[\{Na(H_2O)_{12}\} \subset \{Mo^{VI}_{72}Cr^{III}_{30}O_{252}(CH_3COO)_{19}(H_2O)_{94}\}] \cdot ca. 120 H_2O$



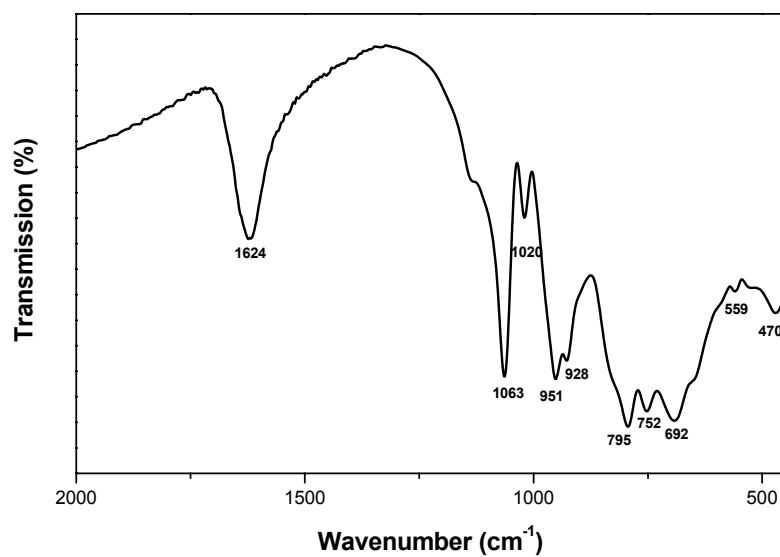
IR spectrum of $Na_{12}K_8H_4[K_8 \subset \{P_8W_{48}O_{184}\} \{V^V_4V^{IV}_2O_{12}(H_2O)_2\}_2] \cdot ca. 80 H_2O$



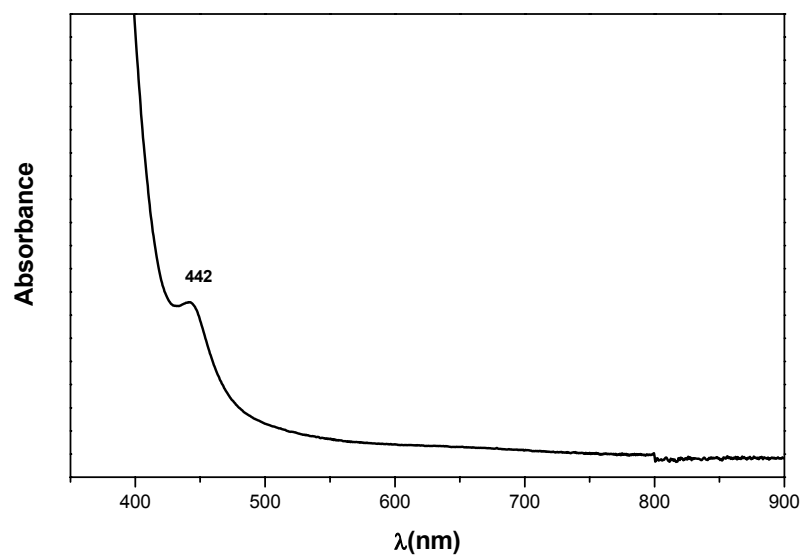
Solid state Raman spectrum of $\text{Na}_{12}\text{K}_8\text{H}_4[\text{K}_8\{\text{P}_8\text{W}_{48}\text{O}_{184}\}\{\text{V}^{\text{V}}_4\text{V}^{\text{IV}}_2\text{O}_{12}(\text{H}_2\text{O})_2\}_2] \cdot \text{ca. } 80 \text{ H}_2\text{O}$



UV-Vis spectrum of $\text{Na}_{12}\text{K}_8\text{H}_4[\text{K}_8\{\text{P}_8\text{W}_{48}\text{O}_{184}\}\{\text{V}^{\text{V}}_4\text{V}^{\text{IV}}_2\text{O}_{12}(\text{H}_2\text{O})_2\}_2] \cdot \text{ca. } 80 \text{ H}_2\text{O}$



IR spectrum of $\text{Na}_9\text{K}_{11}[\text{P}_8\text{W}_{48}\text{O}_{184}\text{Fe}_{16}(\text{OH})_{28}(\text{OH}_2)_4] \cdot 100\text{H}_2\text{O}$



UV-Vis spectrum of $\text{Na}_9\text{K}_{11}[\text{P}_8\text{W}_{48}\text{O}_{184}\text{Fe}_{16}(\text{OH})_{28}(\text{OH}_2)_4] \cdot 100\text{H}_2\text{O}$

Chapter 4

Curriculum Vitae

Ana Maria Todea
Wellensiek 19
33619 Bielefeld
Deutschland
Tel: +4917626065299
Email: *todeaanamaria@yahoo.com*

PERSONALS

Born on 27th February, 1979 in Cluj-Napoca, Romania, single, Romanian nationality

PROFESSIONAL EXPERIENCE

02/2004 - present Doctoral student, University of Bielefeld, Germany, Faculty of Chemistry, supervisor: Prof. Dr. Dr. h. c. mult. Achim Müller

EDUCATION

06/2003 Licentiate in Electrochemistry, topic of the thesis: Biosensors for electrochemical detection of glucose and nitrates, supervisor: Prof. Dr. Liana Muresan

10/2002 - 06/2003 Master student of the "Babes-Bolyai" University, Cluj-Napoca, Romania, Faculty of Chemistry and Chemical Engineering, specialization: Electrochemistry

07/2002 Licentiate in Chemistry, topic of the thesis: Kinetics and oxidation mechanism of tiodipropionic acid with chromate in acidic medium, supervisor: Lector. Dr. Ing. Alexandra Rustoiu-Csavdari

10/1998 - 06/2002 Student of the "Babes-Bolyai" University, Cluj-Napoca, Romania, Faculty of Chemistry and Chemical Engineering, specialization: Chemistry - Physics;

09/1994 - 07/1998 "Avram Iancu" National Colleg, Cluj-Napoca, Romania

HONORS

02/2003 - 05/2003 ERASMUS fellowship, Universite Joshep Fourier, Grenoble, France

10/1998 - 06/2002 Studentship granted by the "Babes-Bolyai" University Cluj-Napoca, Romania

COMPUTER SKILLS

Microsoft Office (Word, Excel, PowerPoint), Origin, Corel Draw, Internet related software.

LANGUAGES

Fluent English and French, Romanian (mother language).

LIST OF PUBLICATIONS

1. A. Müller, A. M. Todea, J. van Slageren, M. Dressel, H. Bögge, M. Schmidtman, M. Luban, L. Engelhardt, M. Rusu, **"Triangular Geometrical and Magnetic Motifs Uniquely Linked on a Spherical Capsule Surface"**, *Angew. Chem.*, **2005**, *117*, 3925-3929, *Angew. Chem. Int. Ed.*, **2005**, *44*, 3857-3861.
2. A. Müller, A. M. Todea, H. Bögge, J. van Slageren, M. Dressel, A. Stammer, M. Rusu, **"Formation of a "less stable" polyanion directed and protected by electrophilic internal surface functionalities of a capsule in growth: $[\{\text{Mo}_6\text{O}_{19}\}^{2-}$ in $\{\text{Mo}^{\text{VI}}_{72}\text{Fe}^{\text{III}}_{30}\text{O}_{252}(\text{ac})_{20}(\text{H}_2\text{O})_{92}\}^{4-}$ "**, *Chem. Commun.*, **2006**, 3066-3068.

3. A. Müller, M. T. Pope, A. M. Todea, H. Bögge, J. van Slageren, M. Dressel, P. Gouzerh, R. Thouvenot, B. Tsukerblat, A. Bell, **"Metal-Oxide-Based Nucleation Process under Confined Conditions: Two Mixed-Valence V₆-Type Aggregates Closing the W₄₈ Wheel-Type Cluster Cavities"**, *Angew. Chem.*, **2007**, *119*, 4561-4564, *Angew. Chem. Int. Ed.*, **2007**, *46*, 4477-4480.
4. A. M. Todea, A. Merca, H. Bögge, J. van Slageren, M. Dressel, L. Engelhardt, M. Luban, T. Glaser, M. Henry, A. Müller, **"Extending the {(Mo)Mo₅}₁₂M₃₀ Capsule Sequence: New Cr₃₀ Cluster of $s = 3/2$ Metal Centres with a {Na(H₂O)₁₂} Encapsulate"**, *Angew. Chem.*, **2007**, *119*, 6218-6222, *Angew. Chem. Int. Ed.*, **2007**, *46*, 6106-6110.
5. E. Balogh, A. M. Todea, A. Müller, W. H. Casey, **"Rates of Ligand Exchange between >Fe^{III}-OH₂ Functional Groups on a Nanometer-Sized Aqueous Cluster and Bulk Solution"**, *Inorg. Chem.*, **2007**, *46*, 7087-7092.
6. S. S. Mal, M. H. Dickman, U. Kortz, A. M. Todea, A. Merca, H. Bögge, T. Glaser, A. Müller, S. Nellutla, N. Kaur, J. van Tol, N. S. Dalal, B. Keita, L. Nadjo, **"Nucleation process in the cavity of a 48-tungstophosphate wheel resulting in a 16 metal center iron-oxide nanocluster"**, *Chem. Eur. J.*, **2008**, *14*, 1186-1195.